

Blood-CNS barriers in neurodegenerative diseases

Dissertation
zur Erlangung des Grades
„Doktor der Naturwissenschaften“

Am Fachbereich Biologie
der Johannes Gutenberg-Universität
in Mainz



JOHANNES GUTENBERG
UNIVERSITÄT MAINZ

von

Sabrina Meister

geboren am 31. Januar 1984 in Mainz

Mainz, im November 2013

Dekan:

1. Berichtstatter:

2. Berichtstatter:

Tag der mündlichen Prüfung: 22. Januar 2014

I hereby declare that I wrote this dissertation submitted without any unauthorized external assistance and used only sources acknowledged in the work. All textual passages which are appropriated verbatim or paraphrased from published and unpublished texts as well as all information obtained from oral sources are duly indicated and listed in accordance with bibliographical rules. In carrying out this research, I complied with the rules of standard scientific practice as formulated in the statutes of the Johannes Gutenberg-University Mainz to insure standard scientific practice.

Sabrina Meister

Summary

The blood-brain barrier (BBB) and the blood-spinal cord barrier (BSCB) separate the brain and the spinal cord from the circulating blood and are important for the maintenance of the CNS homeostasis. They build a physical barrier thereby protecting the CNS from pathogens and toxic agents, and their disruption plays a crucial role in the pathogenesis of several CNS disorders. In this thesis, the blood-CNS-barriers were studied via *in vitro* models in two case studies for neurodegenerative disorders, in particular Alzheimer's disease (AD) and amyotrophic lateral sclerosis (ALS). The first model evaluates treatment possibilities of AD using nanotechnology-based strategies. Since the toxic amyloid- β_{42} ($A\beta_{42}$) peptide plays a crucial role in the pathogenesis of AD, reduced generation or enhanced clearance of $A\beta_{42}$ peptides are expected to modify the disease course in AD. Therefore, several $A\beta_{42}$ -lowering drugs like flurbiprofen had been tested in clinical trials, but most of them failed due to their low brain penetration. Here, flurbiprofen was embedded in polylactide (PLA) nanoparticles and its transport was examined in an *in vitro* BBB model. The embedding of flurbiprofen into the nanoparticles disguised its cytotoxic potential and enabled the administration of higher drug concentrations which resulted in a sufficient transport of the drug across an endothelial cell monolayer. These results demonstrate that non-permeable drugs can be transported efficiently via nanoparticles and that these nanotechnology-based strategies are a promising tool to generate novel therapeutic options for AD and other CNS diseases.

The focus of the second project was to investigate the impaired integrity of the BSCB in a mouse model for ALS. About 20% of all familial ALS cases are associated with missense mutations or small deletions in the gene that encodes Cu/Zn-superoxide dismutase 1 (SOD1). To date, the molecular mechanisms resulting in ALS are still unknown, but there is evidence that the disruption of the BSCB is one of the primary pathological events. In both familial and

sporadic ALS patients, loss of endothelial integrity and endothelial cell damage was observed, and studies with SOD1 transgenic mice demonstrated that the BSCB disruption was found prior to motor neuron degeneration and neurovascular inflammation. Thus, an *in vitro* model for ALS endothelial cells was generated which exhibited comparable integrity characteristics and tight junction (TJ) protein expression profiles as isolated primary endothelial cells of the BSCB of SOD1 transgenic mice. In this, an alteration of the β cat/AKT/FoxO1 pathway, which regulates the expression of the TJ protein claudin-5, could be observed. These data furthermore indicate that ALS is a neurovascular disease, and understanding of the primary events in ALS pathogenesis will hopefully provide ideas for the development of new therapeutic strategies.

Zusammenfassung

Die Blut-Hirn Schranke („*blood-brain barrier*“, BBB) und die Blut-Rückenmark Schranke („*blood-spinal cord barrier*“, BSCB) bilden eine physiologische Barriere zwischen dem Blut und dem zentralen Nervensystem (ZNS). Sie schützen das ZNS vor Pathogenen und toxischen Substanzen und sind für die ZNS Homöostase essentiell, weshalb Störungen oder der Verlust ihrer Integrität eine entscheidende Rolle bei neurodegenerativen Erkrankungen spielt. In dieser Arbeit wurden mit Hilfe von *in vitro* Modellen die Blut-ZNS Schranken anhand zweier Fallstudien für neurodegenerative Erkrankungen untersucht: Morbus Alzheimer („*Alzheimer's disease*“, AD) und Amyotrophe Lateral Sklerose (ALS). Im ersten Modell wurden mögliche Therapieansätze für AD mittels Nanotechnologie-basierender Strategien untersucht. Bei der Pathogenese spielt das Amyloid- β_{42} ($A\beta_{42}$) Peptid eine entscheidende Rolle und es wird angenommen, dass sowohl eine reduzierte Generierung als auch eine gesteigerte Eliminierung der $A\beta_{42}$ Peptide und Plaques den Krankheitsverlauf beeinflussen. Daher wurden bisher einige $A\beta_{42}$ -senkende Substanzen wie z.B. Flurbiprofen in klinischen Studien getestet; allerdings ohne Erfolg, da die meisten Substanzen nicht ins Gehirn gelangten. Hier wurden Polymilchsäure („*Polylactide*“, PLA) Nanopartikel mit Flurbiprofen beladen und ihr Transport in einem *in vitro* BBB Model getestet. Durch die Einbettung in Nanopartikel wurde die Zytotoxizität von Flurbiprofen aufgehoben, und dadurch konnten höhere Konzentrationen von Flurbiprofen eingesetzt werden, welches wiederum im effizienten Transport der Substanz über die Endothelzellen resultierte. Diese Ergebnisse zeigen, dass nicht-permeable Substanzen mit Hilfe von Nanopartikeln effizient transportiert werden können, und dass diese Nanotechnologie-basierenden Strategien vielversprechende und neue therapeutische Ansätze für AD und andere ZNS Erkrankungen liefern können.

Im zweiten Projekt wurde die beeinträchtigte Integrität der BSCB eines Mausmodells für ALS untersucht. 20% aller familiären ALS Fälle sind mit Punktmutationen oder Deletionen mit dem Gen assoziiert, das die Cu/Zn-Superoxid-Dismutase 1 (SOD1) kodiert. Die Ursache für ALS ist bis heute unbekannt, allerdings gibt es viele Hinweise, dass die funktionelle Störung der BSCB eins der primären pathologischen Ereignisse ist. Sowohl in familiären als auch sporadischen ALS Fällen konnten Schäden der Endothelzellen und ein Verlust deren Integrität festgestellt werden. Studien in einem transgenen Mausmodell mit humaner SOD1 zeigten, dass der Zusammenbruch der BSCB bereits vor der Degeneration der Motoneurone und der neurovaskulären Inflammation festgestellt werden kann. Daher wurde hier ein *in vitro* Modell der ALS Endothelzellen hergestellt, welches vergleichbare Eigenschaften bezüglich der Integrität und „*tight junction*“ (TJ) Expression wie isolierte primäre Endothelzellen der BSCB von transgenen SOD1 Mäusen zeigt. Weiterhin konnten Veränderungen im β cat/AKT/FoxO1 Signalweg, der die Expression des TJ Proteins Claudin-5 reguliert, festgestellt werden. Diese und auch die Ergebnisse anderer Gruppen weisen darauf hin, dass ALS eine neurovaskuläre Erkrankung ist. Das Verständnis der primären pathologischen Ereignisse führt in Zukunft hoffentlich dazu, dass neue therapeutische Ansätze für die Behandlung von ALS entwickelt werden können.

Danksagung

Contents

1	Background	1
1.1	Barriers of the central nervous system.....	1
1.1.1	The blood-brain barrier.....	3
1.1.2	The blood-spinal cord barrier.....	6
1.2	Project I: Nanoparticulate flurbiprofen reduces A β ₄₂ generation in an <i>in vitro</i> BBB model.....	7
1.3	Project II: Impaired integrity at the BSCB in a mouse model for ALS.....	11
2	Material & Methods	15
2.1	Reagents.....	15
2.1.1	Chemicals.....	15
2.1.2	Antibiotics.....	17
2.1.1	Kits.....	17
2.1.2	Antibodies.....	18
2.2	Laboratory hardware and equipment.....	18
2.3	Animals.....	19
2.4	Software.....	19
2.5	Cell biological methods.....	20
2.5.1	Cultivation of immortalized cells.....	21
2.5.2	Cryoconservation of immortalized cells.....	21
2.5.3	Revitalization of immortalized cells.....	21
2.5.4	Establishing stable cell lines via retroviral transfection.....	22
2.5.5	Isolation and cultivation of primary mouse endothelial cells.....	23
2.5.6	Impedance measurement.....	23
2.5.6.1	Influence of the TER by nanoparticles.....	24
2.5.6.2	Measurement of the integrity of endothelial cells.....	24
2.5.7	Measurement of cytotoxicity.....	25
2.5.8	Endocytosis of nanoparticles.....	26
2.5.9	Treatment with nanoparticles.....	26
2.5.9.1	Biological activity of the nanoparticles.....	26
2.5.9.2	Transport of nanoparticles across endothelial cells.....	27
2.5.9.3	Enzyme-linked immunosorbent assay (ELISA).....	28
2.5.10	Immunofluorescence.....	28

2.6	Protein biochemical methods	29
2.6.1	Cell lysis and protein extraction.....	29
2.6.2	SDS-Polyacrylamide gel electrophoresis (SDS-PAGE)	30
2.6.3	Western blot analysis.....	30
2.6.4	Cell surface biotinylation.....	31
2.7	Molecular biological methods.....	33
2.7.1	Cultivation of bacteria	33
2.7.1.1	Small scale liquid cultures.....	33
2.7.1.2	Large scale liquid cultures.....	33
2.7.2	Generation of chemically competent <i>E.coli</i>	34
2.7.3	Transformation of chemically competent <i>E.coli</i>	35
2.7.4	Isolation of plasmid DNA.....	35
2.7.5	Determination of DNA concentrations	36
2.7.6	Amplification of DNA by polymerase chain reaction (PCR).....	36
2.7.7	Agarose gel electrophoresis of DNA	37
2.7.8	Gel extraction of DNA fragments.....	38
2.7.9	Restriction enzyme digestion of DNA	38
2.7.10	Ligation of DNA fragments	39
2.7.11	Cloning of expression constructs	40
2.7.11.1	Subcloning of hSOD1 in pLBCX.....	40
2.7.12	Sequencing of DNA.....	41
3	Results & Discussion.....	43
3.1	Project I: Nanoparticulate flurbiprofen reduces A β ₄₂ generation in an <i>in vitro</i> BBB model.....	43
3.1.1	Preparation and characterization of the PLA-flurbiprofen nanoparticles.....	44
3.1.2	Flurbiprofen is released over time from the nanoparticles.....	46
3.1.3	PLA-flurbiprofen nanoparticles exhibit no cytotoxic potential.....	46
3.1.4	Cellular binding and uptake of the nanoparticles	48
3.1.5	The biological activity of nanoparticulate flurbiprofen is comparable to free flurbiprofen.....	50
3.1.6	Transport of flurbiprofen across endothelial cells	51
3.1.7	The protein corona of the PLA nanoparticles contains bioactive proteins.....	54
3.2	Project II: Impaired integrity of the BSCB in a mouse model for ALS	57
3.2.1	Expression of hSOD1 ^{G93A} lead to an impaired integrity in endothelial cells	58
3.2.2	The expression of TJ proteins is decreased in hSOD1 ^{G93A} endothelial cells	62

3.2.3	The β cat/AKT/FoxO1 pathway is altered in hSOD1 ^{G93A} cells.....	64
3.2.4	Endothelial cells expressing ALS-causing SOD1 variants G37R and G85R exhibit similar characteristics like the G93A variant	69
4	Conclusion & Outlook.....	75
5	References	81
6	Appendix.....	95
6.1	Supplementary material and methods.....	95
6.1.1	Nanoparticles preparation and characterization	95
6.1.1.1	Reagents and chemicals.....	95
6.1.1.2	Nanoparticle preparation.....	96
6.1.1.3	Freeze-drying of the samples	96
6.1.1.4	Nanoparticle characterization	96
6.1.1.5	Determination of flurbiprofen loading.....	96
6.1.1.6	<i>In vitro</i> release of flurbiprofen.....	97
6.1.2	Measurement of A β species by ELISA	97
6.1.3	Cellular binding of the nanoparticles	98
6.1.4	Nanoparticle plasma protein binding assay.....	99
	List of Acronyms.....	101
	List of Scientific Contributions	103
	Curriculum vitae.....	119

1

Background

Neurodegenerative disorders are characterized by the progressive loss of function or structure of the nervous system and are often associated with neuronal death. They include diseases such as Alzheimer's disease (AD) and other dementias, Parkinson's disease (PD), prion disorders, multiple sclerosis, amyotrophic lateral sclerosis (ALS), and there are presently no effective therapies for many of them. This thesis deals with two independent projects regarding the role of blood-CNS barriers in neurodegenerative disorders. The following chapter provides first background information about blood-CNS barriers in general and is then subdivided into the two different projects.

1.1 Barriers of the central nervous system

The nervous system is subdivided in the central nervous system (CNS), consisting of the brain and the spinal cord, and the peripheral nervous system (PNS), composed of specialized clusters of neurons and peripheral nerves. The PNS relays information to the CNS and executes motor commands generated in the brain and spinal cord. One special feature of the brain and the spinal cord is that they are protected by the skull and the vertebrae against external damages. The protection against internal toxic agents and pathogens is facilitated by blood-CNS barriers which separate the blood and the CNS. This includes the blood-brain barrier (BBB, described under 1.1.1), the blood

spinal-cord barrier (BSCB, described under 1.1.2) and the blood-cerebrospinal fluid (CSF) barrier. The history of the blood-CNS barrier already started in 1695 when Humphrey Ridley observed the specific protective nature of the brain in human subjects (Ridley, 1695; Liddelow, 2011). However, the concept of a barrier between the blood and the CNS is coined from Paul Ehrlich's observation in 1885: he observed that intravenously administered dyes stained all organs apart from the brain and spinal cord. He presumed that the different staining is due to the different binding affinities of different tissues to different dyes (Ehrlich, 1885). Later, Edwin Goldmann completed Ehrlich's dye experiment by injecting the dye trypan blue directly into the CSF of the brain (Figure 1.1). He observed that the brain and the spinal cord were stained but not the peripheral organs. After intravenous injection of trypan blue, Goldmann observed no staining in the CNS (Goldmann, 1909). This clearly demonstrated the existence of a compartmentalization of the CNS and the peripheral organs.

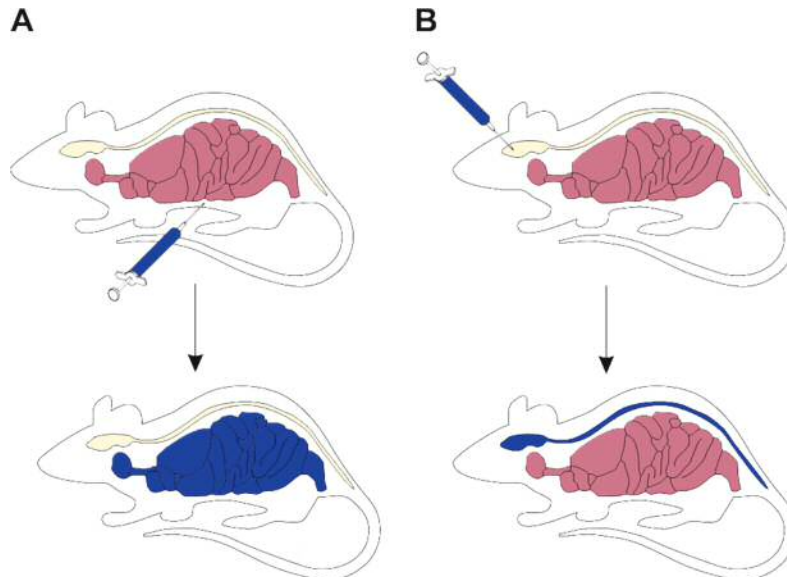


Figure 1.1: Illustration of the early experiments by Ehrlich and Goldmann. The injection of the dye trypan blue demonstrates the compartmentalization of the CNS and the peripheral organs. When trypan blue is injected intravenously (A), only the peripheral organs are stained and the dye does not penetrate the CNS. Vice versa, if trypan blue is injected into the CSF (B), the brain and the spinal cord are stained and not the peripheral organs (adapted from Liddelow, 2011).

In 1900, the existence of a physical barrier at the level of the cerebral vessels was first hypothesized by Max Lewandowsky who coined the term “bluthirnschranke” or “blood brain barrier” (Lewandowsky, 1900). Later, Reese and Karnovsky showed by electron microscope studies that the endothelial cells in the brain vasculature, and more precisely the junctions between these cells, form the BBB (Reese and Karnovsky, 1967).

1.1.1 The blood-brain barrier

The BBB separates the circulating blood from the brain, and it plays a crucial role in the regulation of the constancy of the internal environment of the brain. The cellular components of the BBB are specialized endothelial cells, which form tight junctions (TJ) to limit the paracellular space, astrocytes, whose endfeet surround the endothelial cells, pericytes between the astrocytes and endothelial cells, and the basement membrane (Palmer, 2010).

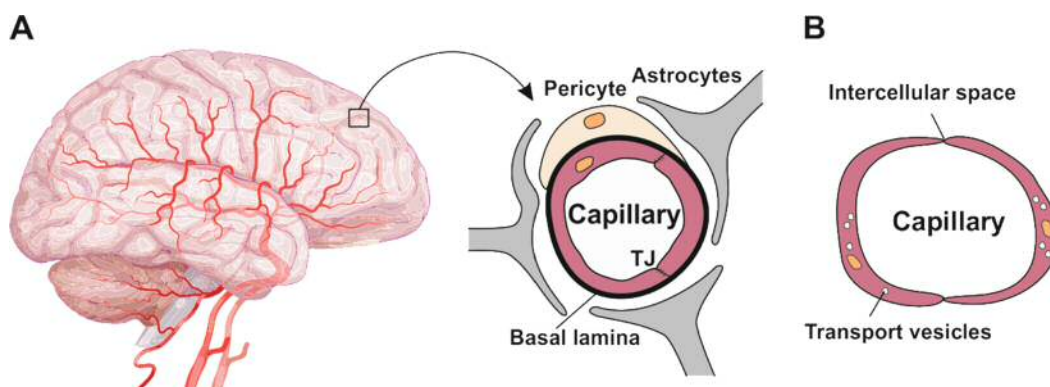


Figure 1.2: The vasculature of the brain and the BBB. The BBB separates the circulating blood from the brain and is comprised of endothelial cells, astrocytes and pericytes (A). The brain capillaries differ from those of the periphery (B): they lack fenestrae and pinocytotic vesicles, and the TJ between the endothelial cells close the intracellular space to limit the paracellular flux of hydrophilic molecules across the BBB (adapted from Deeken and Löscher, 2007).

Anatomically, the endothelial cells of the BBB are distinguished from those of the periphery by increased mitochondrial content, a lack of fenestrations, minimal pinocytotic activity, and the presence of TJ (Figure 1.2) (Hawkins and Davis, 2005).

The TJ is an intricate complex of transmembrane and cytoplasmic proteins linked to the actin cytoskeleton (Figure 1.3). These TJs consist of three transmembrane proteins: claudin, occludin and junctional adhesion molecule (Huber *et al.*, 2001). Claudins form dimers and bind homotypically to claudins on adjacent endothelial cells to form the primary seal of the TJ (Furuse *et al.*, 1999). Claudins comprise a multigene family with currently 27 members. (Mineta *et al.*, 2011). The family members exhibited distinct tissue expression patterns whereby claudin-1, claudin-3, claudin-5 and claudin-12 were detected at the BBB (Liebner *et al.*, 2000; Wolburg *et al.*, 2003; Morita *et al.*, 1999; Nitta *et al.*, 2003). Newborn claudin-5-deficient mice die within one day after birth although the vascularization and the brain morphology are not impaired. Nitta and colleagues observed that the BBB was loosened in a size-selective manner indicating a crucial role for claudin-5 for the formation of TJ (Nitta *et al.*, 2003).

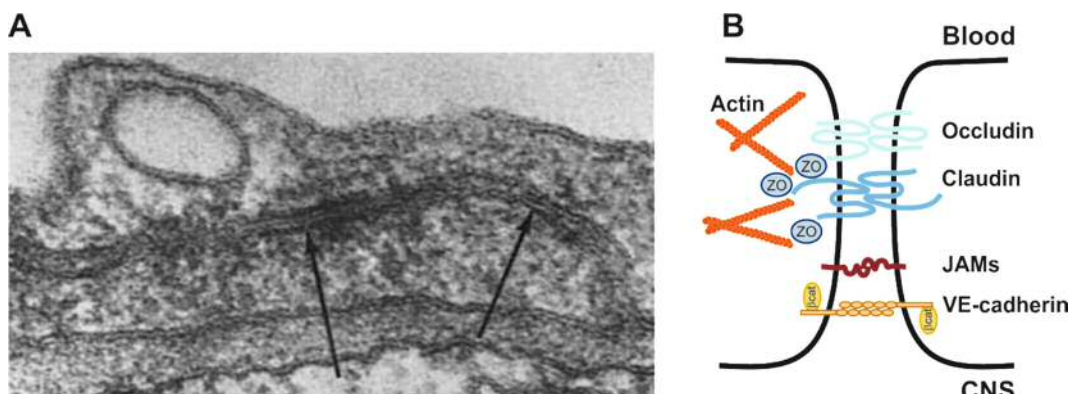


Figure 1.3: Structural and molecular characteristics of the TJ. TJ between the endothelial cells of the BBB restrict the paracellular diffusion of water-soluble substances from the blood to the brain. **(A)** Electron microscope pictures of the TJs (arrows) between the endothelial cells (adapted from Reese and Karnovsky, 1967). **(B)** The TJs are composed of an intricate combination of transmembrane and cytoplasmic proteins linked to an actin-based cytoskeleton that allow the TJ to form a seal while remaining capable of rapid modulation and regulation (adapted from Hawkins and David, 2005).

Occludin was the first tight junctional transmembrane protein discovered (Furuse *et al.*, 1993), but its functional role is still unclear. The TJ of occludin-deficient mice are not affected regarding to TJ formation, strand morphology or barrier function (Saitou *et al.*, 2000; Schulzke *et al.*, 2005). Recent data demonstrated that occludin has a regulatory function and that its phosphorylation state regulates TJ permeability (Hirase *et al.*, 2001; Feldman

et al., 2005). Junctional adhesion molecule (JAM)-1 is a member of the IgG superfamily and is believed to mediate the early attachment of adjacent cell membranes via hemophilic interactions (Dejana *et al.*, 2000).

The TJ also consists of several accessory proteins that are necessary for structural support. Zonula occludens proteins (ZO1, ZO2 and ZO3) belong to a family known as membrane-associated guanylate kinase-like proteins (MAGUKs) and serve as recognition proteins for TJ replacement and as a support structure for signal transduction proteins (Haskins *et al.*, 1998). The cytoskeletal protein actin has known binding sites on all ZO proteins, and for instance, the C-terminus of occludin is linked to the actin cytoskeleton via ZO1 (Itoh *et al.*, 1999). This interaction is likely critical to the stability and function of the TJ, because dissociation of ZO1 or the structural organization of actin is associated with tight junctional integrity (Stevenson and Begg, 1994; Fischer *et al.*, 2002).

Other junctional complexes that are present in the interendothelial space are adherens junctions (AJ). AJ, or more precisely their major component vascular endothelial (VE)-cadherin, are required for correct vascular development in the embryo (Carmeliet *et al.*, 1999). The cytoplasmic tail of VE-cadherin binds to β -catenin (β cat) and other proteins, which in turn binds to the actin cytoskeleton, stabilizing the AJ complex (Yap *et al.*, 1997).

Although the movement of most molecules between the blood and the brain is severely constrained by the junctional complexes, the movement of essential nutrients such as glucose and amino acids has to be permitted. Therefore, the brain endothelial cells express a large number of specialized transporters (Qutub and Hunt, 2005; Hawkins *et al.*, 2006; Bernacki *et al.*, 2008). Larger essential molecules such as insulin, leptin and iron transferrin are transported into the CNS by receptor-mediated transcytosis (Pardridge, 2007). Furthermore, they express a large number of transporters, the ATP-binding cassette transporters, which remove xenobiotics and drugs from the CNS (Ueno, 2007; Bernacki *et al.*, 2008; Aszalos, 2008; Dauchy *et al.*, 2008). Thus,

the BBB is a natural defense which restricts the transport of many therapeutically important drugs from the blood into the brain including Alzheimer drugs, anticancer drugs, antibiotics, and a wide variety of CNS-active drugs, but is otherwise crucial for the nutrient supply and homeostasis of the brain (Madara, 1988; Abbott *et al.*, 1999; Abbott *et al.*, 2006).

1.1.2 The blood-spinal cord barrier

The BSCB is the functional equivalent to the BBB that plays a similar protective and regulatory role for the spinal cord parenchyma (Bartanusz *et al.*, 2011). Like the BBB, the BSCB is comprised of endothelial cells, which form TJ, astrocytes, pericytes and a basement membrane (Figure 1.4). However, there exist morphological and functional differences between the two barriers.

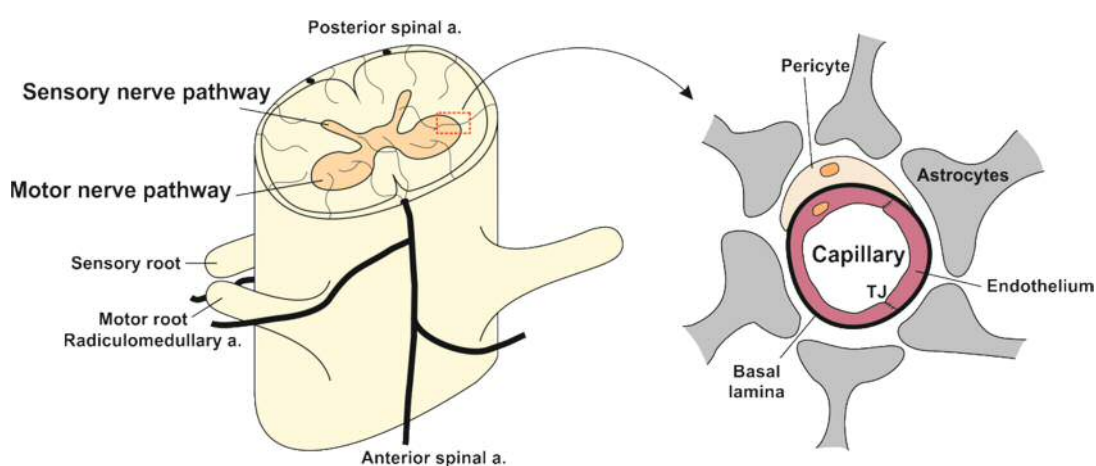


Figure 1.4: Schematic illustration of the BSCB. The BSCB is the functional equivalent of the BBB. It is comprised of endothelial cells, astrocytes and pericytes and has a protective and regulatory role for the spinal cord parenchyma (adapted from Bartanusz *et al.*, 2011).

Several studies have shown that the rodent BSCB has an increased permeability to mannitol and inulin (Daniel *et al.*, 1985; Prockop *et al.*, 1995), interferons (Pan *et al.*, 1997b), albumin, sucrose and tumor necrosis factor α (Pan *et al.*, 1997a). Furthermore, a specifically decreased expression of ZO1 and occludin has been reported whereby the expression of claudin-1 and claudin-5 remained unchanged. The expression of VE-cadherin and β cat were

investigated as well, since the tight junction assembly is dependent on the AJ proteins. Both proteins showed a significant reduction in spinal cord microvessels and cultured spinal cord endothelial cells. (Ge and Pachter, 2006). Thus, differences in the ultrastructure of the BBB and the BSCB endothelial exist, which in turn may have an impact on its physiology and pathophysiology.

1.2 Project I: Nanoparticulate flurbiprofen reduces A β ₄₂ generation in an *in vitro* BBB model

AD is the most common neurodegenerative disorder in the elderly and is currently affecting more than 35 million people worldwide (Querfurth and LaFerla, 2010). AD is named after the German psychiatrist Alois Alzheimer, who described the symptoms and the changes in the brain of his patient Auguste Deter. He observed deposits of insoluble proteins in the brain of his patient and associated their presence with the symptoms of the disease (Alzheimer, 1906). To date, the treatment of AD is only symptomatic and there is no cure for the disease, and with increased life expectancy the number of patients will increase to more than 140 million AD patients by 2050 (Pahnke *et al.*, 2009; Alzheimer's, 2012).

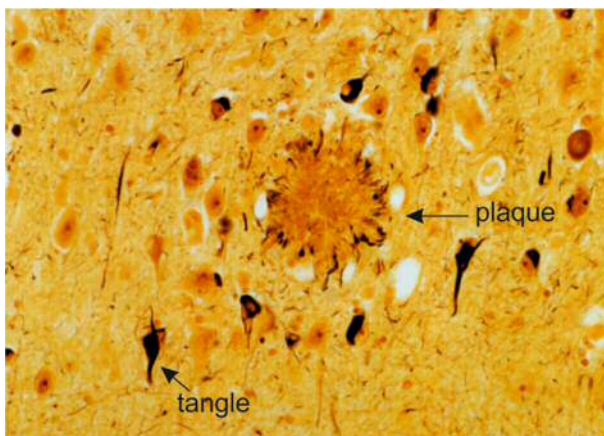


Figure 1.5: The histopathological characteristics in an AD brain. AD is characterized by the presence of intracellular deposits of the hyperphosphorylated tau protein in so-called neurofibrillary tangles and extracellular deposits of the A β peptide in so-called senile plaques. These plaques are furthermore surrounded by dystrophic dendrites and axons, activated microglia, and reactive astrocytes (A β : Amyloid- β ; adapted from Selkoe, 1991).

The pathological characteristics of AD are neuronal and synaptic loss, neurofibrillary tangle formation and extracellular deposits of amyloid- β (A β)

peptides in susceptible brain regions (Figure 1.5) which result in learning and memory impairment (Selkoe, 1991; LaFerla and Oddo, 2005). A β is generated through the sequential processing of the amyloid precursor protein (APP) and occurs in various isoforms between 36 and 46 amino acids in length with A β_{40} and A β_{42} being the most prevalent variants (Burdick *et al.*, 1992; Haass and Selkoe, 1993; Kuo *et al.*, 1996; Pietrzik and Behl, 2005). APP can be cleaved first by α -secretase or β -secretase representing the so-called non-amyloidogenic or amyloidogenic pathway, respectively (Figure 1.6).

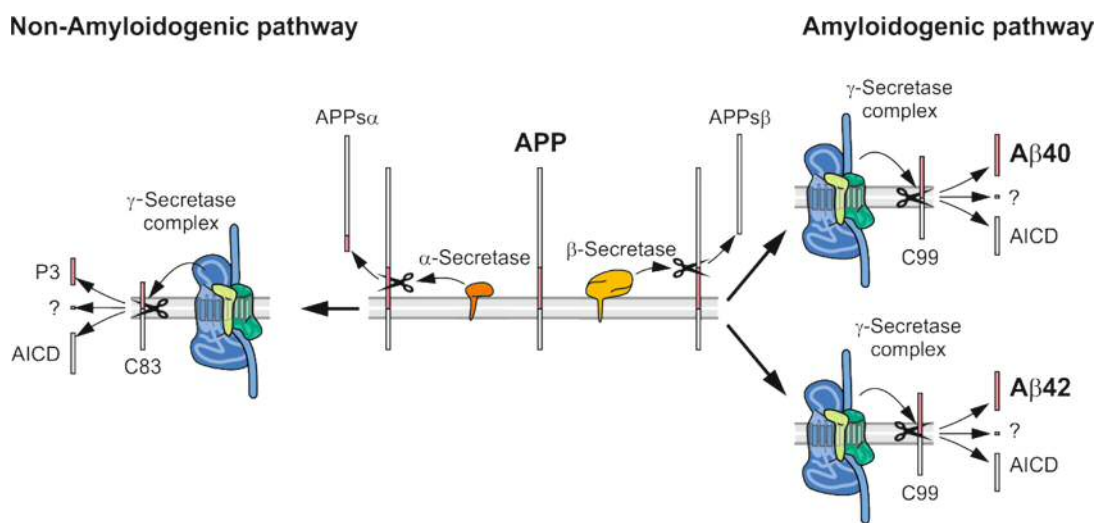


Figure 1.6: The physiological processing of APP. Schematic illustration of the processing of APP, which can be processed by two different pathways: In the non-amyloidogenic pathway, APP is cleaved first by α -secretase producing APPs α and a C-terminal fragment C83 peptide. C83 is cleaved by γ -secretase as well and this cleavage produces the p3 peptide. In the amyloidogenic pathway, APP is cleaved first by β -secretase producing APPs β and a C-terminal fragment C99 peptide. This peptide is cleaved afterwards by γ -secretase producing A β peptides with variation in length, whereby A β_{40} and A β_{42} are the most prominent (A β : Amyloid- β ; AICD: APP intracellular domain; APP: Amyloid precursor protein; CTF: C-terminal fragment; APPs: Soluble APP; adapted from Pietrzik and Behl, 2005).

In the non-amyloidogenic pathway, APP is first cleaved by the α -secretase. This cleavage generates the soluble APPs α peptide and the C-terminal fragment C83 peptide which remains in the cell membrane. This peptide is cleaved afterwards by the γ -secretase complex generating a soluble p3 peptide and the remaining APP intracellular domain (AICD) peptide. In the amyloidogenic pathway, APP is cleaved by the β -secretase generating the soluble APPs β and

the remaining C-terminal fragment C99 peptide. A β peptides are produced after the cleavage of C99 by γ -secretase complex (Haass *et al.*, 1993; Haass and Selkoe, 1993). According to the amyloid hypothesis (Selkoe, 1991; Hardy and Allsop, 1991; Hardy and Higgins, 1992), which states that the accumulation or increased generation of A β_{42} peptides in the brain is one of the primary events in the pathogenesis of AD (Selkoe, 2001; Golde, 2003; McGowan *et al.*, 2005; Wyss-Coray, 2006), it is thought that reduced generation or enhanced clearance of A β_{42} peptides and plaques would modify the disease course of AD (Hardy, 2009). Thus, there have been many efforts for the development of disease-modifying therapies focused on suppressing A β production by small molecule inhibitors of β - or γ -secretase. But none of the approaches has yielded clinically viable therapies since all of them were confronted with serious technical challenges and safety concerns (Golde, 2006; Hull *et al.*, 2006). The most obstacle concerns the inhibition of the γ -secretase itself, because it has more than 50 substrates with critical functions like cell signaling (*e.g.*, the Notch receptor), cell adhesion, and apoptosis (Haapasalo and Kovacs, 2011). This was demonstrated in one of the latest clinical trial of the γ -secretase inhibitor semagacestat, which was developed by Eli Lilly. The trial was terminated before completion, because semagacestat did not improve the cognitive status of the probands, and it was furthermore associated with more adverse events, including skin cancers and infections (Doody *et al.*, 2013). Nevertheless, there is still a promising approach to reduce A β_{42} levels: the application of so-called γ -secretase modulators (GSM). In 2001, Weggen and colleagues showed that the treatment of Chinese Hamster Ovary (CHO) cells with some nonsteroidal anti-inflammatory drugs (NSAIDs) such as indomethacin, ibuprofen and flurbiprofen specifically decreased the secretion of the A β_{42} peptides. This was accompanied by an increase of shorter, nontoxic A β isoforms (*e.g.*, A β_{37} and A β_{38}), indicating that NSAIDs subtly altered γ -secretase activity without significant impairment of other APP processing pathways or Notch signaling (Weggen *et al.*, 2001). NSAIDs exert their principal therapeutic effects, reducing fever, pain and inflammation by

blocking the cyclooxygenase (COX)-mediated synthesis of inflammatory prostaglandins (Warner and Mitchell, 2004). However, some NSAIDs were shown to selectively lower A β ₄₂ production *in vitro* and in mouse models of AD independently of COX activity (Weggen *et al.*, 2001; Eriksen *et al.*, 2003). Furthermore, the so-called Rotterdam study showed evidence that the long-term use of NSAIDs may protect against AD (in t' Veld *et al.*, 2001). The Rotterdam study is a prospective, population-based study of 6989 subjects with 55 years of age or older who were free of dementia at base line. During an average follow-up period of 6.8 years, AD was only developed in 293 subjects. The relative risk of AD was 0.95 in subjects with short-term use of NSAIDs, and 0.20 in those with long-term use. These results strongly suggest that the long-term use of NSAIDs has a beneficial effect on the risk of AD. However, the clinical development of the A β ₄₂ lowering agent tarenflurbil, the COX-inactive *R*-enantiomer of the NSAID flurbiprofen, has been stopped after failure in a Phase III clinical trial (Green *et al.*, 2009). The results of this multicenter, randomized, double-blind, placebo-controlled trial did not show any slowing of cognitive decline after 18 months of treatment with tarenflurbil. The reasons for the clinical failure of tarenflurbil are unknown, but low penetration across the BBB and, consequently, insufficient target engagement in the brain may be likely explanations (Green *et al.*, 2009). Since the BBB restricts the transport of CNS-active drugs, a number of different strategies have been devised to overcome the BBB such as osmotic opening of the TJ, the direct surgical administration of drugs into the brain, or the development of drug carriers such as liposomes or nanoparticles (Brightman *et al.*, 1973; Rapoport and Robinson, 1986; Pardridge, 2007; Craparo *et al.*, 2011; Sahni *et al.*, 2011). However, the most notable and promising progression has been achieved by the use of nanotechnology. Liposomes as well as solid lipid nanoparticles or different polymeric nanoparticles have been successfully used for the transport of drugs across the BBB and into the brain (Silva, 2010). Compared to free drug molecules or pro-drugs, the usage of nanoparticles possesses advantages such as their high drug-loading capacity. Furthermore, the drugs

are protected against chemical or enzymatic degradation and nanoparticles can be actively targeted to a tissue via surface modifications of the nanoparticles (Tosi *et al.*, 2008). To date, these drug carriers have been studied intensively for neurological disorders, cancer and other diseases and some of them are in different trial phases or even commercially available (Kumari *et al.*, 2010; Re *et al.*, 2012). In this project, polymeric nanoparticles were investigated if they can serve as drug carriers for nonpermeable drugs in an *in vitro* BBB model (chapter 3.1).

1.3 Project II: Impaired integrity at the BSCB in a mouse model for ALS

ALS is a severe progressive motor neuron disease that affects both lower motor neurons in the brainstem and spinal cord and the upper motor neurons in the motor cortex. The degeneration of these neurons leads to muscle atrophy, paralysis, fasciculation, and spasticity (Mulder, 1982).

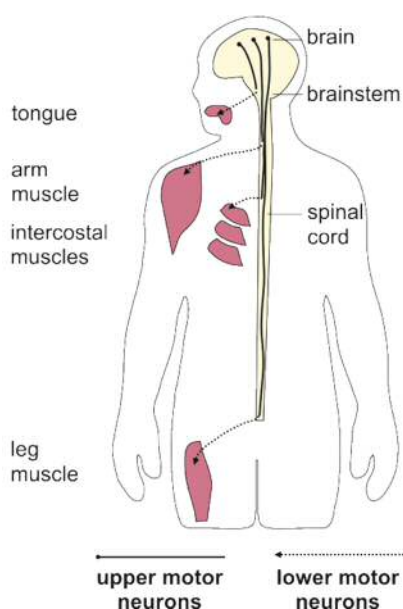


Figure 1.7: Schematic illustration of upper and lower motor neurons affected in ALS. In ALS, both lower motor neurons in the brainstem and spinal cord, and the upper motor neurons in the motor cortex are affected. The most typical features of this progressive lethal disease is the degeneration of motor neurons, muscle atrophy and weakness, speech and swallowing disabilities, progressive paralysis and death caused by respiratory failure (adapted from Mulder, 1982).

The incidence and prevalence of ALS are 1-2 and 4-6 in 100.000 in a population, with a lifetime ALS risk of 1/600 to 1/1000 (Mitsumoto *et al.*, 1998; McGuire *et al.*, 1996; Boillee *et al.*, 2006). Most patients with ALS die

within 3 to 5 years after symptom onset which is caused by respiratory failure, but the clinical disease duration is very variable and ranges from death within months after onset to more than 20 years after onset (Robberecht and Philips, 2013). To date, there exist no therapeutical treatment of the disease, and the only treatments include the single drug approved for ALS, riluzole (which only slightly prolongs survival), respiratory support and the application of feeding tubes. Approximately 90% of all patients have sporadic ALS which is clinically indistinguishable to patients with a familial history (FALS). The first causative mutations for familial forms of ALS were found in 1993 within the *superoxide dismutase 1 (SOD1)* gene (Rosen *et al.*, 1993). The gene encodes a 153 amino acid metalloenzyme, which is ubiquitous expressed and highly conserved across species (Fridovich, 1995). SOD1 binds copper and zinc, and forms a functional homodimer that converts the superoxide anion (a by-product of the oxidative phosphorylation in the mitochondria) to hydrogen peroxide and oxygen by the cyclical reduction and oxidation (dismutation) of the copper atom (Figure 1.8) (Cleveland and Liu, 2000; Barber *et al.*, 2006).

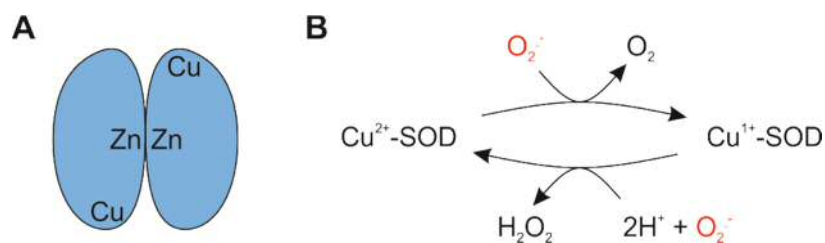


Figure 1.8: SOD1 catalyzes the removal of superoxide radicals in a dismutation reaction. The functional SOD1 enzyme consists of two monomers (A), whereby each subunit binds one copper and one zinc atom. (B) Through cyclical reduction and oxidation of copper, SOD1 converts the superoxide anion to hydrogen peroxide and oxygen (adapted from Barber *et al.*, 2006 and Cleveland and Liu, 2000).

Mutations in the *SOD1* gene underlie about 20% of all FALS cases and to date, more than 150 mutations have been reported to be pathogenic. The current reported mutations are illustrated in Figure 1.9, whereby three of these missense mutations are highlighted because they were studied in this project.

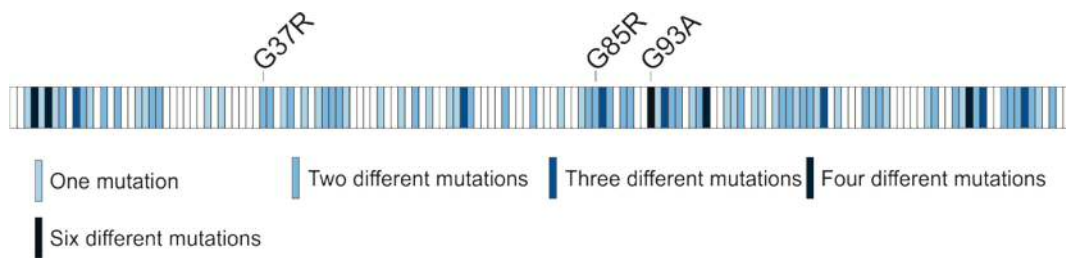


Figure 1.9: Schematic illustration of human SOD1 and the reported pathogenic mutations. Mutations in the *SOD1* gene underlie about 20% of familial ALS cases. To date, more than 150 different mutations have been reported to be pathogenic. The data are taken from the ALS online database (ALSoD, <http://alsod.iop.kcl.ac.uk>, October 2013) (adapted from Robberecht and Philips, 2013).

Transgenic mice carrying mutated human SOD1 genes have been generated to elucidate SOD1 mediated motor neuron degeneration. The first generated mouse model carries the hSOD1^{G93A} mutation (Gurney *et al.*, 1994). To date, more than 12 different published human mutant SOD1 transgenic strains exist and all develop a progressive adult-onset motor phenotype (Joyce *et al.*, 2011). In post-mortem examinations of ALS patients and in the rodent models of the disease a loss of neurons in the brainstem and in the ventral horn of the spinal cord were observed, and this cell loss was accompanied by astrocytic activation and microglia proliferation. In addition to these neuroinflammatory reactions, inclusions of aggregated proteins could be detected in the remaining motor neurons (Robberecht and Philips, 2013). Thus, numerous hypothesis for the pathogenesis of ALS have been proposed which include glutamate toxicity, oxidative stress, mitochondrial dysfunction, autoimmune mechanisms, protein aggregation, SOD1 accumulation, neuroinflammation, and neuronal death (Wong *et al.*, 1998; Cleveland, 1999; Philips and Robberecht, 2011). Recently, a new possible pathogenic mechanism in ALS has been proposed concerning the impairment of the BSCB (Garbuzova-Davis *et al.*, 2011). First studies regarding the role of the BSCB in ALS focused on its functional competence in hSOD1^{G93A} mice at different stages of disease (Garbuzova-Davis *et al.*, 2007a; Garbuzova-Davis *et al.*, 2007b). Ultrastructural changes at the BSCB and endothelial cell degeneration could be observed, as well as the leakage of the BSCB to Evans Blue dye throughout the disease's progression. In an important study of Zhong and colleagues the authors showed that the BSCB is disrupted in different

transgenic mice (hSOD1^{G37R}, hSOD1^{G85R} and hSOD1^{G93A}) by the reduction of the TJ proteins ZO-1, occludin and claudin-5 (Zhong *et al.*, 2008). Furthermore, they observed that this early breakdown occurred before inflammatory changes and motor neuron degeneration and suggested that the disease initiator may be this barrier damage. Analyzes of post-mortem tissues of ALS patients (both SALS and FALS) also indicated the evidence of BSCB impairment in the disease (Donnenfeld *et al.*, 1984; Engelhardt and Appel, 1990; Henkel *et al.*, 2009; Garbuzova-Davis *et al.*, 2012). However, it still has to be elucidated if the barrier damage is an initial disease factor of the disease, or if the impairment is just an element in the ALS pathogenesis. In this project, an *in vitro* model of the BSCB in ALS was generated and the molecular mechanisms leading to the impaired integrity were analyzed (chapter 3.2).

2

Material & Methods

In this chapter, only the experimental techniques and methods which were carried out in person are presented and explained. For the experimental techniques and methods which were performed in cooperation, the reader is encouraged to consult the supplementary material and methods in chapter 6.

2.1 Reagents

2.1.1 Chemicals

30% Acrylamide 37.5 : 1 Bis-Acrylamide	National Diagnostics, Atlanta, GA, USA
Agar	Carl Roth, Karlsruhe, Germany
Ammoniumpersulfate (APS)	Sigma-Aldrich, Steinheim, Germany
alamarBlue®	Invitrogen, Karlsruhe, Germany
Bacto-tryptophane	BD, Heidelberg, Germany
Bis-Tris	Carl Roth, Karlsruhe, Germany
Basic fibroblast growth factor (bFGF)	R&D Systems, Wiesbaden, Germany
Bovine Serum Albumin (BSA)	Sigma-Aldrich, Steinheim, Germany
Calcium chloride (CaCl ₂)	Merck, Darmstadt, Germany
Chloroquine	Sigma-Aldrich, Steinheim, Germany
Collagen IV	Sigma-Aldrich, Steinheim, Germany

Material & Methods

Collagenase CLS2	Worthington, Lakewood, NJ
Collagenase-Dispase	Roche, Mannheim, Germany
DNaseI	Sigma, Schnelldorf, Germany
Desoxynucleotide-tri-phosphate (dNTP)	NEB, Frankfurt, Germany
DRAQ5™	Biostatus Limited, Leicestershire, UK
Dry-milk (fat-free)	VONS, USA
Dithiothreitol (DTT)	Sigma-Aldrich, Steinheim, Germany
Dulbecco's modified Eagle medium (DMEM)	Invitrogen, Karlsruhe, Germany
Ethanol	Carl Roth, Karlsruhe, Germany
Ethidiumbromide (EtBr)	Sigma-Aldrich, Steinheim, Germany
Ethylendiaminetetraacetic acid (EDTA)	Carl Roth, Karlsruhe, Germany
Fetal Calf Serum (FCS)	Invitrogen, Karlsruhe, Germany
Fibronectin	Sigma-Aldrich, Steinheim, Germany
Glacial Acid	Carl Roth, Karlsruhe, Germany
L-Glutamine	Invitrogen, Karlsruhe, Germany
Glycerol	Carl Roth, Karlsruhe, Germany
Glycine	Merck, Darmstadt, Germany
Goat Serum	Invitrogen, Karlsruhe, Germany
Heparin	Sigma-Aldrich, Steinheim, Germany
HEPES	Invitrogen, Karlsruhe, Germany
Immobilon™ Western HRP Substrate Reagents	Millipore, Schwalbach, Germany
Inulin-carboxyl, [carboxyl- ¹⁴ C]	Perkin Elmer, MA, USA
Isopropanol	Carl Roth, Karlsruhe, Germany
Lipofectamine® 2000	Invitrogen, Karlsruhe, Germany
Methanol	Carl Roth, Karlsruhe, Germany
MOPS	Carl Roth, Karlsruhe, Germany
NeutrAvidin Agarose resin	Pierce Chemicals, Rockford, IL, USA
Nitrocellulose membrane	Hartenstein, Würzburg
Nonidet P40	Roche, Mannheim, Germany
Paraformaldehyde	Sigma-Aldrich, Steinheim, Germany
Percoll	GE Healthcare, Munich, Germany
Plasma-derived bovine serum (PDS)	First Link, Birmingham, UK
Polybrene	Sigma-Aldrich, Steinheim, Germany
Poly lactide (PLA)	Sigma-Aldrich, Steinheim, Germany
Ponceau S	Sigma-Aldrich, Steinheim, Germany
Prolong® Gold antifade reagent	Invitrogen, Darmstadt, Germany
Protease inhibitor cocktail tablets, EDTA-free	Roche, Mannheim, Germany

RotiLoad® (4 x Protein loading buffer)	Carl Roth, Karlsruhe, Germany
Rubidium chloride (RbCl)	AppliChem, Darmstadt, Germany
Sodiumazide (NaN ₃)	Carl Roth, Karlsruhe, Germany
Sodiumchloride (NaCl)	Carl Roth, Karlsruhe, Germany
Sodium dodecyl sulfate (SDS)	BioRad, Munich, Germany
Sodiumpyruvate	Invitrogen, Karlsruhe, Germany
Sucrose	Sigma-Aldrich, Steinheim, Germany
Sulfo-NHS-LC-LC-biotin	Pierce Chemicals, Rockford, IL, USA
TEMED (N,N,N+,N+-Tetramethylendiamine)	BioRad, Munich, Germany
Tris-acetate	Carl Roth, Karlsruhe, Germany
Tris-base (Tris-OH)	Carl Roth, Karlsruhe, Germany
Tris-hydrochloride (Tris-HCl)	Carl Roth, Karlsruhe, Germany
Triton-X 100	Sigma-Aldrich, Steinheim, Germany
Trypsin/EDTA	Invitrogen, Karlsruhe, Germany
Tween-20	Carl Roth, Karlsruhe, Germany
Yeast Extract	Carl Roth, Karlsruhe, Germany

2.1.2 Antibiotics

Ampicillin	Sigma-Aldrich, Steinheim, Germany
Blasticidin	Sigma-Aldrich, Steinheim, Germany
Geneticin	Sigma-Aldrich, Steinheim, Germany
Puromycin	Alexis, Loerrach, Germany
Penicillin/Streptomycin (Pen/Strep)	Invitrogen, Karlsruhe, Germany

2.1.1 Kits

BCA™ Protein Assay Kit	Pierce, Bonn, Germany
GenElute™ Mammalian Genomic DNA Miniprep Kit	Sigma-Aldrich, Schnellendorf, Germany
High Pure Plasmid Isolation Kit	Roche, Mannheim, Germany
NucleoBond® Xtra Midi Kit	Macherey Nagel, Düren, Germany
“NucleoSpin® Extract II”-PCR Clean-up and Gel Extraction Kit	Macherey Nagel, Düren, Germany

2.1.2 Antibodies

Table 2.1: Primary antibodies. WB: Western blot, ICC: Immunocytochemistry.

Antigen	Species	Type	Dilution	Reference/Supplier
β -Actin	rabbit	polyclonal	1:5000 (WB)	Sigma-Aldrich
AKT	rabbit	polyclonal	1:1000 (WB)	Cell Signaling
p[S473]AKT	mouse	monoclonal	1:1000 (WB)	Cell Signaling
β cat	mouse	monoclonal	1:1000 (WB)	BD Biosciences
p[S675] β cat	rabbit	monoclonal	1:2000 (WB)	Cell Signaling
<i>c-myc</i>	mouse	monoclonal	1:500 (WB)	Hybridoma cellline
Claudin-5	rabbit	polyclonal	1:1000 (WB) 1:100 (ICC)	Zymed, Invitrogen
FoxO1	rabbit	monoclonal	1:1000 (WB)	Cell Signaling
p[S256]FoxO1	rabbit	polyclonal	1:1000 (WB)	Cell Signaling
Occludin	mouse	monoclonal	1:1000 (WB)	Zymed, Invitrogen
Occludin	rabbit	monoclonal	1:500 (WB)	Santa Cruz
SOD1	rabbit	polyclonal	1:500 (WB)	Epitomics
α -Tubulin	mouse	monoclonal	1:5000 (WB)	Sigma-Aldrich

Table 2.2: Secondary antibodies.

Antigen	Conjugate	Dilution	Reference/Supplier
Goat-anti-rabbit IgG	HRP	1:5000 (WB)	Sigma-Aldrich
Donkey-anti-mouse IgG	HRP	1:5000 (WB)	Dianova
Goat-anti-Rabbit IgG	Alexa-Fluor 546	1:1000 (ICC)	Invitrogen

2.2 Laboratory hardware and equipment

Anthos plate reader 2010	Anthos Labtec, Salzburg, Austria
Cell culture dishes (6cm, 10 cm)	TPP, Trasadingen, Switzerland
CellZscope®	nanoAnalytics, Münster, Germany
Chamber slides	Nunc, Langenselbold, Germany
Coverslips	Marienfeld, Lauda-Königshofen, Germany
Cryovials	Nunc
LAS-3000mini	Fujifilm, Duesseldorf, Germany
LSM 710	Zeiss, Jena, Germany

Mini Trans-Blot® Cell	Bio-Rad
SmartSpec 3000	Bio-Rad
Thermoshaker	
Tri-Carb 2800 TR Liquid Scintillation Analyzer,	PerkinElmer MA, USA
Wallac 1420 Multilabel Counter	PerkinElmer MA, USA
Well plates (6, 24, 96)	Greiner, Frickenhausen, Germany

2.3 Animals

hSOD1^{G93A}-transgenic mice (strain B6.Cg-Tg(SOD1-G93A)^{dl1Gur/J}, Jackson Laboratories, Bar Harbor, Maine, USA) were kept in the local animal facility under a 12 h light cycle with food and drinking water ad libitum. Mice were housed, anesthetized and sacrificed according to the European and German guidelines for the care and use of laboratory animals. The animals were kindly provided by Albrecht Clement and Christian Behl (Institute of Pathobiochemistry, University Medical Center of the Johannes Gutenberg University Mainz, Mainz, Germany).

2.4 Software

Adobe Photoshop CS3
Chromas 2.33
CorelDRAW X6
EndNote X5
GraphPad Prism 4
ImageJ 1.44, NIH
Microsoft Office 2010
SECentral 7.0/ Clonemanager
ZEN 2008

2.5 Cell biological methods

In general, cell culture routine was performed in S1 and S2 qualified laboratories under sterile working conditions. The equipment including culture dishes, pipettes, filter tips, 15-50 ml tubes, 1.5-2 ml tubes, syringes and sterile filters were single-use plastic items and cell culture qualified. Media and reagents were warmed to 37 °C in a water bath before use. Cells were cultured at 37 °C and 5% CO₂ and the cell morphology and proliferation was checked every day.

Table 2.3: Immortalized cell lines and the respective culture media.

Cell line	Cell type	Reference/Supplier	Culture Media
bEnd.3	Mouse brain endothelium	(Montesano <i>et al.</i> , 1990)	DMEM high glucose, 10% FCS, 1% Pen/Strep
bEnd.3 hSOD1 ^{WT} myc	Mouse brain endothelium		DMEM high glucose, 10% FCS, 1% Pen/Strep, 5 µg/ml blasticidin
bEnd.3 hSOD1 ^{G37R} myc	Mouse brain endothelium		DMEM high glucose, 10% FCS, 1% Pen/Strep, 5 µg/ml blasticidin
bEnd.3 hSOD1 ^{G85R} myc	Mouse brain endothelium		DMEM high glucose, 10% FCS, 1% Pen/Strep, 5 µg/ml blasticidin
bEnd.3 hSOD1 ^{G93A} myc	Mouse brain endothelium		DMEM high glucose, 10% FCS, 1% Pen/Strep, 5 µg/ml blasticidin
CHO 7WD10	Chinese Hamster Ovary	(Koo and Squazzo, 1994)	DMEM high glucose, 10% FCS, 1 mM sodium pyruvate, 1% Pen/Strep, 400 µg/ml geneticin
GP2-293	Human Embryonic Kidney	Clontech, France	DMEM high glucose, 10% FCS, 1 mM sodium pyruvate, 1% Pen/Strep

2.5.1 Cultivation of immortalized cells

Immortalized cell lines were cultured in 10-cm culture dishes, and before confluence, cells were passaged using 0.05% Trypsin-EDTA. Therefore, cells were washed with 1 x PBS and trypsinized for 1-5 min at 37 °C. Detached cells were resuspended using fresh growth medium until a single cell suspension was obtained. Aliquots of the suspension were plated in culture dishes containing 10 ml fresh medium and cells were equally distributed by gently shaking.

For all experiments bEnd.3 were seeded at a density of 5×10^4 cells per cm^2 and the experiments were performed after 3 days when cells were post-confluent. 7WD10 were seeded at a density of 3×10^4 cells per cm^2 and after 24 h, cells were either treated (2.5.9.1) or co-cultured with the bEnd.3 in the *in vitro* BBB model (2.5.9.2).

2.5.2 Cryoconservation of immortalized cells

For the long term storage cells were washed and trypsinized as described in 2.5.1. The cell suspension was transferred to 15 ml tubes, centrifuged at 1200 rpm for 4 min, and cells were resuspended in growth medium containing 10% DMSO. Aliquots were transferred into cryovials and stored overnight at -80 °C. The next day, cryovials were transferred into a liquid nitrogen tank for long term storage.

2.5.3 Revitalization of immortalized cells

For the revitalization frozen cells were quickly thawed in a 37 °C water bath and transferred into a 10 cm dish containing 20 ml growth medium. The medium was replaced the next day to remove the remaining DMSO or passaged if necessary.

2.5.4 Establishing stable cell lines via retroviral transfection

The generation of stably expressing cells was performed by retroviral transfection using the packaging cell line GP2-293. This HEK-293 based cell line stably express the *gag* and *pol* genes, and for the generation of infectious viral particles, GP2-293 must be co-transfected with the *env* gene and a retroviral expression vector. The *env* gene encodes an envelope glycoprotein from the vesicular stomatis virus (VSV), which mediates the viral entry through lipid binding and plasma membrane fusion (Emi *et al.*, 1991).

To generate the viral particles, GP2-293 cells were seeded at 10-cm dishes and at a density of about 50%, cells were treated with 25 μ M chloroquine for 2 h prior to transfection. The medium was changed and cells were double transfected with the respective pLBCX constructs and the pVSV-G at a ratio 1:1 using the calcium phosphate transfection method:

Reaction batch for one 10-cm plate to generate infectious virus particles:

450 μ l H₂O
10 μ g pVSV-G
10 μ g pLBCX hSOD1 constructs
50 μ l 2.5 M CaCl₂
500 μ l 2 x HEPES

The reaction batch incubated for 15 min at RT and was dispersed drop-wise to the cells. After 4 h, the medium was changed and viruses were collected for another 48 h. The target bEnd.3 cells were seeded 24 h prior transfection in 6-well plates, and at density of about 50%, medium was replaced to 1 ml fresh medium containing 20 μ g/ml polybrene. This cationic polymer facilitates the adsorption of retroviral particles to eukaryotic cells. Finally, about 2 ml of the medium containing the recombinant viruses was added to the bEnd.3 cells and after 24 h, infected cells were transferred to 10-cm dishes with fresh medium containing 5 μ g/ml blasticidin. The selection medium was changed every 2-3

days and the expression of the transgene was analyzed by western blot analysis.

2.5.5 Isolation and cultivation of primary mouse endothelial cells

The isolation and cultivation of primary mouse endothelial cells was carried out as described previously (Weidenfeller *et al.*, 2005). In brief, spinal cord endothelial cells (pMSCECs) were isolated from 6- to 7-months-old hSOD1^{G93A} mice and their respective littermates. Spinal cords were pooled and the tissue was mechanically dissociated followed by a digest with a mixture of 0.75 mg/ml collagenase CLS2 and 10 U/ml DNaseI in DMEM at 37 °C on a shaker set at 200 rpm for 1 h. The pellet was resuspended in 20% (w/v) BSA-DMEM and centrifuged at 1000 *g* for 20 min to remove myelin. The pellet was further digested with 1 mg/ml collagenase-dispase and 10 U/ml DNaseI in DMEM at 37 °C on a shaker for 1 h. Endothelial capillaries were separated on a 33% continuous Percoll gradient, collected, and seeded in dishes coated with 400 µg/ml collagen IV and 100 µg/ml fibronectin. Cultures were maintained in DMEM supplemented with 20% PDS, 100 U/ml penicillin, 100 µg/ml streptomycin, 2 mM L-glutamine, 4 µg/ml puromycin, 1 ng/ml bFGF and 1 µg/ml heparin at 37 °C and 5% CO₂.

2.5.6 Impedance measurement

The cellZscope® is an automated device for measuring the transendothelial impedance of cell layers under physiological condition (Wegener *et al.*, 2004). By impedance spectroscopy, the transendothelial resistance (TER) and the capacitance (C_{Cl}) of a cell layer can be measured. The TER is a direct measure of the tightness and the C_{Cl} is a direct measure of the confluence of the cells. The *in vitro* BBB model used in this thesis is presented in Figure 2.1, as well as the cellZscope®.

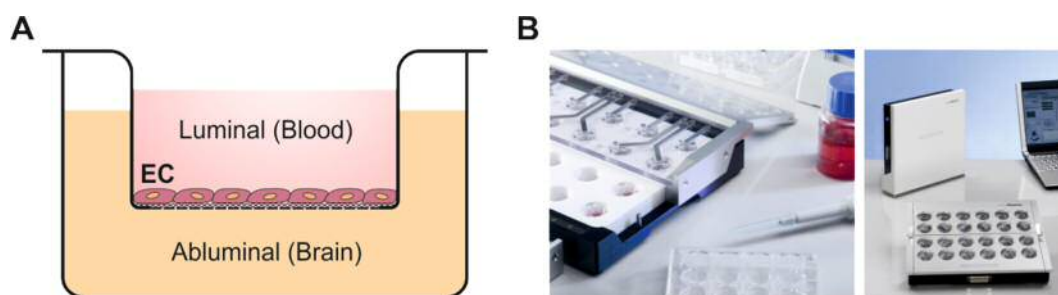


Figure 2.1: Schematic illustration of the *in vitro* BBB model. Immortalized or primary endothelial cells were cultivated on porous membranes (cell culture inserts). The upper compartment represents the luminal side of the blood vessel, whereas the lower compartment represents the brain parenchyma side (A). The inserts were placed in the cellZscope® device (B). The cellZscope® measures online the TER and the C_{Cl} of the cells. These measurements can be used for the verification of the integrity of endothelial.

2.5.6.1 Influence of the TER by nanoparticles

The TER was used to analyze the toxicity of the nanoparticles on endothelial cells. bEnd.3 cells were seeded on 24-transwell cell culture inserts and placed into the cellZscope® device. When cells were post-confluent, equal amount of drug-loaded and unloaded nanoparticles (2.4 mg nanoparticles per cm^2 , which corresponds to 750 μM nanoparticulate flurbiprofen) were added luminally and the TER was measured.

2.5.6.2 Measurement of the integrity of endothelial cells

The TER and the permeability of [^{14}C]-inulin were used to analyze the integrity of pMSCECs or stable hSOD1 bEnd.3 cells. Therefore, cells were seeded on 24-transwell cell culture inserts and placed into the cellZscope® device and the TER was measured. When the capacitance values were between 1.0 and 0.8 $\mu\text{F}/\text{cm}^2$, indicating a confluent monolayer, cells were used for the permeability assay. Culture media was changed to serum-free media containing 40 mM HEPES and 1 $\mu\text{Ci}/\text{ml}$ [^{14}C]-inulin was added to the luminal compartment of the inserts. At each point in time, 10 μl samples were taken from the abluminal compartment and counted on a Tri-Carb 2800 TR Liquid Scintillation Analyzer. The permeability was evaluated by calculating the

apparent permeability coefficient (P_{app}) as previously described (Grabovac and Bernkop-Schnurch, 2007): $P_{app}[cm / s] = dQ / (dt \cdot A \cdot c_0)$ where dQ is the amount of permeated [^{14}C]-inulin in the incubation time, A is the surface area, c_0 is the initial concentration in the luminal compartment and dt is the incubation time.

2.5.7 Measurement of cytotoxicity

The cytotoxicity of free flurbiprofen or PLA-flurbiprofen nanoparticles was assessed using the alamarBlue® reagent. This cell viability indicator is converted by living cells into a fluorescent molecule which can be measured by a plate reader or fluorescence spectrophotometer. The active component of alamarBlue® is the blue and nontoxic dye resazurin, which permeates into living cells and can be converted by the mitochondria to the red fluorescent dye resorufin. Viable cells continuously convert resazurin to resorufin thereby generating a quantitative measure of viability and cytotoxicity.

bEnd.3 cells were seeded on 96-well plates and after reaching post-confluency, cells were treated with increasing concentrations of free or nanoparticulate flurbiprofen ranging from 25 μM to 750 μM (which corresponded to 45.2 $\mu g/cm^2$ to 226.2 $\mu g/cm^2$ nanoparticles). The unit μg per cm^2 refers to the amount of nanoparticles which were administered to the cells and this unit reflects possible local sedimentation on the surface of the cells which might locally lead to different concentrations. After 72 h, cells were incubated for another 4 h with 1 x alamarBlue® in medium. The absorbance was measured with a 570 nm measurement filter and a 600 nm reference filter. The cell viability was calculated as percentage of absorbance in relation to vehicle control treated cells.

2.5.8 Endocytosis of nanoparticles

To study the endocytotic uptake of the PLA nanoparticles, bEnd.3 cells were seeded on glass coverslips. When cells were post-confluent, they were treated with 90.9 $\mu\text{g}/\text{cm}^2$ PLA-flurbiprofen nanoparticles at 4 °C or 37 °C for 1 h or 4 h. After the incubation, cells were put on ice and washed with PBS pH2 to remove the surface-bound nanoparticles mimicking the acidic environment of endosomes where ligands dissociate from their receptor after internalization (Koo and Squazzo, 1994). Cells were fixed with 4% PFA and 0.12 M sucrose in PBS for 10 min at RT. The cell nuclei were stained with 2 μM DRAQ5™ for 10 min at RT. Samples were embedded in Prolong® Gold antifade reagent and analyzed with a confocal laser scanning microscope.

2.5.9 Treatment with nanoparticles

2.5.9.1 Biological activity of the nanoparticles

To examine the biological activity of flurbiprofen-loaded nanoparticles, 7WD10 were treated with free or nanoparticulate flurbiprofen ranging from 50 μM to 250 μM flurbiprofen (Figure 2.2).

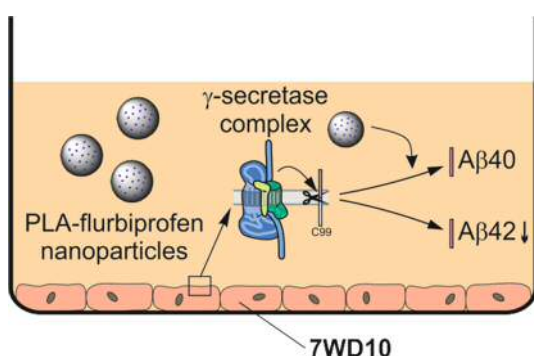


Figure 2.2: Treatment of 7WD10 with PLA-flurbiprofen nanoparticles. 7WD10 were treated with free or nanoparticulate flurbiprofen to assess the biological activity of the flurbiprofen-loaded nanoparticles. The levels of A β_{40} and A β_{42} were measured by an A β specific ELISA in cooperation with Sandra Baches from the lab of Prof. Dr. Sascha Weggen (University of Heinrich Heine University, Duesseldorf).

The administered concentration of the nanoparticles was adjusted to the free flurbiprofen which corresponds to 45.2 $\mu\text{g}/\text{cm}^2$ to 226.2 $\mu\text{g}/\text{cm}^2$ nanoparticles. After 48 h, the supernatants were collected and centrifuged at 18,000 g for

20 min at 4 °C. Levels of A β were measured by an A β specific enzyme-linked immunosorbent assay (ELISA) (see chapter 2.5.9.3).

2.5.9.2 Transport of nanoparticles across endothelial cells

To study the ability of PLA-flurbiprofen nanoparticles to be transported across an *in vitro* BBB model, bEnd.3 cells were seeded on 24-transwell cell culture insert. After reaching post-confluency, bEnd.3 cells were co-cultured with 7WD10 in the lower compartment and bEnd.3 were treated with 300 μ M free flurbiprofen or nanoparticulate flurbiprofen ranging from 300 μ M to 750 μ M flurbiprofen which correspond to 379 μ g/cm² to 942.3 μ g/cm² nanoparticles. The experimental setup is illustrated in Figure 2.3.

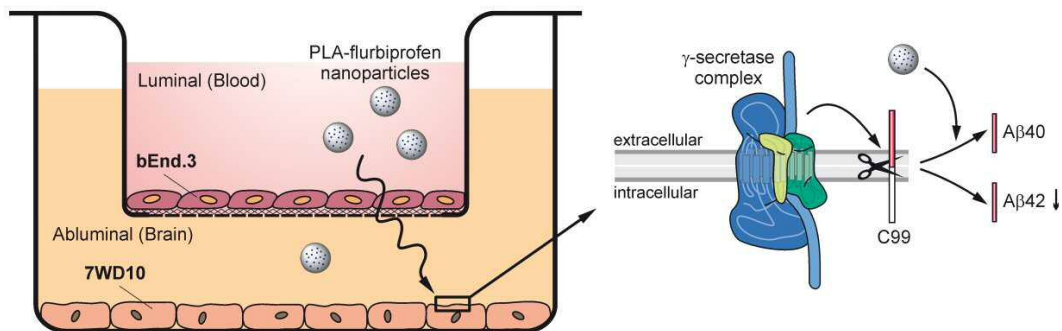


Figure 2.3: Experimental setup to study the transport of PLA-flurbiprofen nanoparticles in an *in vitro* BBB model. bEnd.3 cells were cultivated on porous membranes until a post-confluent monolayer had grown. Then, 7WD10 were co-cultured with the bEnd.3 cells in the lower compartment and bEnd.3 cells were treated with free or nanoparticulate flurbiprofen. The levels of A β ₄₀ and A β ₄₂ in the abluminal compartment were collected after 72 h and measured by an A β specific ELISA in cooperation with Sandra Baches from the lab of Prof. Dr. Sascha Weggen (University of Heinrich Heine University, Duesseldorf).

After 72 h, the supernatants of the lower compartment were collected and centrifuged at 18,000 *g* for 20 min at 4 °C. Levels of A β were measured by an A β specific ELISA (see chapter 2.5.9.3).

2.5.9.3 Enzyme-linked immunosorbent assay (ELISA).

In this immunochemical assay, substances like peptides are detected by a specific antibody followed by an enzymatic reaction. Therefore, the specific antibody is attached to a surface, and the antigen will be applied. Then, another specific antibody, which is often labeled with horseradish peroxidase (HRP), is added and binds to the antigen. A final incubation with a HRP substrate produces a detectable signal, which can be measured by a plate reader.

The measurement of the A β ₄₀ and A β ₄₂ levels generated in 2.5.9.1 and 2.5.9.2 was performed as previously described (Hahn *et al.*, 2011) and in cooperation with Sandra Baches from the lab of Prof. Dr. Sascha Weggen (Department of Neuropathology, Heinrich Heine University, Duesseldorf).

2.5.10 Immunofluorescence

Cells were grown on glass coverslips or chamber slides and fixed with 4% (w/v) PFA and 0.12 M sucrose in 1 x PBS for 30 min at RT. The permeabilization of the cells was achieved by incubating for another 30 min at RT with 0.1% (v/v) Triton X-100 in 1 x PBS. The cells were blocked with 5% (v/v) goat serum and 1% (w/v) BSA for 90 min at RT to reduce unspecific background signals. The respective primary antibodies (Table 2.1) were incubated for 1 h at 37 °C. Unspecific binding of the antibodies was removed by washing the cells five times with the blocking solution. The secondary antibodies (Table 2.2) were incubated for 90 min at RT followed by five wash steps with 1 x PBS. Cell nuclei were stained with 5 μ M DRAQ5™ in 1 x PBS for 10 min at RT. Samples were embedded in Prolong® Gold antifade reagent, dried overnight at RT and analyzed with a confocal laser scanning microscope.

2.6 Protein biochemical methods

2.6.1 Cell lysis and protein extraction

To analyze intracellular and membrane proteins, bEnd.3 were seeded on 6-cm dishes and grown until post-confluency. Dishes were placed on ice and cells were washed with ice-cold 1 x PBS. Cells were harvested with 1 ml 1 x PBS using a cell scraper and transferred to a 1.5 ml tube and pelleted at 4,500 *g* for 4 min. The pellet was lysed in NP-40 lysis buffer supplemented with 1 x protease inhibitor cocktail for 20 min on ice.

NP-40 lysis buffer:

150 mM	NaCl
50 mM	Tris-OH pH 8.0
1% (v/v)	Nonidet P40
0.02% (w/v)	NaN ₃

Cellular debris was removed by centrifugation at 18,000 *g* for 20 min at 4 °C, and clear lysates were transferred to a new 1.5 ml tube. The protein concentration was determined with the bicinchoninic acid (BCA) protein assay (Smith *et al.*, 1985). In an alkaline environment, proteins reduce Cu²⁺ to Cu¹⁺, and this cuprous ion can be detected with BCA by colorimetry. For the determination of the protein concentration, the BCA™ Protein Assay Kit was used. Therefore, samples were diluted 1:10 in ddH₂O and BSA was used as a reference protein ranging from 0 µg/µl to 5 µg/µl. The BCA reagents A and B were mixed in a ratio 50:1, and 1 ml was added to each sample and standard. All samples and standards were incubated for 30 min at 60 °C, and then loaded in duplicates on 96-well plates and measured at a wavelength of 562 nm.

2.6.2 SDS-Polyacrylamide gel electrophoresis (SDS-PAGE)

Cellular proteins were analyzed by SDS-PAGE (Laemmli, 1970), whereby proteins were denatured and separated according to their molecular weight. Therefore, the electrophoresis is performed in presence of the anionic detergent SDS which results in a dissociation of oligomeric proteins into their subunits and an overall negative charge of the proteins. The separation is facilitated by an electrical field which is build up along Bis-Tris-HCl polyacrylamide gels. All gels in this study were handmade according to the following recipe.

Table 2.4: Preparation of Bis-Tris-HCl polyacrylamide gels.

	Stacker gel	Resolving gel	
	4%	10%	12%
30% Acrylamide 37.5 : 1 Bis-Acrylamide	390 µl	3.30 ml	3.96 ml
1.6 M Bis Tris pH 6.4	750 µl	2.48 ml	2.48 ml
ddH ₂ O	1.85 ml	4.05 ml	3.39 ml
10% (w/v) APS	30 µl	49.5 µl	49.5 µl
TEMED	7.5 µl	16.5 µl	16.5 µl

Proteins were separated with 1 x MES buffer at 120 V.

2.6.3 Western blot analysis

The western blot (Burnette, 1981) allows the identification of separated proteins with specific antibodies - the proteins in the polyacrylamide matrix are transferred to a membrane followed by a detection with the appropriate antibodies. The protein transfer is facilitated by an electrical field which is build up between the gel and the membrane.

Transfer buffer:

192 mM Glycine
25 mM Tris-OH
20% (v/v) Methanol

The gel and the membrane were tightly stacked between thick Whatman papers, sponge pads and gel-cassette plates using the Mini Trans-Blot® Cell System. The transfer was performed with ice-cold transfer buffer at 70 V for 90 min at RT. Thereafter, the transfer was checked by a reversible staining of the membrane using Ponceau S-solution for 1 min.

Ponceau S-solution:

0.5% (w/v) Ponceau S red
1% (v/v) Glacial acid

The blots were washed with TBS containing 0.01% (v/v) Tween-20 (TBST) for 5 min, and then blocked for 1 h with 5% (w/v) non-fat dry milk in TBST to block unspecific binding-sites. The blots were incubated with the primary antibodies in TBST or 5% (w/v) non-fat dry milk in TBST overnight at 4 °C in an appropriate dilution (Table 2.1). The next day, blots were washed 3 x 10 min on a shaker with TBST, to remove unspecific binding of the primary antibodies. Blots were incubated for another hour at RT with the in TBST diluted HRP-labeled secondary antibodies (Table 2.2). Thereafter, the blots were washed 3 x 10 min with TBST and the proteins were detected using the HRP substrate Immobilon and were visualized by the LAS-3000mini.

2.6.4 Cell surface biotinylation

The cell surface biotinylation is a method to analyze the expression of proteins at the cell surface by labeling them covalently with biotin. Since biotin binds to avidin or NeutrAvidin with a high affinity, biotinylated proteins can be specifically isolated by pull down assays using NeutrAvidin coated agarose

beads. For the biotinylation, the membrane impermeable reagent sulfo-NHS-SS-Biotin, which reacts rapidly with the primary amines of lysine residues of proteins, was used. bEnd.3 cells were seeded at 6-cm dishes and when cells were post-confluent, the cell surface biotinylation was performed. Therefore, cells were washed three times with ice-cold 1 x PBS and cell surface proteins were biotinylated with 0.25 mg/ml sulfo-NHS-biotin in ice-cold PBS for 40 min at 4 °C. After 20 min, the biotin solution was replaced. Cells were washed four times with ice-cold PBS containing 50 mM NH₄Cl to quench non-conjugated biotin. Cells were lysed in NP40 lysis buffer and the protein concentration was determined by the BCA assay (2.6.1). Equal amounts of total protein lysates were incubated with 20 µl NeutrAvidin Agarose resin beads at 4 °C overnight on a rotated wheel. The next day, the beads were washed 4 times with NP-40 buffer to remove nonspecific binding proteins. The biotinylated cell surface proteins were recovered by boiling the bead-bound fraction with equivalent volumes of 2 x RotiLoad® for 10 min and separated on 12% Bis-Tris HCl polyacrylamide gels followed by western blot. Success of the cell surface biotinylation was verified by the absence of α -tubulin in the cell surface fraction.

2.7 Molecular biological methods

2.7.1 Cultivation of bacteria

For gene cloning experiments, the *Escherichia coli* strain DH5 α was used. Single clones of *E. coli* were used for the amplification of plasmids for the generation of stable cell lines or transient transfections. Bacteria were cultured either in LB medium or on LB agar plates, supplemented with 100 $\mu\text{g/ml}$ ampicillin or 50 $\mu\text{g/ml}$ kanamycin, if required.

LB medium pH 7.0:

0,5% (w/v)	NaCl
1% (w/v)	Bacto-Tryptone
0.5% (w/v)	yeast extract
20 mM	Tris-HCl pH 7.5

LB agar plates pH 7.0:

0,5% (w/v)	NaCl
1% (w/v)	Bacto-Tryptone
0.5% (w/v)	yeast extract
20 mM	Tris-HCl pH 7.5
1,5% (w/v)	Bacto-Agar

2.7.1.1 Small scale liquid cultures

For the extraction of small amounts of plasmid DNA, a single colony was inoculated with 5 ml LB medium supplemented with the appropriate antibiotics and incubated overnight at 37 °C under vigorous shaking. The next day, 4 ml of the culture was used for plasmid DNA extraction (2.7.4).

2.7.1.2 Large scale liquid cultures

For the extraction of large amounts of plasmid DNA, a single colony was inoculated with 5 ml LB medium supplemented with the appropriate

antibiotics and incubated for 8 h at 37 °C under vigorous shaking. Then, 150 µl of this pre-culture was inoculated with 150 ml LB medium supplemented with the appropriate antibiotics and incubated overnight at 37 °C under vigorous shaking. The next day, the whole culture was used for the plasmid DNA extraction (2.7.4).

2.7.2 Generation of chemically competent *E.coli*

Chemically competent bacteria were generated by the RbCl method (Hanahan, 1983). Therefore, a single colony was cultured overnight in 5 ml LB medium without antibiotics at 37 °C under vigorous shaking. The next day, 4 ml were inoculated in 100 ml LB medium and incubated at 37 °C on a shaker until an OD₆₀₀ of 0.5 was reached. Bacteria were pelleted at 4000 rpm and 4 °C for 10 min. The following steps were performed on ice using precooled equipment.

RFI buffer pH 5.8:

100 mM	RbCl
50 mM	MnCl ₂ x 4 H ₂ O
30 mM	CH ₃ CO ₂ K
10 mM	CaCl ₂ x 2 H ₂ O
15% (w/v)	Glycerol

RFII buffer pH 7.0:

10 mM	MOPS
10 mM	RbCl
75 mM	CaCl ₂ x 2 H ₂ O
15% (w/v)	Glycerol

The pellet was resuspended in 40 ml RFI buffer, incubated for 60 min on ice and centrifuged at 4000 rpm and 4 °C for 10 min. The supernatant was discarded and the pellet was resuspended in 10 ml RFII buffer and incubated

for 15 min on ice. 100 µl of the cell suspension were dispensed on 1.5 ml tubes and dropped into liquid nitrogen. Frozen DH5α *E. coli* were stored at -80 °C.

2.7.3 Transformation of chemically competent *E.coli*

The incorporation and expression of foreign DNA by bacteria is called transformation. Therefore, a 100 µl aliquot of competent DH5α *E. coli* was thawed on ice and incubated with 100 ng of plasmid DNA for 20 min on ice. Then, the bacteria were heat shocked for 1 min at 42 °C and cooled on ice for 2 min. 400 µl LB medium was added and bacteria were incubated for 1 h at 37 °C on a thermoshaker at 600 rpm. Afterwards, 50 µl of the suspension were plated on LB agar plates and incubated overnight at 37 °C.

2.7.4 Isolation of plasmid DNA

For the isolation of plasmid DNA from bacteria, commercially available DNA extraction kits were used. The main principle of this isolation relies on an alkaline lysis of the bacterial cells to free the plasmid DNA, which is initially separated from the cell debris and chromosomal DNA by centrifugation, and afterwards purified using ion-exchange columns. The NucleoBond® Xtra Midi kit was used for the large scale plasmid DNA extraction from a 150 ml bacterial culture, and for the extraction of small amounts of plasmid DNA from a 5 ml bacterial culture, the High Pure Plasmid Isolation Kit was used. The kits contained all the necessary reagents and equipment, and the DNA extraction was performed according to the manufacturers' instructions.

2.7.5 Determination of DNA concentrations

To determine the DNA concentration, the absorbance was measured at 260 nm using a spectral photometer, whereby an OD_{260} of 1.0 corresponds to 50 $\mu\text{g/ml}$ double-stranded DNA. Contaminations of the DNA samples with other molecules like proteins or polysaccharides were evaluated by measuring the absorbance at 280 nm and 310 nm which corresponds to the absorption maxima of the contaminants (A_{280} for proteins and A_{310} for polysaccharides). Pure and good-quality DNA will have an A_{260}/A_{280} ratio of 1.8-2.0 with no absorption at A_{310} . Generally, the DNA samples were diluted 1:100 in ddH₂O for the measurement.

2.7.6 Amplification of DNA by polymerase chain reaction (PCR)

The PCR is a method to amplify a defined region of DNA *in vitro* using a thermostable DNA polymerase. Therefore, the DNA becomes thermally denatured and specific oligonucleotides hybridize with the DNA and are subsequently elongated by a DNA polymerase (Mullis and Faloona, 1987). The cycle of denaturation, annealing and elongation is repeated for several times and results in an amplification of the DNA fragment which was flanked by the specific oligonucleotides. Each PCR protocol varies due to the template DNA, the sequence of the oligonucleotides, the DNA polymerase and the length of the amplified fragment. In all experiments, the Phusion™ High-Fidelity DNA polymerase was used, which possesses in addition to the 5'→3' polymerase activity the 3'→5' exonuclease activity ("proof reading").

For a typical PCR, a reaction batch of 50 μ l was prepared as followed:

Reaction batch for the PCR using Phusion™ Polymerase:

200 ng DNA template
 1 U Phusion™ Polymerase
 1 x Phusion™ HF buffer
 500 nM Primer forward
 500 nM Primer reverse
 300 μ M dNTP's Mix
 all in ddH₂O (nuclease free)

The parameters for the PCR were adjusted to the appropriate conditions. Generally, 30-35 cycles were applied for amplification. A standard PCR program using Phusion™ Polymerase was conducted as follows:

Table 2.5: PCR program for the Phusion™ Polymerase.

Cycle step	Temperature	Time	
Initial Denaturation	98 °C	30 sec	
Denaturation	98 °C	10 sec	
Annealing	60 °C	30 sec	x 31
Elongation	72 °C	30 sec/1kb	
Final Elongation	72 °C	5 min	
Hold	4 °C	∞	

2.7.7 Agarose gel electrophoresis of DNA

The separation of DNA fragments was performed by agarose gel electrophoresis where the percentage of the agarose gel was chosen according to the size of the fragments.

1 x TAE buffer:

40 mM Tris-acetate
 1 mM EDTA pH 8.0

In general, agarose was dissolved in 1 x TAE by boiling to obtain 1.0-2.0% (w/v) agarose gels. For the visualization of the DNA, EtBr was added to the cooled agarose solution at a final concentration of 0.75 µg/ml and poured into a horizontal gel chamber. The DNA samples were supplemented with a 6 x loading dye solution and separated at 120 V. In addition, 5 µl of a 1kb DNA ladder was separated as a size reference. Qualitative agarose gels were photographed and printed with a gel documentation device. The DNA fragments which were separated for preparative purposes were cut out from the gel under weaker UV light at 254 nm to avoid DNA damage and transferred into a 1.5 ml tube for the gel extraction.

2.7.8 Gel extraction of DNA fragments

The gel extraction of DNA fragments was performed using the NucleoSpin® Extract II-PCR clean-up and gel extraction kit, according to the manufacturer's instructions. Thereby, the DNA fragments are extracted from the agarose gel and subsequently purified, so that several contaminants like primers, enzymes or buffers are removed, because they may disturb several downstream applications.

2.7.9 Restriction enzyme digestion of DNA

Restriction enzymes make double-stranded cuts in the sugar-phosphate backbone of the DNA, thereby producing blunt or cohesive ends. A DNA fragment with cohesive ends has unpaired nucleotides in the end of the molecule, and this feature is often used for cloning experiments, because different DNA fragments digested by the same enzyme can be annealed together. In nature, restriction enzymes are found in bacteria and archaea and serve to restrict viral growth by destroying foreign DNA. Restriction enzymes are classified into four groups (Types I-IV) based on the nature of their target

sequence, the position of their restriction site relative to the target sequence, their composition and their cofactor requirements. In this study, only recombinant Type II restriction enzymes were used which cut the DNA within their palindromic recognition site that is four-, six-, or eight base pairs long. All restriction enzymes and supplied buffers were purchased from New England Biolabs (NEB) and the double digest was performed as recommended by the company's online software: <https://www.neb.com/tools-and-resources/interactive-tools/double-digest-finder>). For a typical double digest, a reaction batch of 50 μ l was prepared as followed:

Reaction batch for the double digest of DNA:

- DNA template
- 5 U Each restriction enzyme
- 1 x Restriction buffer NEB
- all in ddH₂O (nuclease free)

For qualitative purposes, \sim 1 μ g of DNA was digested overnight at 37 °C with 5 U of each enzyme at the same time. The next day, digested DNA fragments were analyzed by agarose gel electrophoresis. For a preparative digests, 2 μ g of plasmid DNA or purified PCR products (2.7.7) were digested for 3 h at 37 °C with 5 U of each enzyme at the same time. The next day, digested DNA fragments were analyzed by agarose gel electrophoresis and purified by gel extraction (2.7.8).

2.7.10 Ligation of DNA fragments

The T4 DNA ligase catalyzes the formation of a phosphodiester bond of two strands of DNA between the 5'-phosphate and the 3'-hydroxyl groups of adjacent nucleotides at either cohesive or blunt ends. Thus, individually digested plasmid vector and insert DNA were added to a ligation reaction to be circulated. The plasmid vector and DNA insert were digested with the appropriate enzymes and purified as described in 2.7.9 and 2.7.8. The T4 DNA

ligase and supplied buffers were purchased from NEB and the ligation was performed according to the manufacturer's instructions. For a typical ligation, a reaction batch of 30 μ l was prepared as followed:

Reaction batch for the ligation of DNA:

400 U T4 DNA ligase
1 x T4 DNA ligase buffer
1 x Plasmid vector
4 x DNA insert
all in ddH₂O (nuclease free)

The plasmid vector and the DNA insert were ligated in at a molar ratio of 1 : 4 at ~16 °C overnight.

2.7.11 Cloning of expression constructs

2.7.11.1 Subcloning of hSOD1 in pLBCX

The plasmids pEGFP-N1-hSOD1^{WT}, pEGFP-N1-hSOD1^{G37R}, pEGFP-N1-hSOD1^{G85R} and pEGFP-N1-hSOD1^{G93A} (Witan *et al.*, 2009) were used as PCR templates to subclone the several hSOD1 sequences into the retroviral expression vector pLBCX with a 5'-*Hind*III and 3'-*Not*I restriction site containing an additional 3' myc-epitope as listed in Table 2.6. The final PCR products were ligated in a *Hind*III x *Not*I digested pLBCX vector.

Table 2.6: Oligonucleotides for the generation of pLBCX hSOD1 myc tagged constructs

Primer name	5' - 3' sequence	Enzyme site
hSOD1 fwd	CCC AAGCTT TATGGCGACGAAGGCCGTGTGCGTGCTGAA	<i>Hind</i> III
hSOD1 myc rev	ATTT GCGGCCG TTACAGAT CCTCTTCTGAGATGAGTT TTT GTTCT TTGGGCGATCCCAATTACACCACAA	<i>Not</i> I

2.7.12 Sequencing of DNA

For verification, all cDNA constructs were sequenced at SEQ.IT GmbH & Co. KG in Kaiserslautern. The sequencing files were compared with the desired sequence using the Clone Manager 7 Software.

3

Results & Discussion

In this chapter, the experimental results obtained of the two different projects are presented and discussed in the context of the recent literature. The data of Project I (chapter 3.1) was published in *Alzheimer's Research & Therapy* (Meister *et al.*, 2013 Nov 27, doi:10.1186/alzrt225) and the data of Project II (chapter 3.2) was published in *Journal of Cerebral Blood Flow & Metabolism* (Meister *et al.*, 2015, Apr 8, doi: 10.1038/jcbfm.2015.57).

3.1 Project I: Nanoparticulate flurbiprofen reduces A β ₄₂ generation in an *in vitro* BBB model

Over the past years, several strategies and possibilities for the treatment of AD have been studied intensively, but a lot of these strategies as well as the developed compounds failed in clinical studies in part due to their low penetration of the BBB. Following the amyloid hypothesis, the A β ₄₂ peptide plays a crucial role in the pathogenesis of AD. A β is generated through the proteolytic processing of APP, and its accumulation or increased generation is thought to be one of the primary events in the pathogenesis of AD (Selkoe, 1991; Hardy and Allsop, 1991; Hardy and Higgins, 1992; Selkoe, 2001;

Hardy and Selkoe, 2002; Golde, 2003; McGowan *et al.*, 2005; Wyss-Coray, 2006). According to this hypothesis, reduced generation or enhanced clearance of A β ₄₂ peptides and plaques would be expected to modify the disease course in AD (Hardy, 2009). In 2009, the clinical development of the A β ₄₂ lowering agent tarenflurbil (the COX-inactive *R*-enantiomer of the NSAID flurbiprofen) was stopped in a Phase III clinical trial, because it did not show any slowing or improvement of the cognitive decline after 18 months of treatment (Green *et al.*, 2009). Generally, brain penetration of CNS-active drugs is mostly limited by the BBB, and several strategies have been devised to overcome this barrier in order to deliver therapeutic drugs into the brain (Pardridge, 2007). To date, drug carriers like nanoparticles have been studied intensively for neurological disorders, cancer and other diseases and some of them are in different trial phases or even commercially available (Kumari *et al.*, 2010; Re *et al.*, 2012). Therefore, the transport and functionality of racemic flurbiprofen embedded in PLA nanoparticles was analyzed in an *in vitro* BBB system in order to selectively decrease the levels of A β ₄₂ peptides in the brain. PLA-nanoparticle formulations were studied because this starting material is FDA-approved, biodegradable and biocompatible (Li, 1999; Tosi *et al.*, 2008), and flurbiprofen was used as a GSM because it is FDA-approved, commercially available and, most importantly, its GSM activity has been studied intensively *in vivo* and *in vitro* (Weggen *et al.*, 2001; Eriksen *et al.*, 2003).

3.1.1 Preparation and characterization of the PLA-flurbiprofen nanoparticles

The preparation of the nanoparticles was performed by the emulsification-diffusion technique (Kwon *et al.*, 2001), which is basically describes in Figure 3.1 (for detailed formation, please consult chapter 6.1.1). The nanoparticles were analyzed with regard to particle diameter and size distribution (polydispersity) by photon correlation spectroscopy (PCS), and the surface charge (zeta potential) was measured by microelectrophoresis

(Table 3.1). The size of the nanoparticles was between 213.6 and 218.1 nm, and the polydispersity index was less than 0.1 indicating a uniformly distributed dispersion. The amount of incorporated flurbiprofen was determined by high-performance liquid chromatography (HPLC) that resulted in 60.2 μg flurbiprofen per mg nanoparticles and corresponds to a stock solution of 9.86 mM flurbiprofen.

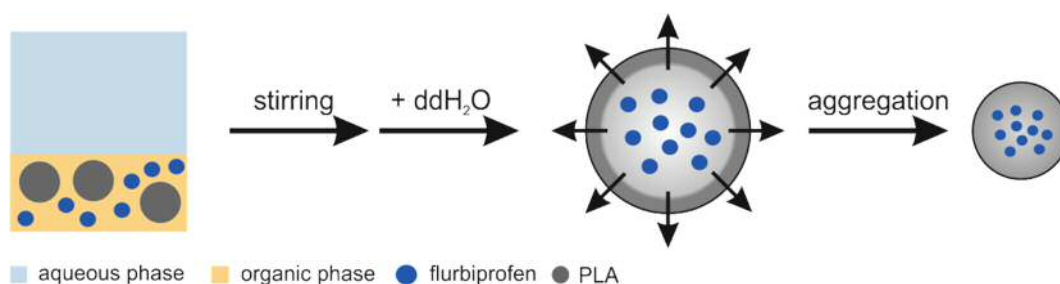


Figure 3.1: Schematic illustration of the formation mechanism of the nanoparticles by emulsification-diffusion method. For the preparation of the nanoparticles, the prospective polymer (PLA) and the racemic flurbiprofen are dissolved in an organic solvent. A water containing stabilizer is added and the solution is stirred. Stirring causes the dispersion of the organic phase as globules in equilibrium with the aqueous phase: the stabilizing agent adsorbs then to the large interfacial area created. The addition of water destabilizes the equilibrium: it causes the organic solvent to diffuse to the external phase. During this transport of solute, new nanometer-sized globules are formed, which gradually become poorer in solvent. As a result, the contained polymer in the globules aggregates because of the presence of a new, continuous non-solvent phase. For the visualization of the cellular uptake of the nanoparticles, Lumogen F Orange[®] 240 (kindly provided by BASF, Ludwigshafen, Germany) was added during the synthesis of the nanoparticles (adapted from Kwon et al, 2001). PLA, polylactide.

Table 3.1: Physicochemical characteristics of PLA nanoparticles. The preparation of the nanoparticles as well as the characterization was performed by Iavor Zlatev (Laboratory of Prof. Klaus Langer, Münster).

Formulation	Mean particle diameter [nm]	Polydispersity index	Zeta potential [mV]	Flurbiprofen loading [$\mu\text{g}/\text{mg}$]
PLA-flurbiprofen nanoparticles	218.1	0.053	-17.4	60.2
PLA nanoparticles	213.6	0.048	-27.6	-

In all subsequent experiments, the administered concentration of the nanoparticles was adjusted to free flurbiprofen to ensure the comparability of the treatments. Furthermore, Lumogen[®] F Orange 240 (kindly provided by

BASF) was added during the preparation to ensure the visualization of the nanoparticles.

3.1.2 Flurbiprofen is released over time from the nanoparticles

Given that the nanoparticle formulation should serve as carrier for flurbiprofen, the release of the drug was studied *in vitro* at a physiological pH. 1 mg PLA-flurbiprofen nanoparticles were incubated in 1 ml phosphate buffer (pH=7.5) at 37 °C and the released flurbiprofen was measured by HPLC at different time points (Figure 3.2).

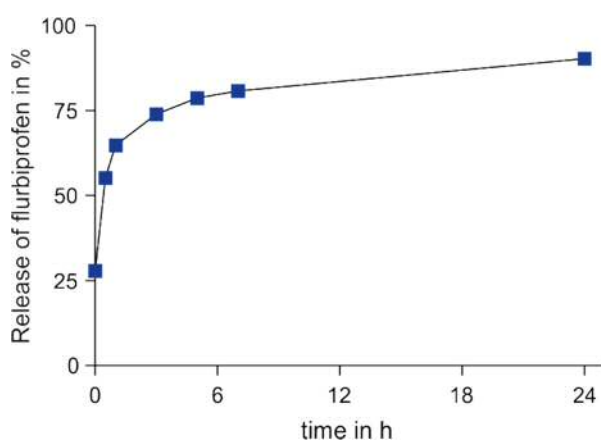


Figure 3.2: Flurbiprofen is released over time from the PLA nanoparticles at a physiological pH. PLA-flurbiprofen nanoparticles were dissolved in an aqueous solution at pH 7.5 and the amount of flurbiprofen in the solution was measured by HPLC at different time points. The release is shown as the percentage of the total amount of incorporated flurbiprofen in the nanoparticles. The experiment was performed by Iavor Zlatev (Laboratory of Prof. Klaus Langer, Münster).

The *in vitro* release shows an asymptotic curve progression which indicates an initial rapid release of flurbiprofen followed by a slower exponential phase. This demonstrates that flurbiprofen is reversibly incorporated into the nanoparticles and that flurbiprofen is constantly released over time.

3.1.3 PLA-flurbiprofen nanoparticles exhibit no cytotoxic potential

The cytotoxic potential of the nanoparticulate formulation to perturb the integrity of endothelial cells was firstly assessed using the alamarBlue® cell viability reagent. Therefore, post-confluent bEnd.3 cells were incubated with

increasing concentrations of free flurbiprofen or PLA-flurbiprofen nanoparticles. For free flurbiprofen, a cytotoxic potential could be observed at concentrations above 300 μM which was reported earlier by several groups (Figure 3.3, A) (Eriksen *et al.*, 2003; Grosch *et al.*, 2003).

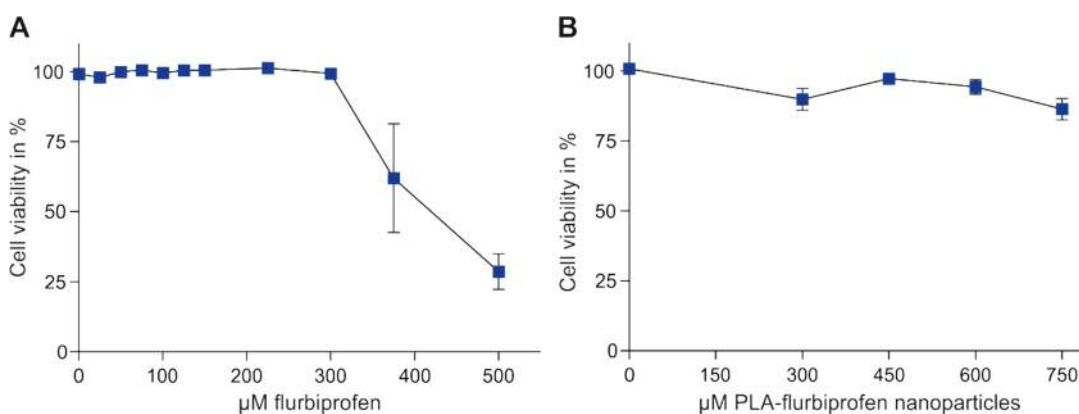


Figure 3.3: Cytotoxicity of free or nanoparticulate flurbiprofen on endothelial cells. bEnd.3 cells were treated with the indicated concentrations of free flurbiprofen (A) or PLA-flurbiprofen nanoparticles (B) for 72 h. The cytotoxicity was assessed after a 4 h incubation with 1 x alamarBlue[®]. The absorbance was measured and the cell viability was calculated as percentage of absorbance in relation to vehicle control treated cells. The data represents mean \pm SEM of $n \geq 3$.

Consequently, flurbiprofen was used in the subsequent experiments only at a highest concentration of 300 μM . In contrast, the nanoparticulate flurbiprofen showed no cytotoxic potential on endothelial cells even at high concentrations of 750 μM flurbiprofen (Figure 3.3, B).

Since the nanoparticles should act as carriers to transport flurbiprofen across endothelial cells, their influence on the integrity of endothelial cells was analyzed. Therefore, the TER of the cells was measured by impedance spectroscopy using a cellZscope[®] device (Wegener *et al.*, 2004). bEnd.3 cells were cultured on cell culture inserts and after reaching post-confluency, cells were treated with 750 μM nanoparticulate flurbiprofen (Figure 3.4).

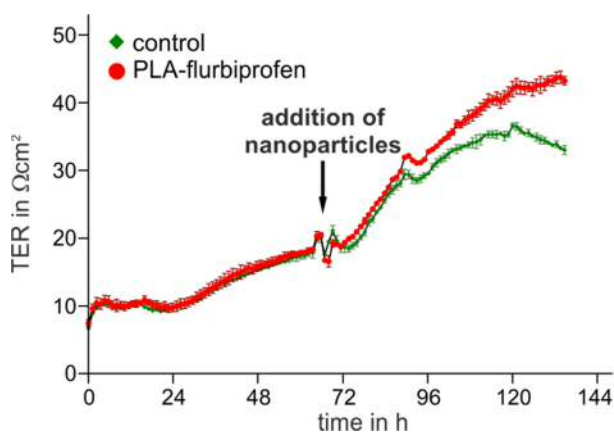


Figure 3.4: Influence of PLA-flurbiprofen nanoparticles on the integrity of the endothelial cell barrier. bEnd.3 cells were cultivated on cell culture inserts in the cellZscope® device. When cells were post-confluent, 750 μM nanoparticulate flurbiprofen were added to the luminal side of the endothelial cells and the TER was measured every hour by impedance spectroscopy.

The nanoparticles showed no interference with the TER development even if high amounts of nanoparticles were administered to the endothelial cells. Considering that the nanoparticles can sediment on the surface of the cells which may lead to different local concentrations these amounts did not perturb the integrity of an endothelial barrier. Thus, the embedding of flurbiprofen in nanoparticles disguised its cytotoxic potential which enables the application of higher concentrations on endothelial cells without any cytotoxicity. In combination with the cell viability assay any cytotoxic effect of the PLA-flurbiprofen nanoparticles could be excluded.

3.1.4 Cellular binding and uptake of the nanoparticles

The prerequisite of an active transport of particles across cells is its cellular binding and uptake by the cells. Thus, the cellular binding as well as the uptake of the PLA-flurbiprofen nanoparticles by endothelial cells was verified. Therefore, bEnd.3 cells were incubated with the PLA-flurbiprofen nanoparticles for 4 h at 37 °C and subsequently analyzed by flow cytometry (Figure 3.5, A). The visualization of the nanoparticles was facilitated by the fluorophor Lumogen F Orange® 240, which was added during the preparation of the nanoparticles. Compared to the untreated control, cellular binding of the PLA-flurbiprofen nanoparticles was detected.

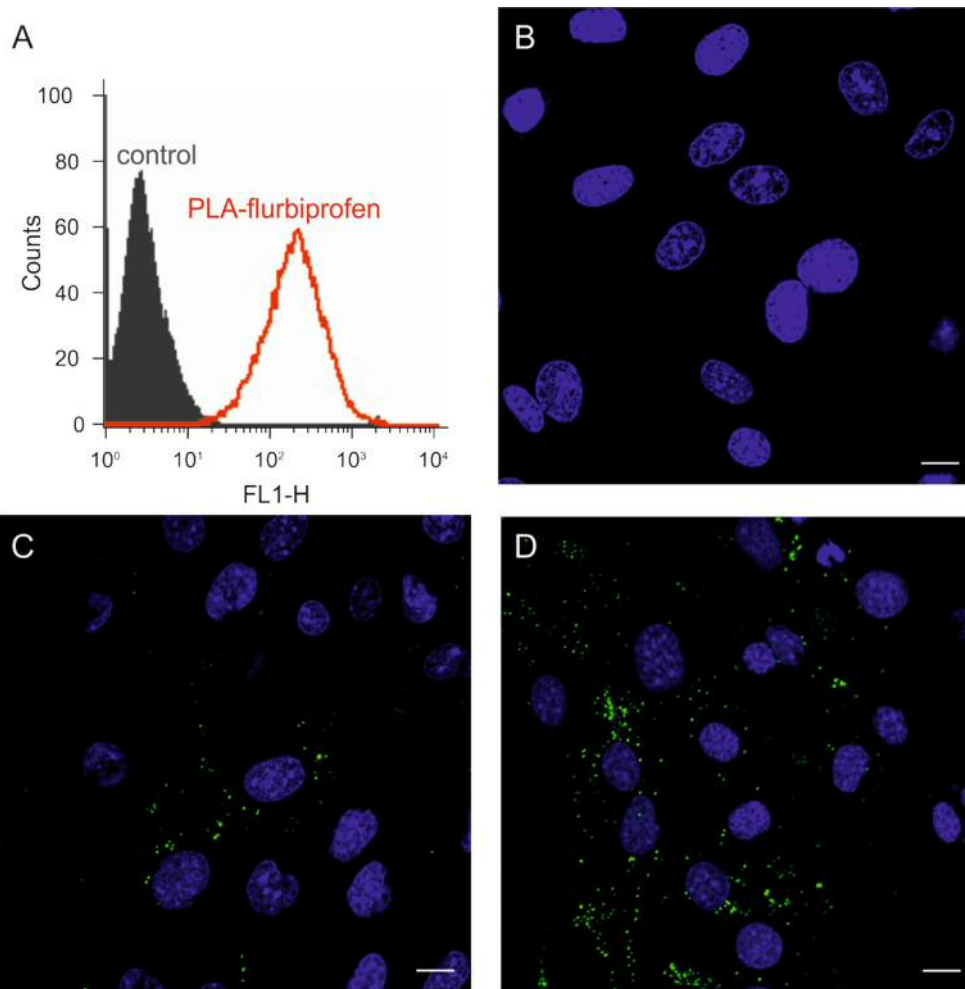


Figure 3.5: Cellular binding and uptake of the PLA-flurbiprofen nanoparticles by endothelial cells. (A) bEnd.3 cells were treated with approx. $100 \mu\text{g}/\text{cm}^2$ PLA-flurbiprofen nanoparticles for 4 h at 37°C and the cellular binding was quantified by flow cytometry. The data are shown as histograms of the FL1-H channel (red: PLA-flurbiprofen nanoparticles, grey: untreated control). This experiment was performed by Julia Stab (Laboratory of Dr. Sylvia Wagner, St. Ingbert). (B-D) bEnd.3 cells were treated with the approx. $100 \mu\text{g}/\text{cm}^2$ nanoparticles. To inhibit endocytosis, the cells were treated at 4°C (B). For the cellular uptake, cells were treated for 1 h (C) or 4 h (D) at 37°C . After the incubation period, the cells were put on ice and washed with acidic PBS to remove the surface-bound nanoparticles. The cells were fixed with 4% (w/v) PFA and cell nuclei were stained with DRAQ5TM. Scale bar, $10 \mu\text{m}$.

Furthermore, the cellular uptake of the nanoparticles was visualized by confocal laser scanning microscopy (CLSM) (Figure 3.5, B-D). Therefore, post-confluent bEnd.3 cells were incubated with the nanoparticles for 1 and -4 h at either 37°C , or at 4°C as a control to inhibit endocytosis. At 4°C , the bEnd.3 cells exhibited no signal of the nanoparticles demonstrating that the nanoparticles were not endocytosed (Figure 3.5, B) (Koo and Squazzo, 1994).

However, the nanoparticles were endocytosed by the bEnd.3 cells at 37 °C (Figure 3.5, C) and this uptake increased with longer incubation time (Figure 3.5, D). Taken together, these results demonstrate that the PLA-flurbiprofen nanoparticles bind to the endothelial cells and were endocytosed which is required for an active transport across the BBB.

3.1.5 The biological activity of nanoparticulate flurbiprofen is comparable to free flurbiprofen

Since the endothelial cells tolerate the PLA-flurbiprofen nanoparticles, and they bind and endocytose the nanoparticles, the biological activity on γ -secretase modulation was verified. As already showed in Figure 3.2, flurbiprofen is constantly released from the nanoparticles, and therefore the ability of the released flurbiprofen to modulate the γ -secretase function was examined using APP overexpressing cells (7WD10) (Koo and Squazzo, 1994). Therefore, 7WD10 were incubated with free flurbiprofen or PLA-flurbiprofen nanoparticles (both ranging from 50 μ M to 250 μ M), and the supernatants were collected for 48 h and the amounts of A β ₄₀ and A β ₄₂ were measured by an A β specific ELISA. Free flurbiprofen specifically decreased A β ₄₂ levels in a concentration-dependent manner with a maximal effect size of approximately 70% in good agreement with previous studies (Figure 3.6, A) (Weggen *et al.*, 2001; Eriksen *et al.*, 2003).

The treatment of the 7WD10 with the nanoparticulate flurbiprofen resulted as well in reduced levels of the A β ₄₂ peptides which decreased also in a concentration dependent manner (Figure 3.6, B). This decrease is comparable to free flurbiprofen although the efficiency of nanoparticulate flurbiprofen is slightly lower compared to free flurbiprofen. Considering that flurbiprofen is released constantly from the nanoparticles, this effect on γ -secretase modulation was expected. Taken together, the nanoparticulate flurbiprofen

exhibited a biological activity to modulate γ -secretase *in vitro* comparable to free flurbiprofen which is required for the following experiments.

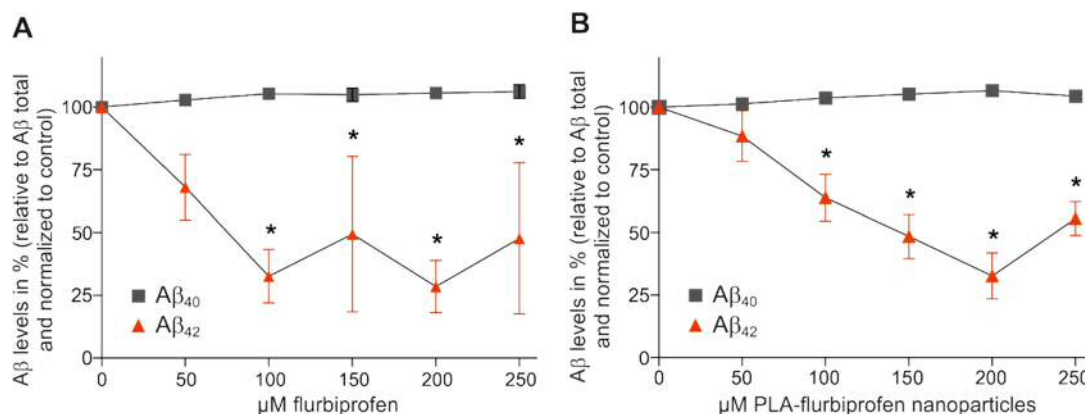


Figure 3.6: Aβ generation in cultured cells treated with free or nanoparticulate flurbiprofen. 7WD10 cells were treated with the indicated concentrations of free flurbiprofen (A) or PLA-flurbiprofen nanoparticles (B). The supernatants were collected after 48 h and the levels of Aβ were measured by an Aβ specific ELISA. The data represents mean ± SEM of 3 independent experiments. * Statistically significant difference ($p < 0.05$, two-way ANOVA) between Aβ levels of vehicle-treated and drug-treated cells are indicated. The ELISA was performed by Sandra Baches (Laboratory of Prof. Dr. Sascha Weggen, Düsseldorf). The levels of the Aβ₄₀ and Aβ₄₂ peptides were normalized to Aβ total (Aβ₄₀ + Aβ₄₂) and the average of triplicate measurements for each concentration was normalized to control condition (DMSO or unloaded PLA nanoparticles).

3.1.6 Transport of flurbiprofen across endothelial cells

The ability of PLA nanoparticles to transport flurbiprofen across an *in vitro* BBB model was studied in a co-culture model as described and illustrated in 2.5.9.2 and Figure 2.3 at page 27. In this model, the bEnd.3 cells were cultivated in the luminal compartment of cell culture inserts until a post-confluent monolayer had grown. Then, abluminally, 7WD10 were co-cultured together with the bEnd.3 cells. The PLA-flurbiprofen nanoparticles or free flurbiprofen was added to the bEnd.3 cells in the luminal compartment after the tightness of the endothelial cell monolayer was confirmed by TER measurement. As readout for the transport of the drug, the medium in the abluminal compartment was collected after 72 h and the γ -secretase activity was measured indirectly by determining the levels of Aβ₄₀ and Aβ₄₂. Additionally, the amount of flurbiprofen in the abluminal compartment was

determined by HPLC. The administration of free flurbiprofen to the bEnd.3 cells showed no influence on the γ -secretase in the abluminal compartment since the levels of $A\beta_{40}$ and $A\beta_{42}$ remained unchanged (Figure 3.7, A). It is noteworthy that only 300 μM free flurbiprofen was administered in this experimental setup due to its cytotoxic potential at higher concentrations (Figure 3.3, A).

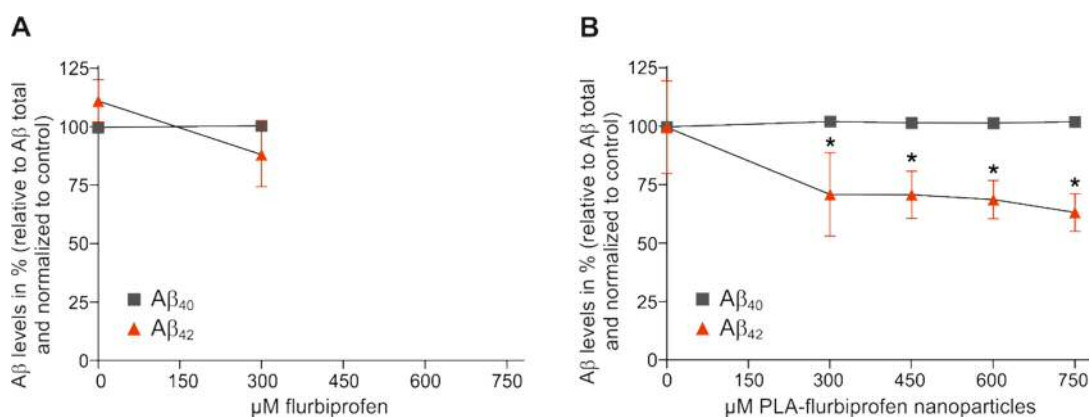


Figure 3.7: Influence of free or nanoparticulate flurbiprofen on $A\beta$ generation in an *in vitro* BBB model. 7WD10 cells were co-cultured abluminal with post-confluent bEnd.3 cells in the luminal compartment. bEnd.3 cells were treated with the indicated concentrations of free flurbiprofen (A) or PLA-flurbiprofen nanoparticles (B). The supernatants were collected after 72 h and the levels of $A\beta$ in the abluminal compartments were measured by an $A\beta$ specific ELISA. The data represents mean \pm SEM of 3 independent experiments. * Statistically significant difference ($p < 0.05$, two-way ANOVA) between $A\beta$ levels of vehicle-treated and drug-treated cells are indicated. The ELISA was performed by Sandra Baches (Laboratory of Prof. Dr. Sascha Weggen, Düsseldorf). The levels of the $A\beta_{40}$ and $A\beta_{42}$ peptides were normalized to $A\beta$ total ($A\beta_{40} + A\beta_{42}$) and the average of triplicate measurements for each concentration was normalized to control condition (DMSO or unloaded PLA nanoparticles).

13.95% of the initial concentration of free flurbiprofen could be detected in the abluminal compartment (Table 3.2), and the resulting concentration was not sufficient to significantly reduce the levels of $A\beta_{42}$. This is in agreement with phase I dosing studies of *R*-flurbiprofen in humans (Galasko *et al.*, 2007). In these studies, healthy volunteers were treated for 21 days with up to 800 mg twice daily of *R*-flurbiprofen. Maximal plasma concentrations of *R*-flurbiprofen up to 185 μM were measured, well in the range of the $A\beta_{42}$ -lowering activity of flurbiprofen in tissue culture experiments. However, flurbiprofen concentrations in the CSF of the volunteers were found to be more than 100-

fold lower with an average CSF to plasma ratio of 0.5%. No significant changes in CSF A β ₄₂ levels were observed in *R*-flurbiprofen treated individuals compared to placebo controls. In the failed Phase III clinical study of *R*-flurbiprofen, CSF drug concentration were not measured, but the highest dose administered in the trial was identical to the phase I study, predicting similarly low brain concentrations (Green *et al.*, 2009).

Table 3.2: Concentration of flurbiprofen in the abluminal compartment measured by HPLC. The determination of flurbiprofen in the abluminal compartment was performed by Iavor Zlatev (Laboratory of Prof. Klaus Langer, Münster).

μM luminally administered	μM abluminally measured by HPLC	% of administered concentration
300 μM flurbiprofen	41.85	13.95
300 μM PLA-flurbiprofen nanoparticles	31.56	10.52
450 μM PLA-flurbiprofen nanoparticles	46.82	10.40
600 μM PLA-flurbiprofen nanoparticles	63.95	10.66
750 μM PLA-flurbiprofen nanoparticles	83.70	11.16

When the flurbiprofen-loaded nanoparticles were added luminally to the endothelial cells, the A β ₄₂ levels decreased in a concentration dependent manner, whereas the levels of A β ₄₀ remained unchanged (Figure 3.7, B). About 10% of the initial concentration of nanoparticulate flurbiprofen could be detected in the abluminal compartment. Although the IC₅₀ for flurbiprofen induced γ -secretase modulation is about 150 to 200 μM , the detected concentrations in the abluminal compartment were sufficient to reduce the A β ₄₂ levels. In a recent study, Wagner and colleagues were able to demonstrate that drug-loaded nanoparticles exhibited a higher biological activity than the free drug alone (Wagner *et al.*, 2010b). The nanoparticulate drug had a lower IC₅₀ value than the free drug molecule, which resulted in a higher efficiency of the nanoparticulate formulation. Moreover, since the nanoparticles may

gradually sediment in the culture medium on the cell surface, this can lead to higher local concentrations of the nanoparticulate flurbiprofen compared to free flurbiprofen. For the HPLC measurements, the total capacity of the abluminal compartment was used and the total concentration of free or nanoparticulate flurbiprofen was measured. Thus, total concentration of the nanoparticulate flurbiprofen may not be higher compared to free flurbiprofen, but if the sedimentation of the nanoparticles is taken into account, the concentrations of the nanoparticulate flurbiprofen can be locally higher resulting in significant decreased levels of A β ₄₂. Taken together, the embedding of flurbiprofen in nanoparticles enabled the administration of higher concentrations of flurbiprofen resulting in a sufficient transport of the drug across the endothelial cell monolayer. These data strongly indicate that even NSAIDs with low GSM activity can efficiently lower A β ₄₂ levels if transported sufficiently across the BBB.

3.1.7 The protein corona of the PLA nanoparticles contains bioactive proteins

When nanoparticles enter a biological fluid, proteins rapidly compete for binding to the nanoparticle surface leading to the formation of a protein corona that critically defines the biological identity of the nanoparticles. Further biological responses of the body as well as the biodistribution of the nanoparticles are expected to be influenced by this nanoparticle-protein complex (Monopoli *et al.*, 2012). Thus, the early time-resolved corona formation of the PLA nanoparticles in human blood plasma was examined. To allow such a snapshot resolution of the corona evolution, PLA nanoparticles were incubated with human plasma for 5, 10, 30 or 60 minutes and centrifuged through a sucrose cushion, which allows a rapid separation of the unbound plasma and the nanoparticles-corona complexes, which is basically describes in Figure 3.8.

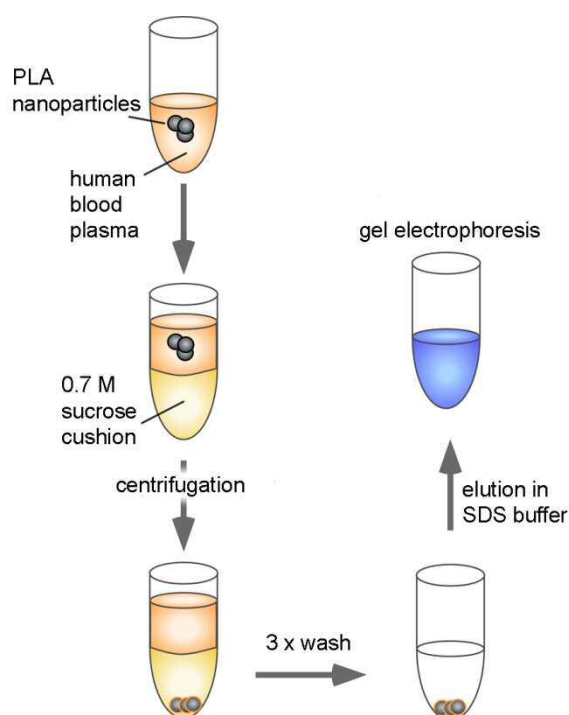


Figure 3.8: Schematic illustration of the experimental protocol to examine the blood plasma corona of PLA nanoparticles. The PLA nanoparticles were incubated with human blood plasma for different time points (5 min to one hour) and subsequently loaded onto a sucrose cushion and centrifuged through the cushion to rapidly separate the nanoparticle-protein complexes from the blood plasma. The plasma remains on the top of the sucrose cushion. Pellets were washed three times with PBS, and proteins eluted in SDS buffer and proteins were separated by gel electrophoreses.

The protein binding profiles demonstrated that already an exposure for 5 min to the blood plasma was sufficient for an efficient corona formation (Figure 3.9, A). Furthermore, the amount of corona proteins increased over time, albeit the corona seems to have changed only quantitatively rather than qualitatively. Apolipoproteins are part of the circulating lipoproteins and serve as receptor ligands for the lipid and cholesterol uptake and metabolism, and since it was proposed that apolipoprotein-functionalized nanoparticles were able to transport drugs across the BBB (Kreuter *et al.*, 2002; Zensi *et al.*, 2009; Wagner *et al.*, 2010a; Wagner *et al.*, 2012), the presence of these bioactive proteins in the protein corona was examined (Figure 3.9, B). After 5 min exposure, apolipoprotein E (ApoE) and apolipoprotein A4 (ApoA4) are present in the nanoparticle-protein complex whereas the amount of ApoA4 slightly had decreased and the ApoE concentrations significantly had increased over time. Members of the apolipoprotein family enable the endocytotic uptake through lipoprotein receptors and it was recently shown that ApoE-modified nanoparticles are actively endocytosed by endothelial cells and that the low

density lipoprotein receptor-related protein 1 (LRP1) is involved in this process (Wagner *et al.*, 2012).

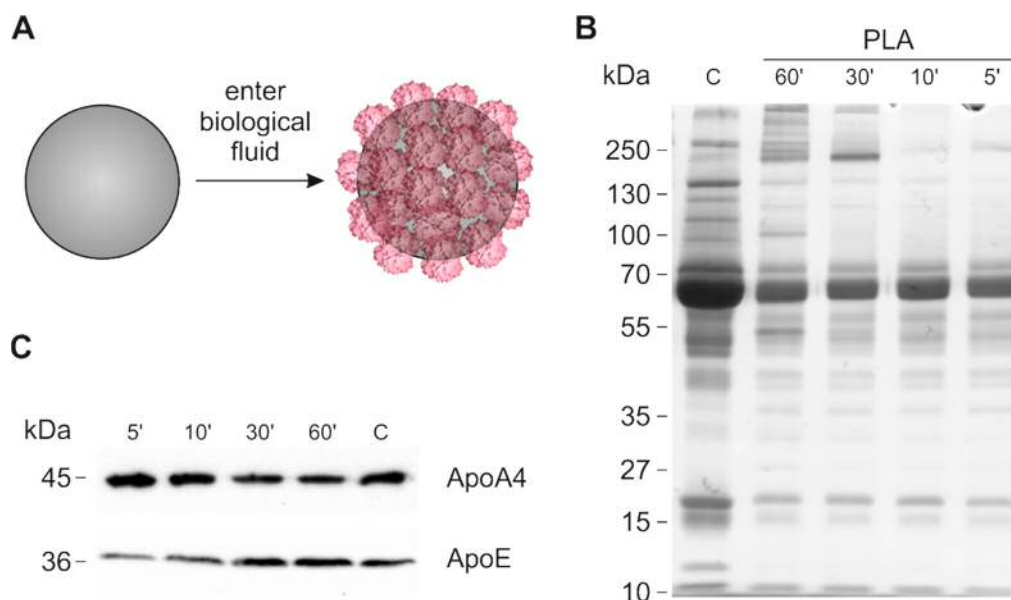


Figure 3.9: Formation of the blood plasma corona results in rapid decoration of PLA nanoparticles with bioactive proteins. When nanoparticles enter a biological fluid, plasma proteins bind to the nanoparticle surface and define thereby their biological identity (A). PLA nanoparticles were incubated with equal amounts of human blood plasma for different time points as indicated. The nanoparticles-protein complexes were separated by gel electrophoresis and stained by Coomassie Blue (B). The lipoproteins ApoA4 and ApoE are present in the protein corona of the PLA nanoparticles (C). This experiment was performed by Dominic Docter (Laboratory of Prof. Dr. Roland Stauber, Mainz). C, control

These data strongly indicate that pristine nanoparticles are not expected to persist in biological environments and the observed formation of the apolipoprotein corona on the PLA nanoparticles proposes a potential transport route of the nanoparticles through a lipoprotein receptor transcytosis pathway (Pflanzner *et al.*, 2011; Wagner *et al.*, 2012). Thus, the transport of the nanoparticulate flurbiprofen may be facilitated by the surface-bound proteins mimicking endogenous lipoproteins via endocytosis by transporters such as LRP1.

3.2 Project II: Impaired integrity of the BSCB in a mouse model for ALS

ALS is a neurodegenerative disease hallmarked by progressive motor neuron degeneration in brain and spinal cord leading to muscle atrophy, paralysis and death typically within 3 to 5 years from diagnosis (Haverkamp *et al.*, 1995; Rowland and Shneider, 2001). Only 5-10% of patients have a genetically inherited form known as familial ALS (FALS) and about 20% of FALS cases are associated with missense mutations or small deletions in the gene that encodes Cu/Zn-superoxide dismutase 1 (SOD1) (Rosen *et al.*, 1993). Transgenic mice carrying mutated human *SOD1* genes have been generated to elucidate SOD1 mediated motor neuron degeneration (Gurney *et al.*, 1994; Wong *et al.*, 1995; Bruijn *et al.*, 1997; Jonsson *et al.*, 2004). To date, numerous hypotheses for ALS pathology exist including glutamate toxicity, oxidative stress, mitochondrial dysfunction, autoimmune mechanisms, protein aggregation, SOD1 accumulation, neuroinflammation, and neuronal death, but the latest hypothesis from Garbuzova-Davis and colleagues (2011) postulates that ALS is a neurovascular disease (Wong *et al.*, 1998; Cleveland, 1999; Garbuzova-Davis *et al.*, 2011; Philips and Robberecht, 2011). A recent study demonstrated that the BSCB of several transgenic mice (hSOD1^{G37R}, hSOD1^{G85R}, hSOD1^{G93A}) is disrupted by reduced levels of the TJ proteins ZO-1, occludin and claudin-5 between the endothelial cells, and that this disruption already occurred at a presymptomatic stage of the disease (Zhong *et al.*, 2008). Therefore, hSOD1 overexpressing endothelial cells were generated to analyze the biochemical processes and involved pathways that may lead to the impaired BSCB integrity of the ALS-causing SOD1 variants. To declare the suitability of this *in vitro* model, the integrity characteristics and the TJ protein expression were compared to isolated pMSCECs.

3.2.1 Expression of hSOD1^{G93A} lead to an impaired integrity in endothelial cells

To elucidate the molecular mechanisms underlying the BSCB breakdown in FALS, the transgenic SOD1 variant G93A was stably transfected in the immortalized murine endothelial cell line bEnd.3 (Figure 3.10). bEnd.3 cells were also stably transfected with wild-type hSOD1, which served as control in the experiments.

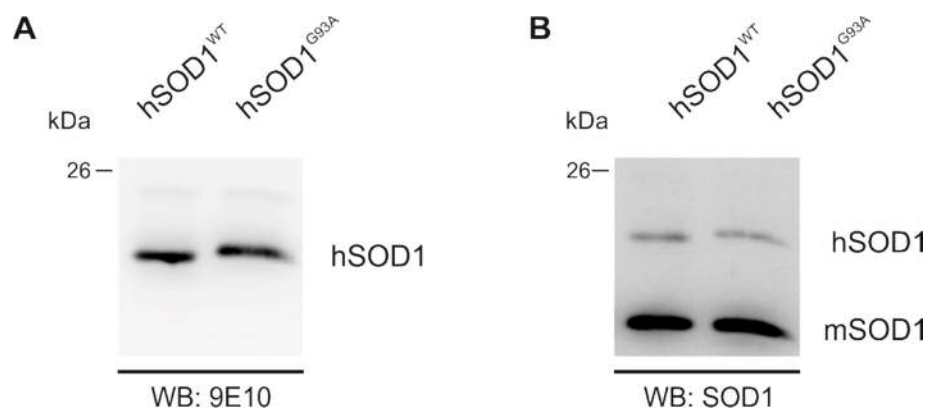


Figure 3.10: Expression of hSOD1^{WT} and hSOD1^{G93A} in bEnd.3 cells. bEnd.3 cells were stably transfected via retroviral transfection. The expression of hSOD1 was analyzed by SDS-PAGE and western blot. The human SOD1 variants were fused to a C-terminal myc-tag. Blots were either incubated with mouse monoclonal 9E10 antibody recognizing the myc-tag (**A**) or rabbit polyclonal SOD1 antibody (**B**), which detects mouse and human SOD1. hSOD1: human SOD1, mSOD1: mouse SOD1.

First, the integrity of bEnd.3 cells was examined. Therefore, cells were seeded on cell culture inserts which were placed into the cellZscope[®] device (described in section 2.5.6, Figure 2.1). The TER of hSOD1^{G93A} bEnd.3 cells was decreased by approx. 20% compared to the hSOD1^{WT} cells (Figure 3.11, A). The C_{Cl} of both cells was comparable (Figure 3.11, B), which demonstrates that the cells built a confluent monolayer and that the decreased TER is due to the impaired tightness of the cells and not to a difference in the confluence. The TER of both hSOD1^{G93A} and hSOD1^{WT} cells increased over time because the expression of TJ proteins is increasingly induced when cells build a confluent monolayer (Koto *et al.*, 2007).

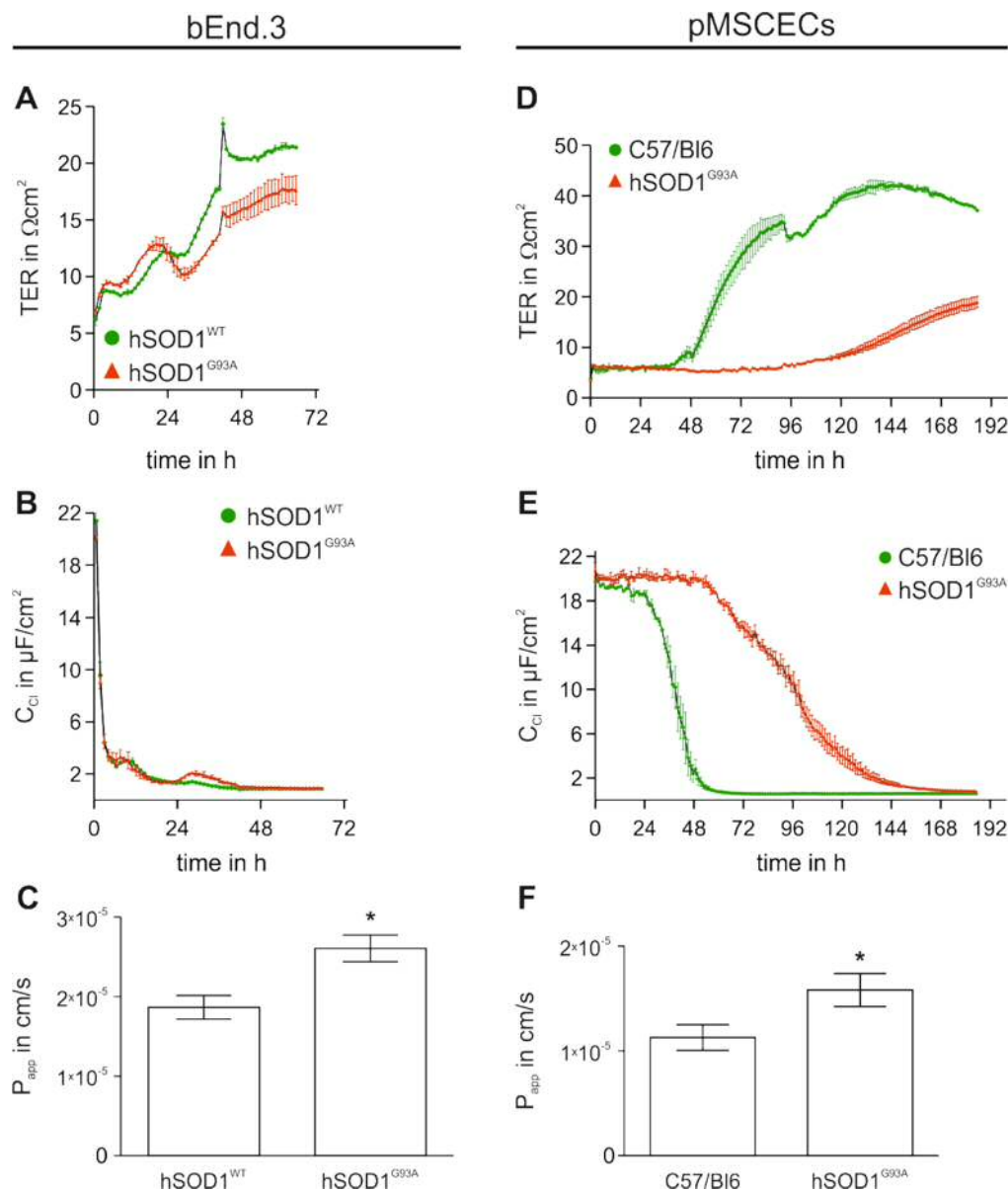


Figure 3.11: Impaired integrity of hSOD1^{G93A} endothelial cells. (A-C) Stable hSOD1^{WT} and hSOD1^{G93A} bEnd.3 cells were cultivated on cell culture insert in the cellZscope® device. (A) Representative TER measurement of stable bEnd.3 cells. (B) Representative C_{Cl} measurement of stable bEnd.3 cells. (C) Apparent permeability of [¹⁴C]-inulin of hSOD1^{G93A} bEnd.3 cells compared to hSOD1^{WT} overexpressing cells. The data represent mean \pm SEM with $n \geq 20$ of 3 independent experiments. * Statistical significance ($p < 0.05$, t-test) between hSOD1^{G93A} and hSOD1^{WT} overexpressing cells is indicated. (D-F) pMSCECs were isolated from 6- to 7-month old hSOD1^{G93A} mice and their littermates. Cells were cultivated on cell culture insert in the cellZscope® device, which measured online the TER and C_{Cl} of the cells. (D) Representative TER and C_{Cl} measurement (E) of cultured pMSCECs. (F) Apparent permeability of [¹⁴C]-inulin of hSOD1^{G93A} pMSCECs compared to their littermates. The data represent mean \pm SEM with $n \geq 9$ of 3 independent experiments. * Statistical significance ($p < 0.05$, t-test) between pMSCECs from hSOD1^{G93A} mice and their littermates is indicated.

The hSOD1^{G93A} cells exhibited a higher permeability of [¹⁴C]-inulin (Figure 3.11, C) which was approx. 40% higher compared to the hSOD1^{WT} cells and demonstrated their impaired integrity. To state the suitability of this *in vitro* model, the integrity of primary mouse spinal cord endothelial cells (pMSCECs) of hSOD1^{G93A} mice was studied as well. The pMSCECs were isolated from presymptomatic mice and their respective littermates and seeded on cell culture inserts which were placed into the cellZscope® device. The TER of hSOD1^{G93A} pMSCECs was decreased by approx. 50% compared to their respective littermates (Figure 3.11, D), even when both pMSCECs cell built a confluent monolayer (Figure 3.11, E). Furthermore, hSOD1^{G93A} pMSCECs exhibited a higher permeability of [¹⁴C]-inulin compared to the littermates pMSCECs, which was increased by approx. 40% (Figure 3.11, C). Although the decrease of the TER values of the immortalized hSOD1^{G93A} is not that striking than in the primary cells, the P_{app} characteristics of these cells are comparable to the pMSCECs. In the hSOD1^{G93A} mice, the transgene is expressed approx. 8 times higher than the endogenous mouse SOD1 (Gurney, 1997; Alexander *et al.*, 2004). In the bEnd.3 cells, the protein levels of hSOD1^{G93A} are approx. 5 times lower than the mSOD1 (Figure 3.10), and importantly, decreased TER and increased P_{app} values were observed in these cells, even though the hSOD1^{G93A} levels are lower than the hSOD1^{WT} in the bend.3 cells. This demonstrates that even low levels of the transgenic hSOD1 lead to a disruption of the endothelial integrity.

In addition, the expression of TJ proteins in the immortalized and primary hSOD1^{G93A} endothelial was examined. Therefore, pMSCECs of hSOD1^{G93A} and hSOD1^{WT} mice were isolated at a presymptomatic stage of the disease, and the expression of the TJ protein claudin-5 was examined in the bEnd.3 cells and pMSCECs by immunofluorescence (Figure 3.12).

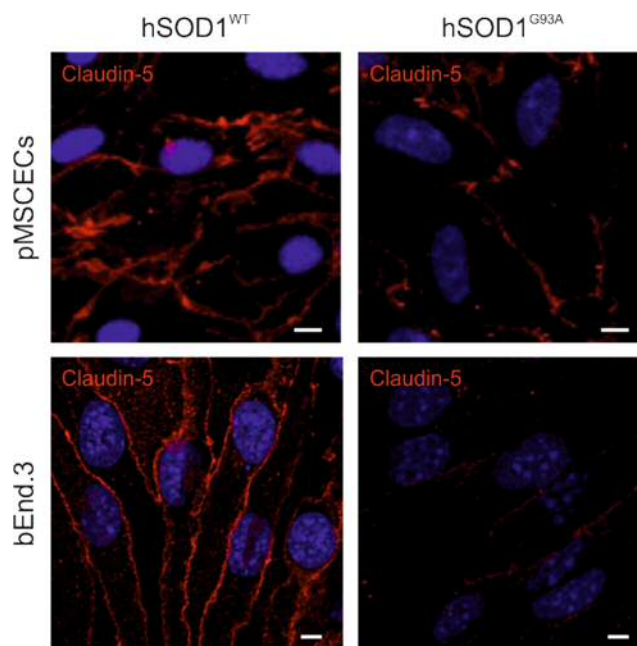


Figure 3.12: Decreased levels of claudin-5 in hSOD1^{G93A} overexpressing endothelial cells. pMSCECs of presymptomatic hSOD1^{WT} and hSOD1^{G93A} mice, and post-confluent bEnd.3 cells overexpressing hSOD1^{WT} or hSOD1^{G93A} were fixed with 4% (w/v) PFA and immunostained for claudin-5, followed by incubation with AlexaFluor 546 secondary antibody. Cell nuclei were stained with DRAQ5TM. Scale bar is 5 μ m.

The levels of claudin-5 are decreased in hSOD1^{G93A} pMSCECs which is in consistence with previous data from Zhong and colleagues. They showed that the expression of claudin-5 and occludin is downregulated in isolated BSCB capillaries of presymptomatic animals (Zhong *et al.*, 2008). Similarly to the pMSCECs, the levels of claudin-5 are decreased in the hSOD1^{G93A} bEnd.3 cells compared to the hSOD1^{WT} cells. This is in consistence with the observed impaired integrity of these cells and the studies of Zhong and colleagues, who postulated that the impaired integrity is due to the reduced expression of the TJ proteins (Zhong *et al.*, 2008). Taken together, the generated hSOD1^{G93A} cell line exhibited comparable integrity characteristics and TJ expression as the isolated pMSCECs from presymptomatic animals demonstrating that this *in vitro* model is suitable for further biochemical studies.

3.2.2 The expression of TJ proteins is decreased in hSOD1^{G93A} endothelial cells

The TJs are the most apical part of the junctional complex on endothelial cells which form a continuous barrier within the intercellular space and the plasma membrane. The expression of TJ proteins is crucial for the tightness of the endothelial cells (Nitta *et al.*, 2003). In both hSOD1^{G93A} pMSCECs and bEnd.3, reduced levels of claudin-5 were observed compared to the respective controls (see section 3.2.1). Previous data demonstrated that the levels of claudin-5 and occludin are downregulated in isolated capillaries from presymptomatic animals (Zhong *et al.*, 2008), but the authors examined the TJ expression in whole lysates of the capillaries and not the decisive surface expression. Thus, the expression of claudin-5 and occludin were examined at the cell surface of post-confluent hSOD1^{G93A} bEnd.3 cells. Therefore, the proteins at the cell surface were covalently labeled with biotin and isolated by a pull down assay using NeutrAvidin coated agarose beads and subsequently analyzed by SDS-PAGE and western blot. The expression of hSOD1^{G93A} led to a decreased expression of claudin-5 in the whole lysate and at the cell surface (Figure 3.13, A): compared to the hSOD1^{WT} cells, the expression in the lysate is reduced by approx. 35% (Figure 3.13, B) and by approx. 32% at the cell surface (Figure 3.13, C). Since the expression of claudin-5 is generally reduced in hSOD1^{G93A} cells and not only at the cell surface, hSOD1^{G93A} may affect the expression of claudin-5.

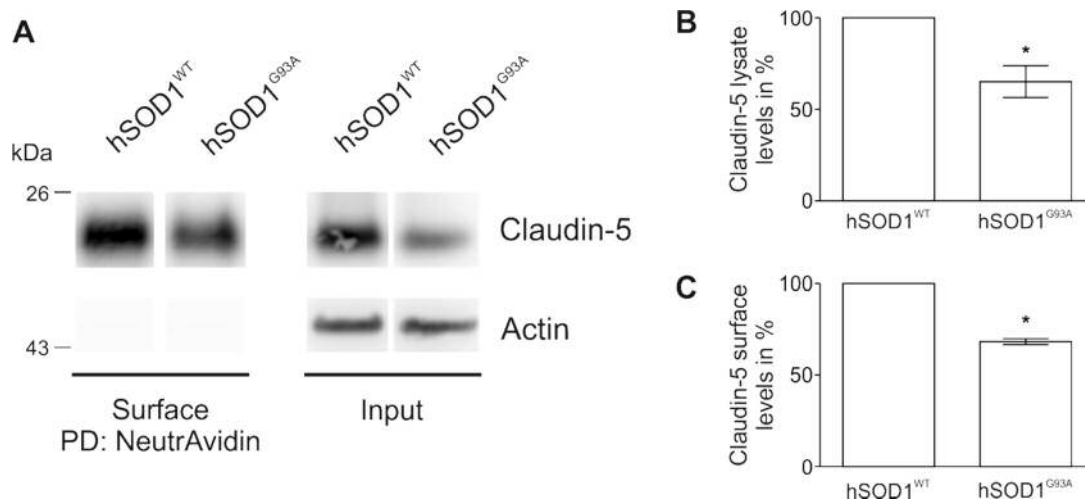


Figure 3.13: Decreased expression and surface levels of the TJ proteins claudin-5 in hSOD1^{G93A} overexpressing cells. (A) Surface proteins of post-confluent bEnd.3 cells stably overexpressing hSOD1^{WT} or hSOD1^{G93A} were biotinylated using sulfo-NHS-biotin. Biotinylated samples were precipitated with NeutrAvidin agarose beads and analyzed by SDS-PAGE and western blot (PD: NeutrAvidin; right panel). As input controls, 20 μ g of cell lysates were used (input; left panel). All samples were analyzed on the same western blot but in a different order and rearranged for better understanding. Polyclonal α -Actin antibody served as loading control to verify the absence of endomembrane contaminants in the biotinylation. (B-C) Claudin-5 levels in the lysate (B) or at the cell surface (C) were quantified by densitometric analysis of western blots. Intensities of hSOD1^{WT} cells were set as 100%. The data represents mean \pm SEM of 6 independent experiments. * Statistically significant difference ($p < 0.05$, t-test) between claudin-5 levels of stable hSOD1^{WT} and hSOD1^{G93A} cells are indicated.

The levels of occludin are also decreased in the hSOD1^{G93A} bEnd.3 compared to hSOD1^{WT} bEnd.3 (Figure 3.14, A). The levels in the lysate are reduced by approx. 18% (Figure 3.14, B) and by approx. 21% (Figure 3.14, B) at the cell surface. Previous studies have shown that reduced levels of occludin result in decreased TER values and higher permeability of fluorescently labeled glucane (Jiang *et al.*, 1999; Ye *et al.*, 2003). Furthermore, it was shown that the localization of claudin-5 at the cell surface correlated with the development of the TER and that the integrity of endothelial cells can be disturbed by silencing the translation of claudin-5 (Koto *et al.*, 2007). Taken together, these data strongly indicate that the expression of hSOD1^{G93A} leads to reduced cell surface levels of claudin-5 and occludin which subsequently results in an impaired integrity of the hSOD1^{G93A} endothelial cells.

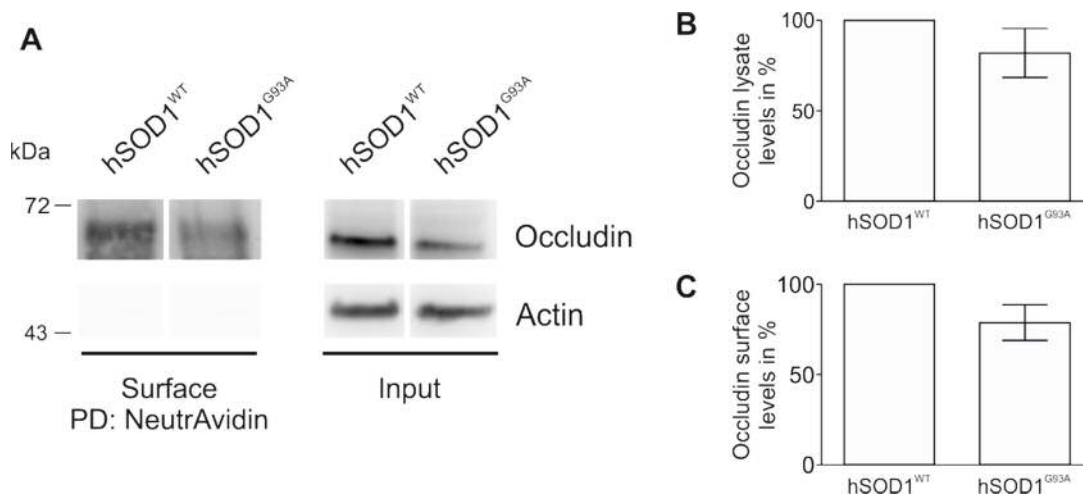


Figure 3.14: Decreased expression and surface levels of the TJ proteins occludin in hSOD1^{G93A} overexpressing cells. (A) Surface proteins of post-confluent bEnd.3 cells stably overexpressing hSOD1^{WT} or hSOD1^{G93A} were biotinylated using sulfo-NHS-biotin. Biotinylated samples were precipitated with NeutrAvidin agarose beads and analyzed by SDS-PAGE and western blot (PD: NeutrAvidin; right panel). As input controls, 20 μ g of cell lysates were used (input; left panel). All samples were analyzed on the same western blot but in a different order and rearranged for better understanding. Polyclonal α -Actin antibody served as loading control to verify the absence of endomembrane contaminants in the biotinylation. (B-C) Occludin levels in the lysate (B) or at the cell surface (C) were quantified by densitometric analysis of western blots. Intensities of hSOD1^{WT} cells were set as 100%. The data represents mean \pm SEM of 4 independent experiments.

3.2.3 The β cat/AKT/FoxO1 pathway is altered in hSOD1^{G93A} cells

Since the previous data strongly indicate that the expression of TJ proteins is affected in hSOD1^{G93A} cells, the pathways that are involved in the *claudin-5* expression were examined. Recently, it was shown that the β cat/AKT/forkhead box protein O1 (FoxO1) pathway regulates the claudin-5 expression (Taddei *et al.*, 2008; Gavard and Gutkind, 2008; Beard *et al.*, 2011). Taddei and colleagues observed that VE-cadherin-mediated adhesion triggers a sustained activation of the phosphatidylinositol-3-kinase (PI3K) and AKT pathway. The phosphorylation of AKT leads to the phosphorylation of FoxO1, which prevents the nuclear accumulation of FoxO1 and leads consequently to the expression of claudin-5 (Figure 3.15, A). In the absence of VE-cadherin or prolonged exposure to pro-permeability factors that disrupt adherens junctions and trigger the local formation of reactive oxygen species (ROS),

unphosphorylated FoxO1 constitutively accumulates in the nucleus, forms a complex with β cat and T-cell factor (TCF), and the FoxO1/ β cat/TCF binds to the promoter of the *claudin-5* gene and represses its transcription (Figure 3.15, B).

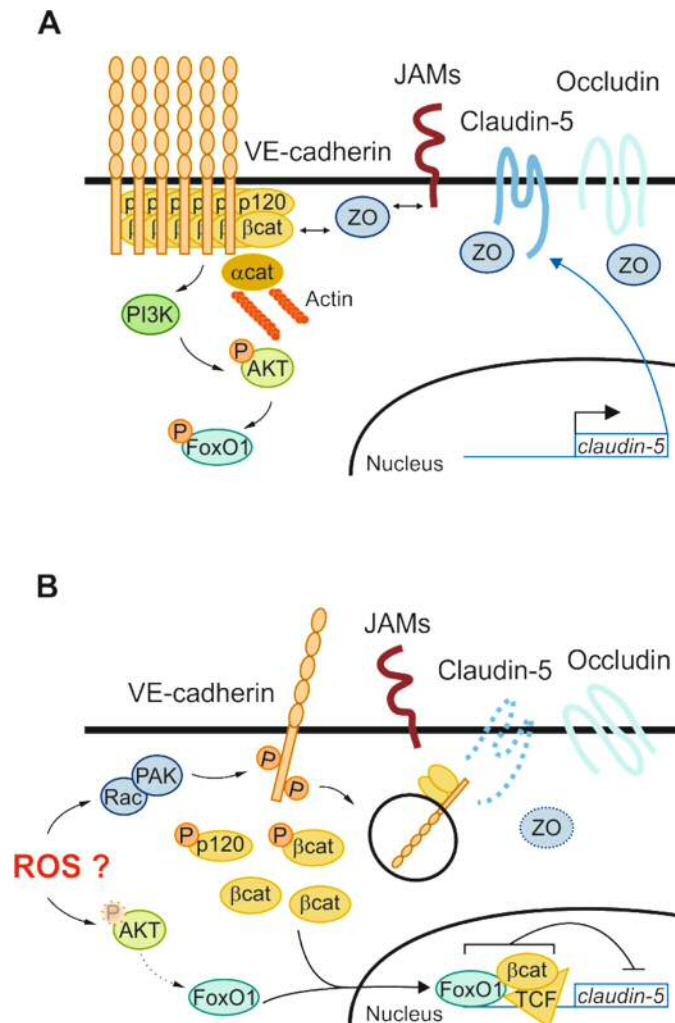


Figure 3.15: The expression of *claudin-5* is regulated by the β cat/AKT/FoxO1 pathway. (A) The crosstalk of adherens and tight junctions (TJ) regulates the barrier function in endothelial cells. The adhesion of VE-cadherin leads downstream to an activation of the PI3K and AKT pathway. Phosphorylation of FoxO1 through AKT activation (pAKT) prevents the nuclear accumulation of β cat and FoxO1 and leads consequently to the expression of *claudin-5*. (B) The local formation of ROS causes an accumulation of β cat and FoxO1 in the nucleus, which leads to a complex formation of β cat and FoxO1 with TCF, and this complex binds to the *claudin-5* promoter and inhibits its transcription. This results in the loss of claudin-5 in TJs, in the disruption of the endothelial barrier function and in enhanced permeability (β cat: β -catenin, JAM: Junctional adhesion molecule, PI3K: phosphatidylinositol-3-kinase, ROS: reactive oxygen species, TCF: T-cell factor; adapted from Gavard and Gutkind, 2008 and Taddei et al., 2008).

Thus, some proteins of this pathway were analyzed in the hSOD1^{G93A} cells. Therefore, the phosphorylation states of β cat, AKT and FoxO1 were examined by SDS-PAGE and western blot (Figure 3.16). A recent study demonstrated that the translocation of β cat to the nucleus and its attachment to the *claudin-5* promoter results in reduced levels of claudin-5 (Beard *et al.*, 2011). The nuclear translocation is induced by the phosphorylation of β cat at Ser675 (Taurin *et al.*, 2006; Hino *et al.*, 2005). In the nucleus, β cat can interact with members of TCF transcription factors and subsequently regulate the expression of downstream target genes. Here, increased levels of p β cat in the hSOD1^{G93A} cells were observed compared to the wild-type (Figure 3.16, A-B) indicating an increased transcriptional activity. Since the nuclear accumulation of β cat was shown to regulate the *claudin-5* expression, and as well decreased levels of claudin-5 and increased levels of p β cat, these results strongly indicates that the impaired integrity of hSOD1^{G93A} is a result of an altered pathway responsible for TJ protein expression. In addition, it was shown that the nuclear levels of β cat are increased in ALS spinal cords of hSOD1^{G93A} mice (Chen *et al.*, 2012). In contrary to the study performed by Chen and colleagues, endothelial cells were used in this study, and it was previously shown that the expression of *claudin-5* is affected in bEnd.3 cells by the β cat/FoxO1 pathway (Beard *et al.*, 2011). Since pAKT is involved in this pathway as well, the phosphorylation state of AKT was examined in hSOD1^{G93A} cells. Decreased levels of pAKT compared to the wild-type could be detected in hSOD1^{G93A} cells (Figure 3.16, C-D). The role of AKT in ALS has been studied in various systems, but the results are contradictory (Lunn *et al.*, 2009). For instance, decreased levels of phosphorylated AKT were observed in motor neurons of both familial and sporadic ALS patients and in hSOD1^{G93A} mice prior to symptom onset (Dewil *et al.*, 2007), as well as in atrophic muscles of symptomatic hSOD1^{G93A} mice (Dobrowolny *et al.*, 2011). No changes on phosphorylated AKT were examined in an alternate study of hSOD1^{G93A} mouse spinal cords (Peviani *et al.*, 2007). AKT plays a crucial role in several cellular processes including survival, apoptosis, cell cycle progression, and cell growth and furthermore regulates

glycogen metabolism and the expression of T) proteins (Franke *et al.*, 1997; Burgering and Coffey, 1995; Franke *et al.*, 1995; Testa and Bellacosa, 2001; Fresno Vara *et al.*, 2004; Taddei *et al.*, 2008).

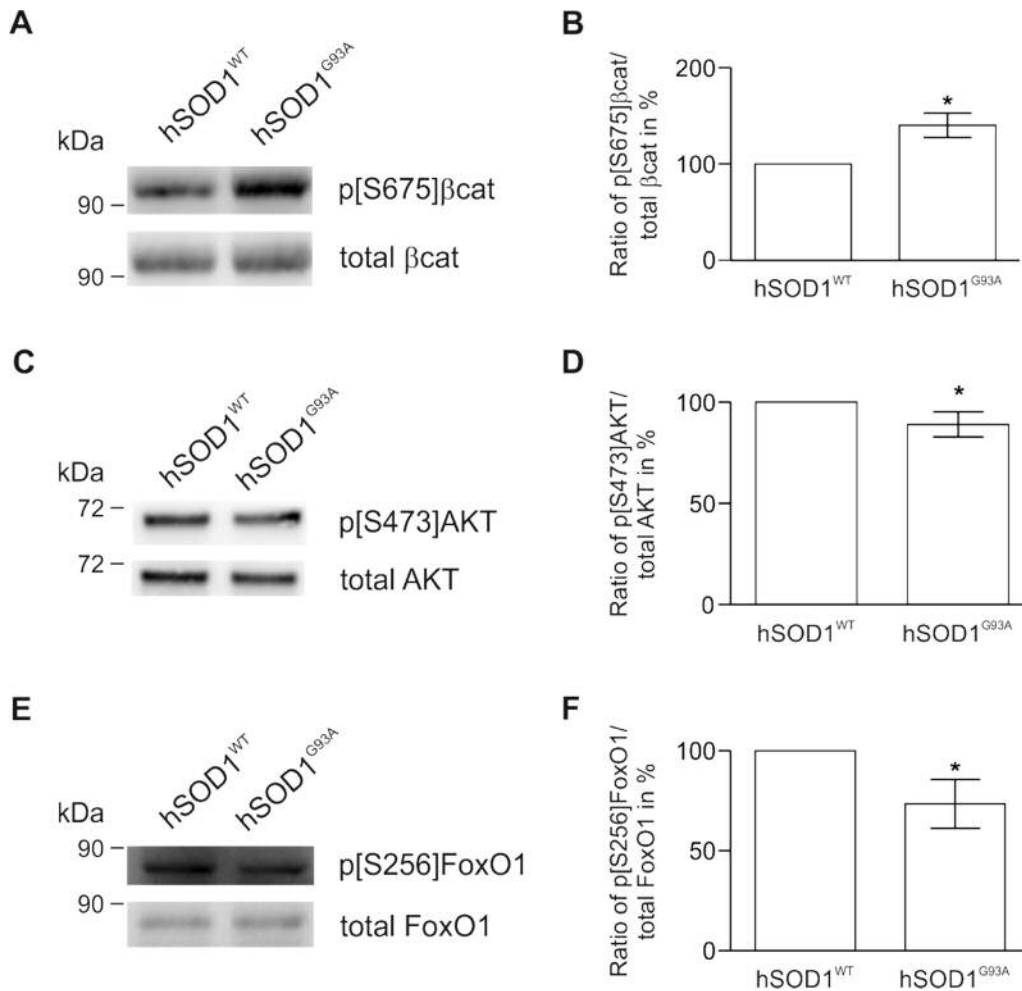


Figure 3.16: Decreased levels of p[S675]βcat, p[S473]AKT and p[S256]FoxO1 in stable hSOD1^{G93A} bEnd.3 cells. The phosphorylation states of p[S675]βcat (A-B), p[S473]AKT (C-D) and p[S256]FoxO1 (E-F) were analyzed in post-confluent hSOD1^{WT} and hSOD1^{G93A} bEnd.3 cells by SDS-PAGE and western blot (A, C, E). Levels of phosphorylated and total proteins were quantified by densitometric analysis of western blots (B, D, F). Intensities were quantified by densitometric analysis of western blots. Intensities were normalized to β-tubulin and the ratio of phosphorylated to total protein was calculated. Ratios of hSOD1^{WT} cells were set as 100%. The data represents mean ± SEM of at least 5 independent experiments. * Statistically significant difference (p<0.05, t-test) between ratios of stable hSOD1^{WT} and hSOD1^{G93A} cells are indicated.

It is complicated to generalize the function of AKT in such a multifactorial disease like ALS. However, the phosphorylation state of AKT in endothelial cells was examined, and according to previous studies in endothelial cells it has

been shown that an inactivation of AKT leads to a decrease of TJ protein expression (Taddei *et al.*, 2008). Since FoxO1 is one of the downstream targets of AKT, and FoxO1 regulates the expression of *claudin-5*, its phosphorylation state was examined in hSOD1^{G93A} cells as well. Unphosphorylated FoxO1 is translocated to the nucleus to repress the expression of its target genes, and the phosphorylation of FoxO1 prevents its transfer to the nucleus. Indeed, decreased levels of pFoxO1 in hSOD1^{G93A} cells compared to the hSOD1^{WT} cells could be detected (Figure 3.16, E-F). AKT was shown to directly phosphorylate FoxO1 (Rena *et al.*, 1999), and reduced levels of pAKT imply its decreased activity which results in an reduced phosphorylation of its target proteins including FoxO1, and this eventually leads to an cytosolic accumulation of FoxO1 and a repression of the *claudin-5* expression (Taddei *et al.*, 2008). Taken together, these data strongly indicate that the protein expression of claudin-5 in hSOD1^{G93A} cells is altered via the β cat/AKT/FoxO1 pathway by repression of the *claudin-5* promoter. Although these data and additional observations by other groups strongly indicate that this alteration is a result of the hSOD1^{G93A} expression, it remains to be determined how exactly this pathway is affected by hSOD1^{G93A} and if this effect is exclusively altered in hSOD1^{G93A} endothelial cells or an overall affect which could be detected in several ALS-causing SOD1 mutant cells.

3.2.4 Endothelial cells expressing ALS-causing SOD1 variants G37R and G85R exhibit similar characteristics like the G93A variant

Since Zhong and colleagues observed that the BSCB is disrupted in hSOD1^{G37R} and hSOD1^{G85R} transgenic mice as well (Zhong *et al.*, 2008), it was investigated if the integrity, the expression of TJ proteins, and the β cat/AKT/FoxO1 pathway is altered in a comparable manner in hSOD1^{G37R} and hSOD1^{G85R} endothelial cells. Therefore, bEnd.3 cells stably overexpressing hSOD1^{G37R} or hSOD1^{G85R} were generated. First, the integrity of these cells was compared to bEnd.3 expressing hSOD1^{WT} (Figure 3.17).

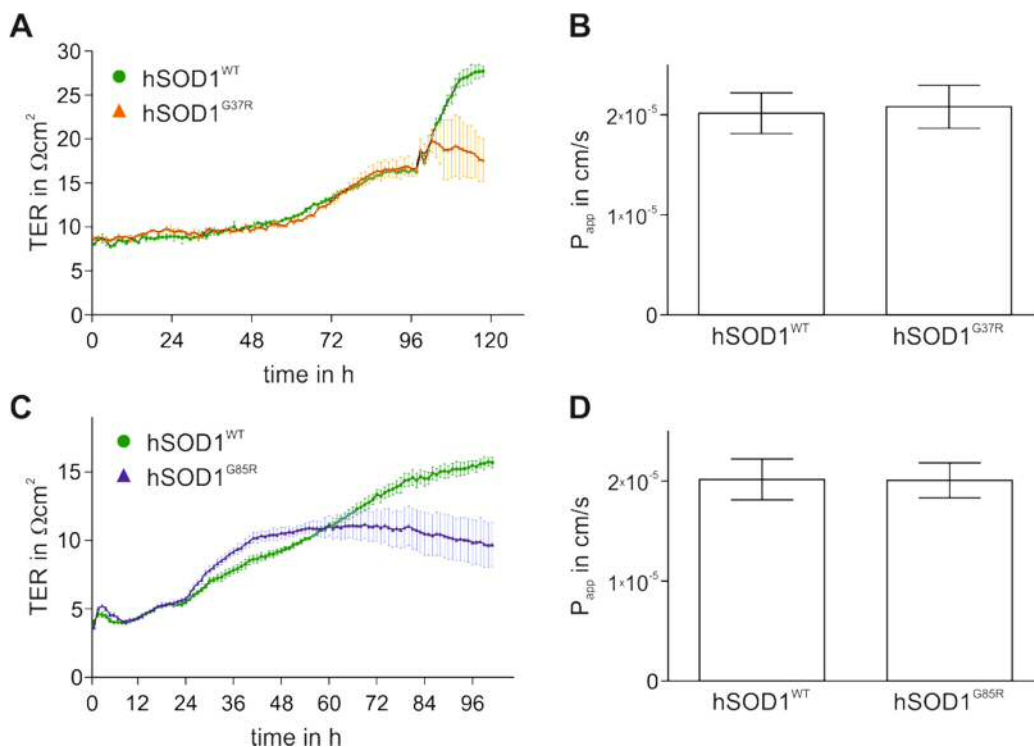


Figure 3.17: Impaired integrity in hSOD1^{G37R} and hSOD1^{G85R} endothelial cells. (A-D) Stable hSOD1^{WT}, hSOD1^{G37R} and hSOD1^{G85R} bEnd.3 cells were cultivated on cell culture insert in the cellZscope® device. (A) Representative TER measurement of stable hSOD1^{G37R} bEnd.3 cells and the respective control. (B) Apparent permeability of [¹⁴C]-inulin of hSOD1^{G37R} bEnd.3 cells compared to hSOD1^{WT} overexpressing cells. The data represent mean \pm SEM with $n \geq 20$ of 3 independent experiments. (C) Representative TER measurement of stable hSOD1^{G85R} bEnd.3 cells and the respective control. (D) Apparent permeability of [¹⁴C]-inulin of hSOD1^{G85R} bEnd.3 cells compared to hSOD1^{WT} overexpressing cells. The data represent mean \pm SEM with $n \geq 20$ of 3 independent experiments.

The expression of hSOD1^{G37R}, as well as of hSOD1^{G85R}, leads to decreased TER values compared to control hSOD1^{WT} bEnd.3 cells (Figure 3.17, A and C). However, mutant SOD1 bEnd.3 cells exhibited no difference of the P_{app} to [¹⁴C]-inulin compared to the control cells (Figure 3.17, B and D). In the hSOD1^{G93A} cells, a nonlinear correlation between the TER and the P_{app} was observed. However, a decreased TER does not necessarily indicate increased paracellular permeability of the cells, because changes in the activity of ion channels or pumps in the plasma membrane may also decrease the TER (Madara, 1988). Otherwise, this could be a gene doses effect, since the levels of hSOD1^{G37R} and hSOD1^{G85R} are not equal to the levels of hSOD1^{WT} (Figure 3.18). However, even small levels of ALS-causing SOD1 variants lead to a decreased TER value in these cells.

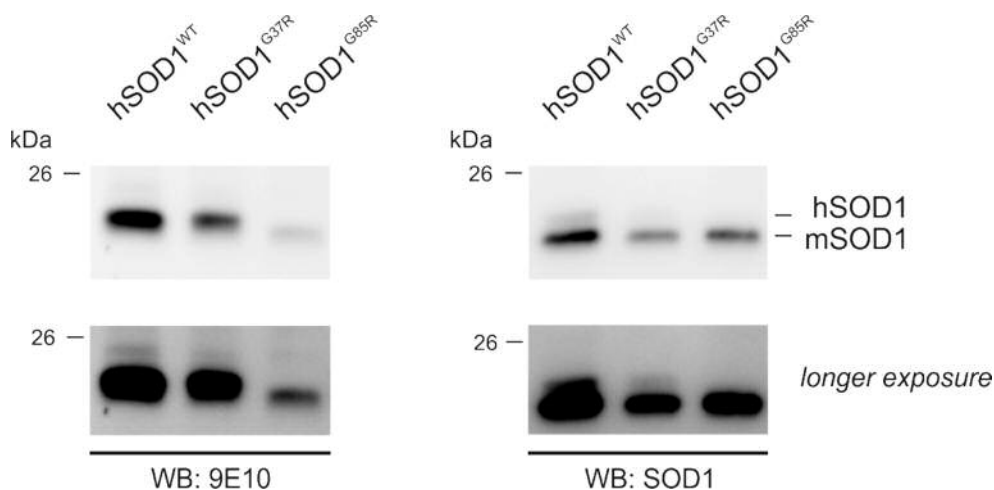


Figure 3.18: Expression of hSOD1^{WT}, hSOD1^{G37R} and hSOD1^{G85R} in bEnd.3 cells. bEnd.3 cells were stably transfected via retroviral transfection. The expression of hSOD1 was analyzed by SDS-PAGE and western blot. The human SOD1 variants were fused to a C-terminal myc-tag. Blots were either incubated with mouse monoclonal 9E10 antibody recognizing the myc-tag (A) or rabbit polyclonal SOD1 antibody (B), which detects mouse and human SOD1. hSOD1: human SOD1, mSOD1: mouse SOD1.

The levels of claudin-5 and occludin were analyzed in hSOD1^{G37R} and hSOD1^{G85R} bEnd.3 cells as well. By immunofluorescence, decreased levels of claudin-5 were observed in the transgenic hSOD1 variants compared to the wild-type (Figure 3.19).

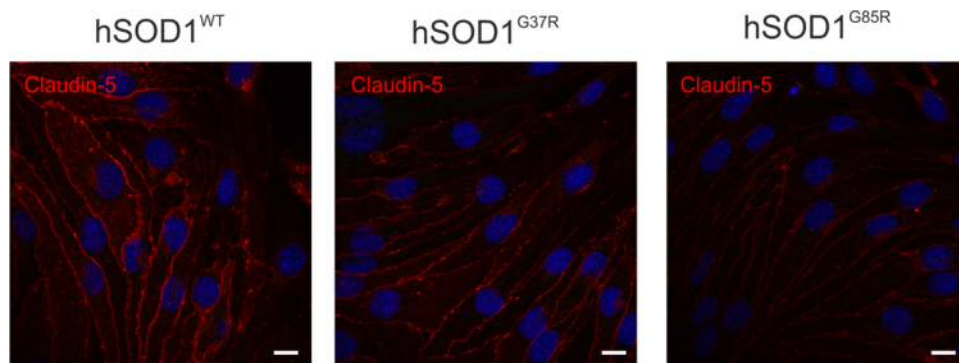


Figure 3.19: Decreased levels of claudin-5 in hSOD1^{G37R} and hSOD1^{G85R} overexpressing cells. hSOD1^{WT}, hSOD1^{G37R}, hSOD1^{G85R} were fixed with 4% (w/v) PFA and immunostained for the TJ protein claudin-5, followed by incubation with AlexaFluor 546 secondary antibody. Cell nuclei were stained with DRAQ5TM. Scale bar is 10 μ m.

These observations indicate that the expression of mutant SOD1 leads to an overall reduction of claudin-5 expression in affected endothelial cells. This is in consistence with previous data from Zhong and colleagues, demonstrating that the BSCB of hSOD1^{G37R}, hSOD1^{G85R} and hSOD1^{G93A} transgenic mice is disrupted by decreased levels of TJ proteins (Zhong *et al.*, 2008). Furthermore, levels of claudin-5 and occludin at the cell surface were examined the in post-confluent hSOD1^{G37R} and hSOD1^{G85R} bEnd.3 cells (Figure 3.20). Analogously to hSOD1^{G93A} cells, the expression of hSOD1^{G37R} and hSOD1^{G85R} led to decreased levels of claudin-5 in the whole lysate and at the cell surface (Figure 3.20, A). Compared to the hSOD1^{WT} cells, claudin-5 levels are reduced by approx. 43% and approx. 45% in the lysate of hSOD1^{G37R} and hSOD1^{G85R} cells (Figure 3.20, B) and by approx. 18% and approx. 20% at the cell surface (Figure 3.20, C). The levels of occludin are also decreased in hSOD1^{G37R} and hSOD1^{G85R} cells compared to the wild-type (Figure 3.20, A): the levels in the lysate are reduced by approx. 21% and 39% (hSOD1^{G37R} and hSOD1^{G85R} (Figure 3.20, D) and by approx. 25% and 40% at the cell surface (Figure 3.20, E). Thus, these data further indicate that the expression of ALS-causing hSOD1 variants leads to reduced cell surface levels of TJ proteins which results in an impaired integrity of the respective endothelial cells.

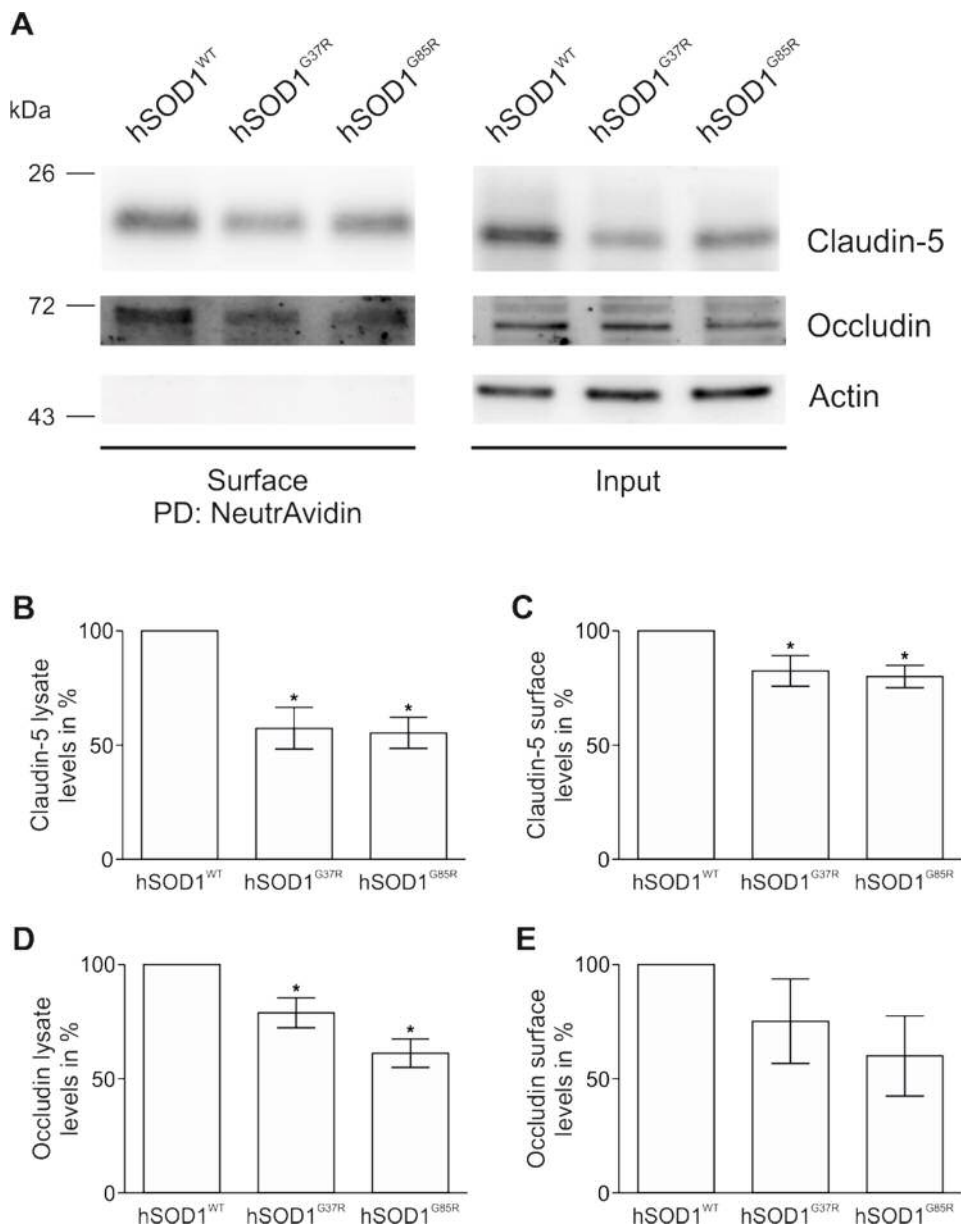


Figure 3.20: Decreased expression and surface levels of the TJ proteins claudin-5 and occludin in hSOD1^{G37R} and hSOD1^{G85R} overexpressing cells. (A) Surface proteins of post-confluent bEnd.3 cells stably overexpressing hSOD1^{WT}, hSOD1^{G37R} or hSOD1^{G85R} were biotinylated using sulfo-NHS-biotin. Biotinylated samples were precipitated with NeutrAvidin agarose beads and analyzed by SDS-PAGE and western blot (PD: NeutrAvidin; right panel). As input controls, 20 μ g of cell lysates were used (input; left panel). Polyclonal α -Actin antibody served as loading control to verify the absence of endomembrane contaminants in the biotinylation. (B-C) Claudin-5 levels in the lysate (B) or at the cell surface (C) were quantified by densitometric analysis of western blots. Intensities of hSOD1^{WT} cells were set as 100%. The data represents mean \pm SEM of 6 independent experiments. (D-E) Occludin levels in the lysate (D) or at the cell surface (E) were quantified by densitometric analysis of western blots. Intensities of hSOD1^{WT} cells were set as 100%. The data represents mean \pm SEM of at least 3 independent experiments. * Statistically significant difference ($p < 0.05$, one-way ANOVA) between the claudin-5 and occludin levels are indicated.

Since decreased levels of the TJ protein claudin-5 in hSOD1^{G37R} and hSOD1^{G85R} were observed, the phosphorylation state of proteins involved in the β cat/AKT/FoxO1 pathway was examined in these cells. Analogously to hSOD1^{G93A} cells, increased levels of p β cat in hSOD1^{G37R} and hSOD1^{G85R} cells could be observed compared to hSOD1^{WT} cells (Figure 3.21, A-B) indicating that the increased transcriptional activity is not limited to the G93A variant of hSOD1 but may be furthermore increased in mutant SOD1 expressing cells. The phosphorylation states of AKT and its downstream target FoxO1 was studied as well in hSOD1^{G37R} and hSOD1^{G85R} cells. Indeed, reduced levels of pAKT and pFoxO1 in the mutant hSOD1 expressing cells were observed compared to the wild-type (Figure 3.21, C-D and E-F). These data furthermore indicate that the protein expression of claudin-5 in mutant hSOD1 cells is altered via the β cat/AKT/FoxO1 pathway which results in impaired integrity of the BSCB and consequently leads to ALS. This hypothesis could be examined in future studies in more detail analyzing the direct interaction of β cat and FoxO1 to the *claudin-5* promoter by chromatin immunoprecipitation (ChIP), or the activity of the claudin-5 promoter could be studied using a reporter gene assay. However, it still remains to be determined how exactly mutant hSOD1 affects this pathway. A recent study postulated a direct link between ALS-causing mutants of SOD1 and the production of ROS (Harraz *et al.*, 2008). Harraz and colleagues proposed a redox sensor model by which SOD1 can regulate NADPH oxidase-dependent (Nox-dependent) production of O₂^{·-} through its ROS-sensitive control of Rac1-GTP hydrolysis. Under reducing conditions, SOD1 binds to Rac1 and inhibits its GTPase activity which consequently leads to an increased production of O₂^{·-}. When the local concentrations of H₂O₂ rise (spontaneously or caused by SOD1), SOD1 dissociates from Rac1, Rac1 is inactivated by GTP hydrolysis, and this leads to an inactivation of the Nox-complex and a reduction in ROS production. The authors observed that this redox-sensitive uncoupling of SOD1 was defective in hSOD1^{G93A} cells leading to an overproduction of ROS (Harraz *et al.*, 2008; Boillee and Cleveland, 2008). The

altered production of ROS may subsequently alter the expression of the TJ proteins which leads to the impaired integrity in SOD1 mutants causing ALS.

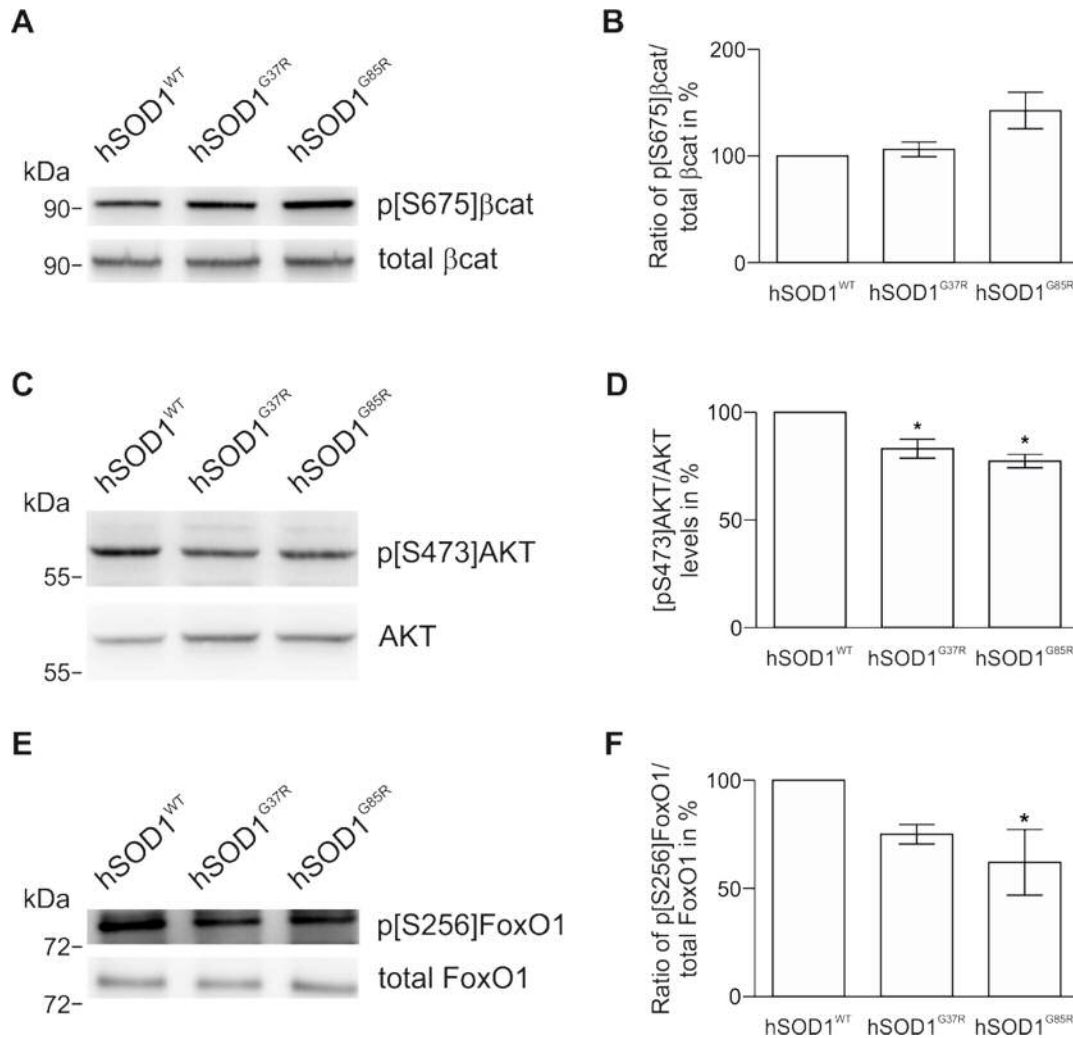


Figure 3.21: Decreased levels of p[S675]βcat, p[S473]AKT and p[S256]FoxO1 in hSOD1^{G37R} and hSOD1^{G85R} overexpressing bEnd.3 cells. The phosphorylation states of p[S675]βcat (A-B), p[S473]AKT (C-D) and p[S256]FoxO1 (E-F) were analyzed in post-confluent hSOD1^{WT}, hSOD1^{G37R} and hSOD1^{G85R} bEnd.3 cells by SDS-PAGE and western blot (A, C, E). Levels of phosphorylated and total proteins were quantified by densitometric analysis of western blots (B, D, F). Intensities were quantified by densitometric analysis of western blots. Intensities were normalized to β-tubulin and the ratio of phosphorylated to total protein was calculated. Ratios of hSOD1^{WT} cells were set as 100%. The data represents mean ± SEM of at least 3 independent experiments. * Statistically significant difference (p<0.05, one-way ANOVA) are indicated.

4

Conclusion & Outlook

Blood-CNS barriers build the physical barrier between the blood and the CNS thereby protecting the CNS from both toxic and pathogenic agents, and their disruption plays a crucial role in the pathogenesis of several CNS disorders (Palmer, 2010). To date, disorders of the CNS are currently affecting over 1.5 billion people worldwide which account for about a third of the global disease burden and constitute 12% of total deaths globally (Palmer, 2010; Murray and Lopez, 1996; Masserini, 2013). They can be classified into three different groups depending on the gradual and progressive loss and the rate of neurodegenerative change. They include chronic neurodegenerative disorders like AD, PD, and ALS, whereby the cause for most of these diseases is still unknown. By contrast, the cause of disorders associated with acute neurodegenerative changes like stroke, traumatic brain and spinal cord injury is clearly known. Lastly, they include CNS disorders like obesity, anxiety, schizophrenia without pronounced neurodegenerative pathology. In this thesis, the role of blood-CNS barriers in neurodegenerative disorders was investigated in two independent projects: Project I: “Nanoparticulate flurbiprofen reduces A β ₄₂ generation in an *in vitro* BBB model” and Project II: “Impaired integrity of the BSCB in a mouse model for ALS”. The first project used a nanotechnology-based strategy to transport therapeutically effective concentrations of AD drugs in an *in vitro* BBB model. Over the past years, the

application of nanotechnology-based strategies for the treatment or diagnosis of AD has been investigated by many groups (Re *et al.*, 2012; Roney *et al.*, 2005). Some approaches focused on the encapsulation of molecules into nanoparticles for the delivery to the brain; others dealt with a reduction of amyloid plaques toxicity, or focused on the early detection of the disease (Brambilla *et al.*, 2011). In this project, embedding of flurbiprofen in polymeric nanoparticles resulted in transport of flurbiprofen across the BBB with retaining its biological activity. However, many improvements and optimizations of the nanoparticles are required for future applications. Usage of GSMs with higher potency or surface modifications of the nanoparticles with peptides or ligands which can achieve a higher bioavailability or a specific targeting to the brain are just some examples (Sahni *et al.*, 2011; Bulic *et al.*, 2011). To date, the number of commercially available nanoparticle-based therapeutic products increased progressively. More than 150 companies are developing nanoscale therapeutics and, so far, 24 nanotechnology-based therapeutics products have been approved for clinical use (Wagner *et al.*, 2006). Among all nanoscale formulations, polymeric nanoparticles have the best combination of characteristics since they are stable, allow high loading of many agents, provide controlled drug release kinetics, and can be modified by a variety of surface-attached ligands (Saltzman, 2001). The first polymer-based formulations for the drug delivery to the CNS were poly(butylcyanoacrylate) (PBCA) nanoparticles (Kreuter *et al.*, 1995). Polyester formulations, such as PLA, polyglycolide (PGA) or poly(lactic-co-glycolic) acid (PLGA), have been shown to penetrate the BBB in a size-dependent manner, as well (Patel *et al.*, 2013). However, polymeric nanoparticles have not yet been studied in clinical trials for the CNS drug delivery, but there are two polymeric nanoparticle drug delivery systems on the market for non-CNS applications: Abraxane[®], which is an albumin-based nanoparticle loaded with paclitaxel and used for the treatment of breast cancer and Abdoscan[®], which is an iron oxide and dextran-based nanoparticle used for diagnostic imaging of liver and spleen (Service, 2010). Over the past years, extensive research demonstrated that the so-called

nanomedicine can afford the drug delivery to the CNS. Taken together, the clinical translation of this technology offers new possibilities for the treatment of CNS disorders including CNS malignancies, ischemic disease and neurodegenerative disorders like AD.

The second project focused on the pathogenesis of SOD1-related familial cases of ALS. ALS is an unrelenting progressive neurodegenerative disorder causing progressive motor neuron degeneration in the brain and spinal cord and leads ultimately to death typically within 3 to 5 years from diagnosis (Haverkamp *et al.*, 1995; Rowland and Shneider, 2001). The only drug that was clinically proven to enhance the survival of ALS patients is Riluzole, but the benefits are only modest and extend ventilator-free survival by approx. 3 months (Bensimon *et al.*, 1994). There are currently more than 50 actively enrolling clinical trials for ALS listed on <http://clinicaltrials.gov/>, which include antiglutamate drugs, antioxidant/mitochondrial preservation drugs, immunosuppressive drugs, muscle-maintenance drugs, stem cell implantations and SOD1 specific treatments (Gibson and Bromberg, 2012). Since the clinical and pathological profiles of sporadic and familial ALS are similar, it is thought that insights from studies of ALS-causing gene mutations can be applied to sporadic ALS cases (Pasinelli and Brown, 2006). However, the determination of the disease-causing mechanism is challenging due to the disease's complexity. Vascular impairment has recently been recognized to be crucial in the ALS pathogenesis: comprised integrity of the blood-CNS barriers in ALS patients and in a mouse model for ALS were demonstrated, as well as structural and functional impairments of these barriers at an early stage of the disease which worsened with the disease progression (Garbuzova-Davis *et al.*, 2007a; Garbuzova-Davis *et al.*, 2007b; Zhong *et al.*, 2008; Nicaise *et al.*, 2009a; Nicaise *et al.*, 2009b; Garbuzova-Davis *et al.*, 2011). Vascular leakage, decreased capillary length and blood flow, microhemorrhages, reduced expression of TJ proteins and basement membrane components have been shown in spinal cord of SOD1 transgenic animals, as well. More important, the breakdown of the BSCB in SOD1 transgenic mice and rats was found prior to

motor neuron degeneration and neurovascular inflammation (Zhong *et al.*, 2008; Nicaise *et al.*, 2009a; Miyazaki *et al.*, 2011). Since neurovascular inflammation, consisting of activated microglia, astrocytes, and inflammatory T-cells, is a common characteristic in ALS, these observations strongly indicate that the BSCB breakdown may be a primary event in ALS. In ALS patients, the loss of endothelial integrity was shown by significant reductions of ZO-1 and occludin mRNAs in the spinal cords (Henkel *et al.*, 2009). In a recent study, Garbuzova-Davis and colleagues investigated the blood-CNS integrity in postmortem tissues of patients with sporadic ALS. Their major findings include endothelial cell damage and pericyte degeneration, several intra- and extracellular edema, IgG microvascular leakage and reduced TJ and adhesion protein expressions (Garbuzova-Davis *et al.*, 2012). In the second project of this thesis, an *in vitro* model for ALS endothelial cells was generated that exhibit comparable integrity characteristics and TJ expression profiles as isolated pMSCECs of SOD1 transgenic mice. Furthermore, an altered regulation of the β cat/AKT/FoxO1 pathway was observed in hSOD1^{G93A} cells that potentially result in an impaired integrity and correspondingly to the disruption of the BSCB in ALS-causing SOD1 mutants. Thus, there is evidence that ALS is a neurovascular disease. And when the endothelial damage is one of the primary events in ALS pathology leading to the infiltration of immunoreactive cells and substances into the CNS and subsequently to neuronal cell death, immunosuppressive drugs may be promising for the treatment of ALS. Multiple immunosuppressive drugs have been studied, but most failed to alter disease progression (Gibson and Bromberg, 2012). In the phase III clinical trial of minocycline, a tetracycline antibiotic that decreases inflammation by inhibiting microglial activation, treated patients had a significantly greater decline in the ALS Functional Rating Scale (ALSF_{RS}-R) score (Gordon *et al.*, 2007). Furthermore, a nonsignificant trend toward a faster decline in breathing function, muscle strength, and mortality could be also observed. The treatment of symptomatic hSOD1^{G93A} mice with minocycline showed that minocycline given at a symptomatic stage caused an

increased inflammatory response which is likely the reason for its failure in the clinical trial (Keller *et al.*, 2011). However, another new drug, NP001, targets a different mechanism of neuroinflammation by regulating macrophage activation and potentially returning macrophages back to their neuroprotective state (Neuraltus, 2012). Recently, the phase II clinical trial was completed (<http://clinicaltrials.gov/> #NCT01281631) and the drug was determined to be safe and tolerable at doses given. Furthermore, the levels of ALS progression biomarkers had a statistically significant dose-dependent decrease for NP001 treatment, and the clinical trial phase III is planned. Thus, understanding of the primary events in ALS pathogenesis will hopefully provide ideas for the development of new therapeutic strategies, if not even therapeutic options to decline the disease progression, better living conditions for the patients or even causal therapeutic options.

5

References

- Abbott, N.J., Chugani, D.C., Zaharchuk, G., Rosen, B.R., Lo, E.H., 1999. Delivery of imaging agents into brain. *Adv Drug Deliv Rev.* 37, 253-77.
- Abbott, N.J., Ronnback, L., Hansson, E., 2006. Astrocyte-endothelial interactions at the blood-brain barrier. *Nature Reviews Neuroscience.* 7, 41-53.
- Alexander, G.M., Erwin, K.L., Byers, N., Deitch, J.S., Augelli, B.J., Blankenhorn, E.P., Heiman-Patterson, T.D., 2004. Effect of transgene copy number on survival in the G93A SOD1 transgenic mouse model of ALS. *Brain Res Mol Brain Res.* 130, 7-15.
- Alzheimer's, A., 2012. 2012 Alzheimer's disease facts and figures. *Alzheimers Dement.* 8, 131-68.
- Alzheimer, A., 1906. Über einen eigenartigen schweren Krankheitsprozess der Hirnrinde. *Neurologisches Zentralblatt, Leipzig.* 25, 1134.
- Aszalos, A., 2008. Role of ATP-binding cassette (ABC) transporters in interactions between natural products and drugs. *Current Drug Metabolism.* 9, 1010-8.
- Barber, S.C., Mead, R.J., Shaw, P.J., 2006. Oxidative stress in ALS: a mechanism of neurodegeneration and a therapeutic target. *Biochim Biophys Acta.* 1762, 1051-67.
- Bartanusz, V., Jezova, D., Alajajian, B., Digicaylioglu, M., 2011. The blood-spinal cord barrier: morphology and clinical implications. *Ann Neurol.* 70, 194-206.
- Beard, R.S., Jr., Reynolds, J.J., Bearden, S.E., 2011. Hyperhomocysteinemia increases permeability of the blood-brain barrier by NMDA receptor-dependent regulation of adherens and tight junctions. *Blood.* 118, 2007-14.
- Bensimon, G., Lacomblez, L., Meininger, V., 1994. A controlled trial of riluzole in amyotrophic lateral sclerosis. ALS/Riluzole Study Group. *New England Journal of Medicine.* 330, 585-91.

References

- Bernacki, J., Dobrowolska, A., Nierwinska, K., Malecki, A., 2008. Physiology and pharmacological role of the blood-brain barrier. *Pharmacol Rep.* 60, 600-22.
- Boillee, S., Vande Velde, C., Cleveland, D.W., 2006. ALS: a disease of motor neurons and their nonneuronal neighbors. *Neuron.* 52, 39-59.
- Boillee, S., Cleveland, D.W., 2008. Revisiting oxidative damage in ALS: microglia, Nox, and mutant SOD1. *J Clin Invest.* 118, 474-8.
- Brambilla, D., Le Droumaguet, B., Nicolas, J., Hashemi, S.H., Wu, L.P., Moghimi, S.M., Couvreur, P., Andrieux, K., 2011. Nanotechnologies for Alzheimer's disease: diagnosis, therapy, and safety issues. *Nanomedicine.* 7, 521-40.
- Brightman, M.W., Hori, M., Rapoport, S.I., Reese, T.S., Westergaard, E., 1973. Osmotic opening of tight junctions in cerebral endothelium. *J Comp Neurol.* 152, 317-25.
- Bruijn, L.I., Becher, M.W., Lee, M.K., Anderson, K.L., Jenkins, N.A., Copeland, N.G., Sisodia, S.S., Rothstein, J.D., Borchelt, D.R., Price, D.L., Cleveland, D.W., 1997. ALS-linked SOD1 mutant G85R mediates damage to astrocytes and promotes rapidly progressive disease with SOD1-containing inclusions. *Neuron.* 18, 327-38.
- Bulic, B., Ness, J., Hahn, S., Rennhack, A., Jumpertz, T., Weggen, S., 2011. Chemical Biology, Molecular Mechanism and Clinical Perspective of gamma-Secretase Modulators in Alzheimer's Disease. *Current Neuropharmacology.* 9, 598-622.
- Burdick, D., Soreghan, B., Kwon, M., Kosmoski, J., Knauer, M., Henschen, A., Yates, J., Cotman, C., Glabe, C., 1992. Assembly and aggregation properties of synthetic Alzheimer's A4/beta amyloid peptide analogs. *J Biol Chem.* 267, 546-54.
- Burgering, B.M., Coffey, P.J., 1995. Protein kinase B (c-Akt) in phosphatidylinositol-3-OH kinase signal transduction. *Nature.* 376, 599-602.
- Burnette, W.N., 1981. "Western blotting": electrophoretic transfer of proteins from sodium dodecyl sulfate--polyacrylamide gels to unmodified nitrocellulose and radiographic detection with antibody and radioiodinated protein A. *Analytical Biochemistry.* 112, 195-203.
- Carmeliet, P., Lampugnani, M.G., Moons, L., Breviario, F., Compernelle, V., Bono, F., Balconi, G., Spagnuolo, R., Oosthuysse, B., Dewerchin, M., Zanetti, A., Angellilo, A., Mattot, V., Nuyens, D., Lutgens, E., Clotman, F., de Ruiter, M.C., Gittenberger-de Groot, A., Poelmann, R., Lupu, F., Herbert, J.M., Collen, D., Dejana, E., 1999. Targeted deficiency or cytosolic truncation of the VE-cadherin gene in mice impairs VEGF-mediated endothelial survival and angiogenesis. *Cell.* 98, 147-57.
- Chen, Y., Guan, Y., Liu, H., Wu, X., Yu, L., Wang, S., Zhao, C., Du, H., Wang, X., 2012. Activation of the Wnt/beta-catenin signaling pathway is associated with glial proliferation in the adult spinal cord of ALS transgenic mice. *Biochemical and Biophysical Research Communications.* 420, 397-403.

- Cleveland, D.W., 1999. From Charcot to SOD1: mechanisms of selective motor neuron death in ALS. *Neuron*. 24, 515-20.
- Cleveland, D.W., Liu, J., 2000. Oxidation versus aggregation - how do SOD1 mutants cause ALS? *Nat Med*. 6, 1320-1.
- Craparo, E.F., Bondi, M.L., Pitarresi, G., Cavallaro, G., 2011. Nanoparticulate systems for drug delivery and targeting to the central nervous system. *CNS Neurosci Ther*. 17, 670-7.
- Daniel, P.M., Lam, D.K., Pratt, O.E., 1985. Comparison of the vascular permeability of the brain and the spinal cord to mannitol and inulin in rats. *J Neurochem*. 45, 647-9.
- Dauchy, S., Dutheil, F., Weaver, R.J., Chassoux, F., Daumas-Duport, C., Couraud, P.O., Scherrmann, J.M., De Waziers, I., Declèves, X., 2008. ABC transporters, cytochromes P450 and their main transcription factors: expression at the human blood-brain barrier. *J Neurochem*. 107, 1518-28.
- Dejana, E., Lampugnani, M.G., Martinez-Estrada, O., Bazzoni, G., 2000. The molecular organization of endothelial junctions and their functional role in vascular morphogenesis and permeability. *Int J Dev Biol*. 44, 743-8.
- Dewil, M., Lambrechts, D., Sciot, R., Shaw, P.J., Ince, P.G., Robberecht, W., Van den Bosch, L., 2007. Vascular endothelial growth factor counteracts the loss of phospho-Akt preceding motor neurone degeneration in amyotrophic lateral sclerosis. *Neuropathol Appl Neurobiol*. 33, 499-509.
- Dobrowolny, G., Aucello, M., Musaro, A., 2011. Muscle atrophy induced by SOD1G93A expression does not involve the activation of caspase in the absence of denervation. *Skelet Muscle*. 1, 3.
- Donnenfeld, H., Kascsak, R.J., Bartfeld, H., 1984. Deposits of IgG and C3 in the spinal cord and motor cortex of ALS patients. *Journal of Neuroimmunology*. 6, 51-7.
- Doody, R.S., Raman, R., Farlow, M., Iwatsubo, T., Vellas, B., Joffe, S., Kieburtz, K., He, F., Sun, X., Thomas, R.G., Aisen, P.S., Alzheimer's Disease Cooperative Study Steering, C., Siemers, E., Sethuraman, G., Mohs, R., Semagacestat Study, G., 2013. A phase 3 trial of semagacestat for treatment of Alzheimer's disease. *New England Journal of Medicine*. 369, 341-50.
- Ehrlich, P., 1885. *Das Sauerstoff-Bedürfniss des Organismus, Eine farbenanalytische Studie*. Vol., Berlin.
- Emi, N., Friedmann, T., Yee, J.K., 1991. Pseudotype formation of murine leukemia virus with the G protein of vesicular stomatitis virus. *Journal of Virology*. 65, 1202-7.
- Engelhardt, J.I., Appel, S.H., 1990. IgG reactivity in the spinal cord and motor cortex in amyotrophic lateral sclerosis. *Arch Neurol*. 47, 1210-6.
- Eriksen, J.L., Sagi, S.A., Smith, T.E., Weggen, S., Das, P., McLendon, D.C., Ozols, V.V., Jessing, K.W., Zavitz, K.H., Koo, E.H., Golde, T.E., 2003. NSAIDs and enantiomers

References

- of flurbiprofen target gamma-secretase and lower Abeta 42 in vivo. *J Clin Invest.* 112, 440-9.
- Feldman, G.J., Mullin, J.M., Ryan, M.P., 2005. Occludin: structure, function and regulation. *Adv Drug Deliv Rev.* 57, 883-917.
- Fischer, S., Wobben, M., Marti, H.H., Renz, D., Schaper, W., 2002. Hypoxia-induced hyperpermeability in brain microvessel endothelial cells involves VEGF-mediated changes in the expression of zonula occludens-1. *Microvasc Res.* 63, 70-80.
- Franke, T.F., Yang, S.I., Chan, T.O., Datta, K., Kazlauskas, A., Morrison, D.K., Kaplan, D.R., Tsichlis, P.N., 1995. The protein kinase encoded by the Akt proto-oncogene is a target of the PDGF-activated phosphatidylinositol 3-kinase. *Cell.* 81, 727-36.
- Franke, T.F., Kaplan, D.R., Cantley, L.C., 1997. PI3K: downstream AKTion blocks apoptosis. *Cell.* 88, 435-7.
- Fresno Vara, J.A., Casado, E., de Castro, J., Cejas, P., Belda-Iniesta, C., Gonzalez-Baron, M., 2004. PI3K/Akt signalling pathway and cancer. *Cancer Treat Rev.* 30, 193-204.
- Fridovich, I., 1995. Superoxide radical and superoxide dismutases. *Annual Review of Biochemistry.* 64, 97-112.
- Furuse, M., Hirase, T., Itoh, M., Nagafuchi, A., Yonemura, S., Tsukita, S., Tsukita, S., 1993. Occludin: a novel integral membrane protein localizing at tight junctions. *J Cell Biol.* 123, 1777-88.
- Furuse, M., Sasaki, H., Tsukita, S., 1999. Manner of interaction of heterogeneous claudin species within and between tight junction strands. *J Cell Biol.* 147, 891-903.
- Galasko, D.R., Graff-Radford, N., May, S., Hendrix, S., Cottrell, B.A., Sagi, S.A., Mather, G., Laughlin, M., Zavitz, K.H., Swabb, E., Golde, T.E., Murphy, M.P., Koo, E.H., 2007. Safety, tolerability, pharmacokinetics, and Abeta levels after short-term administration of R-flurbiprofen in healthy elderly individuals. *Alzheimer Dis Assoc Disord.* 21, 292-9.
- Garbuzova-Davis, S., Haller, E., Saporta, S., Kolomey, I., Nicosia, S.V., Sanberg, P.R., 2007a. Ultrastructure of blood-brain barrier and blood-spinal cord barrier in SOD1 mice modeling ALS. *Brain Res.* 1157, 126-37.
- Garbuzova-Davis, S., Saporta, S., Haller, E., Kolomey, I., Bennett, S.P., Potter, H., Sanberg, P.R., 2007b. Evidence of compromised blood-spinal cord barrier in early and late symptomatic SOD1 mice modeling ALS. *PLoS One.* 2, e1205.
- Garbuzova-Davis, S., Rodrigues, M.C., Hernandez-Ontiveros, D.G., Louis, M.K., Willing, A.E., Borlongan, C.V., Sanberg, P.R., 2011. Amyotrophic lateral sclerosis: a neurovascular disease. *Brain Res.* 1398, 113-25.

- Garbuzova-Davis, S., Hernandez-Ontiveros, D.G., Rodrigues, M.C., Haller, E., Frisina-Deyo, A., Mirtyl, S., Sallot, S., Saporta, S., Borlongan, C.V., Sanberg, P.R., 2012. Impaired blood-brain/spinal cord barrier in ALS patients. *Brain Res.* 1469, 114-28.
- Gavard, J., Gutkind, J.S., 2008. VE-cadherin and claudin-5: it takes two to tango. *Nature Cell Biology.* 10, 883-5.
- Ge, S., Pachter, J.S., 2006. Isolation and culture of microvascular endothelial cells from murine spinal cord. *Journal of Neuroimmunology.* 177, 209-14.
- Gibson, S.B., Bromberg, M.B., 2012. Amyotrophic lateral sclerosis: drug therapy from the bench to the bedside. *Semin Neurol.* 32, 173-8.
- Golde, T.E., 2003. Alzheimer disease therapy: can the amyloid cascade be halted? *J Clin Invest.* 111, 11-8.
- Golde, T.E., 2006. Disease modifying therapy for AD? *J Neurochem.* 99, 689-707.
- Goldmann, E.E., 1909. Die äussere und innere Sekretion des gesunden und kranken Organismus im Lichte der "vitalen Färbung". Vol., H. Laupp.
- Gordon, P.H., Moore, D.H., Miller, R.G., Florence, J.M., Verheijde, J.L., Doorish, C., Hilton, J.F., Spitalny, G.M., MacArthur, R.B., Mitsumoto, H., Neville, H.E., Boylan, K., Mozaffar, T., Belsh, J.M., Ravits, J., Bedlack, R.S., Graves, M.C., McCluskey, L.F., Barohn, R.J., Tandan, R., Western, A.L.S.S.G., 2007. Efficacy of minocycline in patients with amyotrophic lateral sclerosis: a phase III randomised trial. *Lancet Neurol.* 6, 1045-53.
- Grabovac, V., Bernkop-Schnurch, A., 2007. Development and in vitro evaluation of surface modified poly(lactide-co-glycolide) nanoparticles with chitosan-4-thiobutylamidine. *Drug Dev Ind Pharm.* 33, 767-74.
- Green, R.C., Schneider, L.S., Amato, D.A., Beelen, A.P., Wilcock, G., Swabb, E.A., Zavitz, K.H., Tarenflur bil Phase 3 Study, G., 2009. Effect of tarenflur bil on cognitive decline and activities of daily living in patients with mild Alzheimer disease: a randomized controlled trial. *JAMA.* 302, 2557-64.
- Grosch, S., Tegeder, I., Schilling, K., Maier, T.J., Niederberger, E., Geisslinger, G., 2003. Activation of c-Jun-N-terminal-kinase is crucial for the induction of a cell cycle arrest in human colon carcinoma cells caused by flurbiprofen enantiomers. *FASEB J.* 17, 1316-8.
- Gurney, M.E., Pu, H., Chiu, A.Y., Dal Canto, M.C., Polchow, C.Y., Alexander, D.D., Caliendo, J., Hentati, A., Kwon, Y.W., Deng, H.X., et al., 1994. Motor neuron degeneration in mice that express a human Cu,Zn superoxide dismutase mutation. *Science.* 264, 1772-5.
- Gurney, M.E., 1997. The use of transgenic mouse models of amyotrophic lateral sclerosis in preclinical drug studies. *J Neurol Sci.* 152 Suppl 1, S67-73.

References

- Haapasalo, A., Kovacs, D.M., 2011. The many substrates of presenilin/gamma-secretase. *J Alzheimers Dis.* 25, 3-28.
- Haass, C., Hung, A.Y., Schlossmacher, M.G., Oltersdorf, T., Teplow, D.B., Selkoe, D.J., 1993. Normal cellular processing of the beta-amyloid precursor protein results in the secretion of the amyloid beta peptide and related molecules. *Ann N Y Acad Sci.* 695, 109-16.
- Haass, C., Selkoe, D.J., 1993. Cellular processing of beta-amyloid precursor protein and the genesis of amyloid beta-peptide. *Cell.* 75, 1039-42.
- Hahn, S., Bruning, T., Ness, J., Czirr, E., Baches, S., Gijzen, H., Korth, C., Pietrzik, C.U., Bulic, B., Weggen, S., 2011. Presenilin-1 but not amyloid precursor protein mutations present in mouse models of Alzheimer's disease attenuate the response of cultured cells to gamma-secretase modulators regardless of their potency and structure. *J Neurochem.* 116, 385-95.
- Hanahan, D., 1983. Studies on transformation of Escherichia coli with plasmids. *Journal of Molecular Biology.* 166, 557-80.
- Hardy, J., Allsop, D., 1991. Amyloid deposition as the central event in the aetiology of Alzheimer's disease. *Trends in Pharmacological Sciences.* 12, 383-8.
- Hardy, J., Selkoe, D.J., 2002. The amyloid hypothesis of Alzheimer's disease: progress and problems on the road to therapeutics. *Science.* 297, 353-6.
- Hardy, J., 2009. The amyloid hypothesis for Alzheimer's disease: a critical reappraisal. *J Neurochem.* 110, 1129-34.
- Hardy, J.A., Higgins, G.A., 1992. Alzheimer's disease: the amyloid cascade hypothesis. *Science.* 256, 184-5.
- Harraz, M.M., Marden, J.J., Zhou, W., Zhang, Y., Williams, A., Sharov, V.S., Nelson, K., Luo, M., Paulson, H., Schoneich, C., Engelhardt, J.F., 2008. SOD1 mutations disrupt redox-sensitive Rac regulation of NADPH oxidase in a familial ALS model. *J Clin Invest.* 118, 659-70.
- Haskins, J., Gu, L., Wittchen, E.S., Hibbard, J., Stevenson, B.R., 1998. ZO-3, a novel member of the MAGUK protein family found at the tight junction, interacts with ZO-1 and occludin. *J Cell Biol.* 141, 199-208.
- Haverkamp, L.J., Appel, V., Appel, S.H., 1995. Natural-History of Amyotrophic-Lateral-Sclerosis in a Database Population - Validation of a Scoring System and a Model for Survival Prediction. *Brain.* 118, 707-719.
- Hawkins, B.T., Davis, T.P., 2005. The blood-brain barrier/neurovascular unit in health and disease. *Pharmacol Rev.* 57, 173-85.
- Hawkins, R.A., O'Kane, R.L., Simpson, I.A., Vina, J.R., 2006. Structure of the blood-brain barrier and its role in the transport of amino acids. *Journal of Nutrition.* 136, 218s-226s.

-
- Henkel, J.S., Beers, D.R., Wen, S., Bowser, R., Appel, S.H., 2009. Decreased mRNA expression of tight junction proteins in lumbar spinal cords of patients with ALS. *Neurology*. 72, 1614-6.
- Hino, S., Tanji, C., Nakayama, K.I., Kikuchi, A., 2005. Phosphorylation of beta-catenin by cyclic AMP-dependent protein kinase stabilizes beta-catenin through inhibition of its ubiquitination. *Mol Cell Biol*. 25, 9063-72.
- Hirase, T., Kawashima, S., Wong, E.Y., Ueyama, T., Rikitake, Y., Tsukita, S., Yokoyama, M., Staddon, J.M., 2001. Regulation of tight junction permeability and occludin phosphorylation by Rho-p160ROCK-dependent and -independent mechanisms. *J Biol Chem*. 276, 10423-31.
- Huber, J.D., Egleton, R.D., Davis, T.P., 2001. Molecular physiology and pathophysiology of tight junctions in the blood-brain barrier. *Trends in Neurosciences*. 24, 719-25.
- Hull, M., Berger, M., Heneka, M., 2006. Disease-modifying therapies in Alzheimer's disease: how far have we come? *Drugs*. 66, 2075-93.
- in t' Veld, B.A., Ruitenbergh, A., Hofman, A., Launer, L.J., van Duijn, C.M., Stijnen, T., Breteler, M.M., Stricker, B.H., 2001. Nonsteroidal antiinflammatory drugs and the risk of Alzheimer's disease. *New England Journal of Medicine*. 345, 1515-21.
- Itoh, M., Furuse, M., Morita, K., Kubota, K., Saitou, M., Tsukita, S., 1999. Direct binding of three tight junction-associated MAGUKs, ZO-1, ZO-2, and ZO-3, with the COOH termini of claudins. *J Cell Biol*. 147, 1351-63.
- Jiang, W.G., Martin, T.A., Matsumoto, K., Nakamura, T., Mansel, R.E., 1999. Hepatocyte growth factor/scatter factor decreases the expression of occludin and transendothelial resistance (TER) and increases paracellular permeability in human vascular endothelial cells. *Journal of Cellular Physiology*. 181, 319-29.
- Jonsson, P.A., Ernhill, K., Andersen, P.M., Bergemalm, D., Brannstrom, T., Gredal, O., Nilsson, P., Marklund, S.L., 2004. Minute quantities of misfolded mutant superoxide dismutase-1 cause amyotrophic lateral sclerosis. *Brain*. 127, 73-88.
- Joyce, P.I., Fratta, P., Fisher, E.M., Acevedo-Arozena, A., 2011. SOD1 and TDP-43 animal models of amyotrophic lateral sclerosis: recent advances in understanding disease toward the development of clinical treatments. *Mammalian Genome*. 22, 420-48.
- Keller, A.F., Gravel, M., Kriz, J., 2011. Treatment with minocycline after disease onset alters astrocyte reactivity and increases microgliosis in SOD1 mutant mice. *Experimental Neurology*. 228, 69-79.
- Koo, E.H., Squazzo, S.L., 1994. Evidence that production and release of amyloid beta-protein involves the endocytic pathway. *J Biol Chem*. 269, 17386-9.
-

References

- Koto, T., Takubo, K., Ishida, S., Shinoda, H., Inoue, M., Tsubota, K., Okada, Y., Ikeda, E., 2007. Hypoxia disrupts the barrier function of neural blood vessels through changes in the expression of claudin-5 in endothelial cells. *American Journal of Pathology*. 170, 1389-97.
- Kreuter, J., Alyautdin, R.N., Kharkevich, D.A., Ivanov, A.A., 1995. Passage of peptides through the blood-brain barrier with colloidal polymer particles (nanoparticles). *Brain Res*. 674, 171-4.
- Kreuter, J., Shamenkov, D., Petrov, V., Ränge, P., Cychutek, K., Koch-Brandt, C., Alyautdin, R., 2002. Apolipoprotein-mediated transport of nanoparticle-bound drugs across the blood-brain barrier. *J Drug Target*. 10, 317-25.
- Kumari, A., Yadav, S.K., Yadav, S.C., 2010. Biodegradable polymeric nanoparticles based drug delivery systems. *Colloids Surf B Biointerfaces*. 75, 1-18.
- Kuo, Y.M., Emmerling, M.R., Vigo-Pelfrey, C., Kasunic, T.C., Kirkpatrick, J.B., Murdoch, G.H., Ball, M.J., Roher, A.E., 1996. Water-soluble A β (N-40, N-42) oligomers in normal and Alzheimer disease brains. *J Biol Chem*. 271, 4077-81.
- Kwon, H.Y., Lee, J.Y., Choi, S.W., Jang, Y.S., Kim, J.H., 2001. Preparation of PLGA nanoparticles containing estrogen by emulsification-diffusion method. *Colloids and Surfaces a-Physicochemical and Engineering Aspects*. 182, 123-130.
- Laemmli, U.K., 1970. Cleavage of structural proteins during the assembly of the head of bacteriophage T4. *Nature*. 227, 680-5.
- LaFerla, F.M., Oddo, S., 2005. Alzheimer's disease: A β , tau and synaptic dysfunction. *Trends in Molecular Medicine*. 11, 170-6.
- Lewandowsky, M., 1900. Zur lehre der cerebrospinalflüssigkeit. *Zeitschrift Klinische Medizin*. 40, 480-494.
- Li, S., 1999. Hydrolytic degradation characteristics of aliphatic polyesters derived from lactic and glycolic acids. *J Biomed Mater Res*. 48, 342-53.
- Liddel, S.A., 2011. Fluids and barriers of the CNS: a historical viewpoint. *Fluids Barriers CNS*. 8, 2.
- Liebner, S., Fischmann, A., Rascher, G., Duffner, F., Grote, E.H., Kalbacher, H., Wolburg, H., 2000. Claudin-1 and claudin-5 expression and tight junction morphology are altered in blood vessels of human glioblastoma multiforme. *Acta Neuropathol*. 100, 323-31.
- Lunn, J.S., Sakowski, S.A., Kim, B., Rosenberg, A.A., Feldman, E.L., 2009. Vascular endothelial growth factor prevents G93A-SOD1-induced motor neuron degeneration. *Dev Neurobiol*. 69, 871-84.
- Madara, J.L., 1988. Tight junction dynamics: is paracellular transport regulated? *Cell*. 53, 497-8.

- Masserini, M., 2013. Nanoparticles for Brain Drug Delivery. *ISRN Biochemistry*. 2013, 18.
- McGowan, E., Pickford, F., Kim, J., Onstead, L., Eriksen, J., Yu, C., Skipper, L., Murphy, M.P., Beard, J., Das, P., Jansen, K., Delucia, M., Lin, W.L., Dolios, G., Wang, R., Eckman, C.B., Dickson, D.W., Hutton, M., Hardy, J., Golde, T., 2005. Abeta42 is essential for parenchymal and vascular amyloid deposition in mice. *Neuron*. 47, 191-9.
- McGuire, V., Longstreth, W.T., Jr., Koepsell, T.D., van Belle, G., 1996. Incidence of amyotrophic lateral sclerosis in three counties in western Washington state. *Neurology*. 47, 571-3.
- Mineta, K., Yamamoto, Y., Yamazaki, Y., Tanaka, H., Tada, Y., Saito, K., Tamura, A., Igarashi, M., Endo, T., Takeuchi, K., Tsukita, S., 2011. Predicted expansion of the claudin multigene family. *FEBS Letters*. 585, 606-12.
- Mitsumoto, H., Chad, D.A., Pioro, E.P., 1998. *Amyotrophic Lateral Sclerosis*. Oxford Univ. Press.
- Miyazaki, K., Ohta, Y., Nagai, M., Morimoto, N., Kurata, T., Takehisa, Y., Ikeda, Y., Matsuura, T., Abe, K., 2011. Disruption of neurovascular unit prior to motor neuron degeneration in amyotrophic lateral sclerosis. *Journal of Neuroscience Research*. 89, 718-28.
- Monopoli, M.P., Aberg, C., Salvati, A., Dawson, K.A., 2012. Biomolecular coronas provide the biological identity of nanosized materials. *Nature Nanotechnology*. 7, 779-86.
- Montesano, R., Pepper, M.S., Mohle-Steinlein, U., Risau, W., Wagner, E.F., Orci, L., 1990. Increased proteolytic activity is responsible for the aberrant morphogenetic behavior of endothelial cells expressing the middle T oncogene. *Cell*. 62, 435-45.
- Morita, K., Sasaki, H., Furuse, M., Tsukita, S., 1999. Endothelial claudin: claudin-5/TMVCF constitutes tight junction strands in endothelial cells. *J Cell Biol*. 147, 185-94.
- Mulder, D.W., 1982. Clinical limits of amyotrophic lateral sclerosis. *Adv Neurol*. 36, 15-22.
- Mullis, K.B., Faloona, F.A., 1987. Specific synthesis of DNA in vitro via a polymerase-catalyzed chain reaction. *Methods in Enzymology*. 155, 335-50.
- Murray, C.J.L., Lopez, A.D., 1996. *The Global Burden of Disease*. Vol., Harvard University Press.
- Neuraltus, P., 2012. Neuraltus Pharmaceuticals reports clinical results from phase 1 NP001 study in the treatment of amyotrophic lateral sclerosis (ALS). Available at: http://www.neuraltus.com/pages/news_rel11_30_10.html. Accessed May 22, 2012

References

- Nicaise, C., Mitrecic, D., Demetter, P., De Decker, R., Authelet, M., Boom, A., Pochet, R., 2009a. Impaired blood-brain and blood-spinal cord barriers in mutant SOD1-linked ALS rat. *Brain Res.* 1301, 152-62.
- Nicaise, C., Soyfoo, M.S., Authelet, M., De Decker, R., Bataveljic, D., Delporte, C., Pochet, R., 2009b. Aquaporin-4 overexpression in rat ALS model. *Anat Rec (Hoboken)*. 292, 207-13.
- Nitta, T., Hata, M., Gotoh, S., Seo, Y., Sasaki, H., Hashimoto, N., Furuse, M., Tsukita, S., 2003. Size-selective loosening of the blood-brain barrier in claudin-5-deficient mice. *J Cell Biol.* 161, 653-60.
- Pahnke, J., Walker, L.C., Scheffler, K., Krohn, M., 2009. Alzheimer's disease and blood-brain barrier function-Why have anti-beta-amyloid therapies failed to prevent dementia progression? *Neurosci Biobehav Rev.* 33, 1099-108.
- Palmer, A.M., 2010. The role of the blood-CNS barrier in CNS disorders and their treatment. *Neurobiol Dis.* 37, 3-12.
- Pan, W., Banks, W.A., Kastin, A.J., 1997a. Blood-brain barrier permeability to ebsiran and TNF in acute spinal cord injury. *Experimental Neurology.* 146, 367-73.
- Pan, W., Banks, W.A., Kastin, A.J., 1997b. Permeability of the blood-brain and blood-spinal cord barriers to interferons. *Journal of Neuroimmunology.* 76, 105-11.
- Pardridge, W.M., 2007. Blood-brain barrier delivery. *Drug Discov Today.* 12, 54-61.
- Pasinelli, P., Brown, R.H., 2006. Molecular biology of amyotrophic lateral sclerosis: insights from genetics. *Nature Reviews Neuroscience.* 7, 710-23.
- Patel, M., Souto, E.B., Singh, K.K., 2013. Advances in brain drug targeting and delivery: limitations and challenges of solid lipid nanoparticles. *Expert opinion on drug delivery.* 10, 889-905.
- Peviani, M., Cheroni, C., Troglia, F., Quarto, M., Pelicci, G., Bendotti, C., 2007. Lack of changes in the PI3K/AKT survival pathway in the spinal cord motor neurons of a mouse model of familial amyotrophic lateral sclerosis. *Molecular and Cellular Neuroscience.* 34, 592-602.
- Pflanzner, T., Janko, M.C., Andre-Dohmen, B., Reuss, S., Weggen, S., Roebroek, A.J., Kuhlmann, C.R., Pietrzik, C.U., 2011. LRP1 mediates bidirectional transcytosis of amyloid-beta across the blood-brain barrier. *Neurobiol Aging.* 32, 2323 e1-11.
- Philips, T., Robberecht, W., 2011. Neuroinflammation in amyotrophic lateral sclerosis: role of glial activation in motor neuron disease. *Lancet Neurol.* 10, 253-63.
- Pietrzik, C., Behl, C., 2005. Concepts for the treatment of Alzheimer's disease: molecular mechanisms and clinical application. *Int J Exp Pathol.* 86, 173-85.

- Prockop, L.D., Naidu, K.A., Binard, J.E., Ransohoff, J., 1995. Selective permeability of [3H]-D-mannitol and [14C]-carboxyl-inulin across the blood-brain barrier and blood-spinal cord barrier in the rabbit. *J Spinal Cord Med.* 18, 221-6.
- Querfurth, H.W., LaFerla, F.M., 2010. Alzheimer's disease. *New England Journal of Medicine.* 362, 329-44.
- Qutub, A.A., Hunt, C.A., 2005. Glucose transport to the brain: a systems model. *Brain Res Brain Res Rev.* 49, 595-617.
- Rapoport, S.I., Robinson, P.J., 1986. Tight-junctional modification as the basis of osmotic opening of the blood-brain barrier. *Ann N Y Acad Sci.* 481, 250-67.
- Re, F., Gregori, M., Masserini, M., 2012. Nanotechnology for neurodegenerative disorders. *Nanomedicine.* 8 Suppl 1, S51-8.
- Reese, T.S., Karnovsky, M.J., 1967. Fine structural localization of a blood-brain barrier to exogenous peroxidase. *J Cell Biol.* 34, 207-17.
- Rena, G., Guo, S., Cichy, S.C., Unterman, T.G., Cohen, P., 1999. Phosphorylation of the transcription factor forkhead family member FKHR by protein kinase B. *J Biol Chem.* 274, 17179-83.
- Ridley, H., 1695. *The Anatomy of the Brain.* Vol., London: Sam Smith and Benjamin Walford, Printers to the Royal Society.
- Robberecht, W., Philips, T., 2013. The changing scene of amyotrophic lateral sclerosis. *Nature Reviews Neuroscience.* 14, 248-64.
- Roney, C., Kulkarni, P., Arora, V., Antich, P., Bonte, F., Wu, A., Mallikarjuana, N.N., Manohar, S., Liang, H.F., Kulkarni, A.R., Sung, H.W., Sairam, M., Aminabhavi, T.M., 2005. Targeted nanoparticles for drug delivery through the blood-brain barrier for Alzheimer's disease. *J Control Release.* 108, 193-214.
- Rosen, D.R., Siddique, T., Patterson, D., Figlewicz, D.A., Sapp, P., Hentati, A., Donaldson, D., Goto, J., O'Regan, J.P., Deng, H.X., et al., 1993. Mutations in Cu/Zn superoxide dismutase gene are associated with familial amyotrophic lateral sclerosis. *Nature.* 362, 59-62.
- Rowland, L.P., Shneider, N.A., 2001. Amyotrophic lateral sclerosis. *New England Journal of Medicine.* 344, 1688-700.
- Sahni, J.K., Doggui, S., Ali, J., Baboota, S., Dao, L., Ramassamy, C., 2011. Neurotherapeutic applications of nanoparticles in Alzheimer's disease. *J Control Release.* 152, 208-31.
- Saitou, M., Furuse, M., Sasaki, H., Schulzke, J.D., Fromm, M., Takano, H., Noda, T., Tsukita, S., 2000. Complex phenotype of mice lacking occludin, a component of tight junction strands. *Molecular Biology of the Cell.* 11, 4131-42.
- Saltzman, W.M., 2001. *Drug Delivery : Engineering Principles for Drug Therapy.* Vol., New York: Oxford University Press.

References

- Schulzke, J.D., Gitter, A.H., Mankertz, J., Spiegel, S., Seidler, U., Amasheh, S., Saitou, M., Tsukita, S., Fromm, M., 2005. Epithelial transport and barrier function in occludin-deficient mice. *Biochim Biophys Acta.* 1669, 34-42.
- Selkoe, D.J., 1991. The molecular pathology of Alzheimer's disease. *Neuron.* 6, 487-98.
- Selkoe, D.J., 2001. Alzheimer's disease: genes, proteins, and therapy. *Physiol Rev.* 81, 741-66.
- Service, R.F., 2010. Nanotechnology. Nanoparticle Trojan horses gallop from the lab into the clinic. *Science.* 330, 314-5.
- Silva, G.A., 2010. Nanotechnology applications and approaches for neuroregeneration and drug delivery to the central nervous system. *Ann N Y Acad Sci.* 1199, 221-30.
- Smith, P.K., Krohn, R.I., Hermanson, G.T., Mallia, A.K., Gartner, F.H., Provenzano, M.D., Fujimoto, E.K., Goeke, N.M., Olson, B.J., Klenk, D.C., 1985. Measurement of protein using bicinchoninic acid. *Analytical Biochemistry.* 150, 76-85.
- Stevenson, B.R., Begg, D.A., 1994. Concentration-dependent effects of cytochalasin D on tight junctions and actin filaments in MDCK epithelial cells. *Journal of Cell Science.* 107 (Pt 3), 367-75.
- Taddei, A., Giampietro, C., Conti, A., Orsenigo, F., Breviario, F., Pirazzoli, V., Potente, M., Daly, C., Dimmeler, S., Dejana, E., 2008. Endothelial adherens junctions control tight junctions by VE-cadherin-mediated upregulation of claudin-5. *Nature Cell Biology.* 10, 923-34.
- Taurin, S., Sandbo, N., Qin, Y., Browning, D., Dulin, N.O., 2006. Phosphorylation of beta-catenin by cyclic AMP-dependent protein kinase. *J Biol Chem.* 281, 9971-6.
- Testa, J.R., Bellacosa, A., 2001. AKT plays a central role in tumorigenesis. *Proc Natl Acad Sci U S A.* 98, 10983-5.
- Tosi, G., Costantino, L., Ruozi, B., Forni, F., Vandelli, M.A., 2008. Polymeric nanoparticles for the drug delivery to the central nervous system. *Expert Opin Drug Deliv.* 5, 155-74.
- Ueno, M., 2007. Molecular anatomy of the brain endothelial barrier: an overview of the distributional features. *Current Medicinal Chemistry.* 14, 1199-206.
- Wagner, S., Kufleitner, J., Zensi, A., Dadparvar, M., Wien, S., Bungert, J., Vogel, T., Worek, F., Kreuter, J., von Briesen, H., 2010a. Nanoparticulate transport of oximes over an in vitro blood-brain barrier model. *PLoS One.* 5, e14213.
- Wagner, S., Rothweiler, F., Anhorn, M.G., Sauer, D., Riemann, I., Weiss, E.C., Katsen-Globa, A., Michaelis, M., Cinatl, J., Jr., Schwartz, D., Kreuter, J., von Briesen, H., Langer, K., 2010b. Enhanced drug targeting by attachment of an anti alpha v integrin antibody to doxorubicin loaded human serum albumin nanoparticles. *Biomaterials.* 31, 2388-98.

- Wagner, S., Zensi, A., Wien, S.L., Tschickardt, S.E., Maier, W., Vogel, T., Worek, F., Pietrzik, C.U., Kreuter, J., von Briesen, H., 2012. Uptake mechanism of ApoE-modified nanoparticles on brain capillary endothelial cells as a blood-brain barrier model. *PLoS One*. 7, e32568.
- Wagner, V., Dullaart, A., Bock, A.K., Zweck, A., 2006. The emerging nanomedicine landscape. *Nat Biotechnol*. 24, 1211-7.
- Warner, T.D., Mitchell, J.A., 2004. Cyclooxygenases: new forms, new inhibitors, and lessons from the clinic. *FASEB J*. 18, 790-804.
- Wegener, J., Abrams, D., Willenbrink, W., Galla, H.J., Janshoff, A., 2004. Automated multi-well device to measure transepithelial electrical resistances under physiological conditions. *BioTechniques*. 37, 590, 592-4, 596-7.
- Weggen, S., Eriksen, J.L., Das, P., Sagi, S.A., Wang, R., Pietrzik, C.U., Findlay, K.A., Smith, T.E., Murphy, M.P., Bulter, T., Kang, D.E., Marquez-Sterling, N., Golde, T.E., Koo, E.H., 2001. A subset of NSAIDs lower amyloidogenic Abeta42 independently of cyclooxygenase activity. *Nature*. 414, 212-6.
- Weidenfeller, C., Schrot, S., Zozulya, A., Galla, H.J., 2005. Murine brain capillary endothelial cells exhibit improved barrier properties under the influence of hydrocortisone. *Brain Res*. 1053, 162-74.
- Witan, H., Gorlovoy, P., Kaya, A.M., Koziollek-Drechsler, I., Neumann, H., Behl, C., Clement, A.M., 2009. Wild-type Cu/Zn superoxide dismutase (SOD1) does not facilitate, but impedes the formation of protein aggregates of amyotrophic lateral sclerosis causing mutant SOD1. *Neurobiol Dis*. 36, 331-42.
- Wolburg, H., Wolburg-Buchholz, K., Kraus, J., Rascher-Eggstein, G., Liebner, S., Hamm, S., Duffner, F., Grote, E.H., Risau, W., Engelhardt, B., 2003. Localization of claudin-3 in tight junctions of the blood-brain barrier is selectively lost during experimental autoimmune encephalomyelitis and human glioblastoma multiforme. *Acta Neuropathol*. 105, 586-92.
- Wong, P.C., Pardo, C.A., Borchelt, D.R., Lee, M.K., Copeland, N.G., Jenkins, N.A., Sisodia, S.S., Cleveland, D.W., Price, D.L., 1995. An adverse property of a familial ALS-linked SOD1 mutation causes motor neuron disease characterized by vacuolar degeneration of mitochondria. *Neuron*. 14, 1105-16.
- Wong, P.C., Rothstein, J.D., Price, D.L., 1998. The genetic and molecular mechanisms of motor neuron disease. *Current Opinion in Neurobiology*. 8, 791-9.
- Wyss-Coray, T., 2006. Inflammation in Alzheimer disease: driving force, bystander or beneficial response? *Nat Med*. 12, 1005-15.
- Yap, A.S., Briehner, W.M., Gumbiner, B.M., 1997. Molecular and functional analysis of cadherin-based adherens junctions. *Annual Review of Cell and Developmental Biology*. 13, 119-46.

References

- Ye, L., Martin, T.A., Parr, C., Harrison, G.M., Mansel, R.E., Jiang, W.G., 2003. Biphasic effects of 17-beta-estradiol on expression of occludin and transendothelial resistance and paracellular permeability in human vascular endothelial cells. *Journal of Cellular Physiology*. 196, 362-9.
- Zensi, A., Begley, D., Pontikis, C., Legros, C., Mihoreanu, L., Wagner, S., Buchel, C., von Briesen, H., Kreuter, J., 2009. Albumin nanoparticles targeted with Apo E enter the CNS by transcytosis and are delivered to neurones. *J Control Release*. 137, 78-86.
- Zhong, Z., Deane, R., Ali, Z., Parisi, M., Shapovalov, Y., O'Banion, M.K., Stojanovic, K., Sagare, A., Boillee, S., Cleveland, D.W., Zlokovic, B.V., 2008. ALS-causing SOD1 mutants generate vascular changes prior to motor neuron degeneration. *Nat Neurosci*. 11, 420-2.

6

Appendix

6.1 Supplementary material and methods

In this chapter, the experimental techniques and methods are presented, which were performed in cooperation with Iavor Zlatev (chapter 6.1.1) from the lab of Prof. Dr. Klaus Langer (Institute of Pharmaceutical Technology and Biopharmacy, University of Muenster), Sandra Baches (chapter 6.1.2) from the lab of Prof. Dr. Sascha Weggen (Department of Neuropathology, Heinrich Heine University, Duesseldorf), Julia Stab (chapter 6.1.3) from the lab of Dr. Sylvia Wagner (Department of Cell Biology and Applied Virology, Fraunhofer Institute for Biomedical Engineering, St. Ingbert) and Dominic Docter (6.1.4) from the lab of Prof. Dr. Roland Stauber (Molecular and Cellular Oncology/Mainz Screening Center (MSC), University Medical Center of the Johannes Gutenberg University Mainz).

6.1.1 Nanoparticles preparation and characterization

6.1.1.1 Reagents and chemicals

Poly(L-lactide) (PLA, viscosity ~ 1.0 dL/g), flurbiprofen and polyvinyl alcohol (PVA) were obtained from Sigma (Steinheim, Germany). Lumogen® F orange 240 was provided by BASF (Ludwigshafen, Germany). All other reagents were of analytical grade and used as received.

6.1.1.2 Nanoparticle preparation

PLA nanoparticles were formed by an emulsification-diffusion technique. Briefly, 100 mg of PLA, 10 mg of flurbiprofen and 150 µg of Lumogen® orange were dissolved in 2 ml dichloromethane (DCM). The organic phase was added to 6 ml aqueous solution of PVA (2%, w/v). This mixture was homogenized in an ice bath for 30 min at 24,000 rpm (Ultra Turrax®, IKA, Staufen, Germany) and diluted with 6 ml PVA solution (1%, w/v). DCM was removed by stirring the emulsion overnight at RT. Finally, the particles were collected by centrifugation 20,000 *g* for 10 min (Eppendorf, Hamburg, Germany) and washed twice with purified water before lyophilization.

6.1.1.3 Freeze-drying of the samples

For the lyophilization process a freeze-dryer Epsilon 1-4 (Martin Christ Gefriertrocknungsanlagen GmbH, Osterode am Harz, Germany) was used. Aliquots of the nanoparticles suspension (100 µl) were dispensed into 2 ml Lyovials and diluted with 100 µl trehalose solution (6%, w/v) as a cryoprotective agent. The freeze-drying cycle was performed according to an established protocol. First, the samples were frozen at -40 °C for 3 h. In the second step, primary drying was performed at a temperature of -34 °C for 24 h and a vacuum of 0.05 mbar followed by a secondary drying phase for 11 h at 20 °C and a vacuum of 0.025 mbar. At the end of the drying process the vials were sealed and removed.

6.1.1.4 Nanoparticle characterization

Nanoparticles were analyzed with regard to particle diameter and polydispersity by photon correlation spectroscopy (PCS) and zeta potential was measured by microelectrophoresis using a Malvern Zetasizer Nano ZS (Malvern Instruments Ltd., Malvern, UK). Prior to measurement the samples were diluted with purified water.

6.1.1.5 Determination of flurbiprofen loading

The amount of flurbiprofen incorporated into the nanoparticles was determined by a high-performance liquid chromatography (HPLC) method.

1 mg nanoparticles were incubated in 1 ml acetonitrile for 5 min at RT. The sample was centrifuged (20,000 *g*; 10 min) and the chromatographic separation was carried out using aliquots of the supernatant. The aliquots (20 μ l) were injected into a Phenomenex Gemini NX 250 x 4.6 mm, 5 μ m particle, C18 column (Phenomenex, Aschaffenburg, Germany). The flow rate was set to 1 ml/min during the separation, with the mobile phase composed of acetonitrile and 0.1% (v/v) trifluoroacetic acid (57.5 : 42.5, v/v). The eluate was analyzed at a wavelength of 245 nm.

6.1.1.6 *In vitro* release of flurbiprofen

For each point in time individual samples were prepared as follows: 1 mg nanoparticles were incubated in 1 ml phosphate buffer (0.1 mM, pH=7.5) at 37 °C under constant shaking. At defined points in time (0, 0.5, 1, 3, 5, 7, 24 h) one sample was centrifuged (20,000 *g* for 10 min). The amount of the released drug was determined in the supernatant by HPLC as described above.

6.1.2 Measurement of A β species by ELISA

The levels of A β ₄₀ and A β ₄₂ peptides were determined using a cell-based sandwich ELISA assay as described (Hahn *et al.*, 2011). Monoclonal antibody IC16 (1:250 in PBS, pH 7.2), raised against amino acids 1-15 of the A β sequence, was used as a capture antibody. To generate standard curves, synthetic A β ₁₋₄₀ and A β ₁₋₄₂ peptides (JPT Peptide Technologies) were used. These A β peptides were solubilized in DMSO at 10 μ g/mL and aliquots were stored at -80 °C. 96-well high-binding microtiter plates were incubated overnight at 4 °C with the capture antibody. After the capture antibody was removed, conditioned media samples (20 μ l for detection of A β ₄₀ and 100 μ l for A β ₄₂) and freshly diluted A β peptide standards (125-6,000 pg/mL in PBS containing 0.05% Tween-20, 1% BSA) were added.

Subsequently, C-terminal detection antibodies specific for A β ₄₀ and A β ₄₂ labeled with horseradish peroxidase (HRP) using the Pierce EZ-Link™ Plus Activated Peroxidase kit (Thermo Fisher Scientific) were diluted in PBS containing 0.05% Tween-20, 1% BSA, added to each well, and incubated overnight at 4 °C. Plates were washed 3 times with PBS containing 0.05% Tween-20 and once with PBS. Then 50 μ l of TMB ELISA Peroxidase Substrate (Interchim) was added and incubated for 1-10 min at RT in the dark. The reaction was stopped by adding 50 μ l of 2 M H₂SO₄ and the absorbance was measured using a Paradigm microplate reader (Beckman Coulter) at 450 nm. The levels of the A β ₄₀ and A β ₄₂ peptides were normalized to A β total (A β ₄₀ + A β ₄₂) and the average of triplicate measurements for each concentration was normalized to control condition (DMSO or unloaded PLA nanoparticles).

6.1.3 Cellular binding of the nanoparticles

bEnd.3 cells were cultured in 24-well plates (Greiner, Frickenhausen, Germany) and treated with the nanoparticle formulations for 4 h at 37 °C. 105.3 μ g nanoparticles per cm² growing surface area were used. After incubation, cells were washed twice with PBS (Invitrogen, Karlsruhe, Germany) and subsequently trypsinized and harvested. Fixing was performed with FACS-Fix (10 g/l paraformaldehyde (PFA) and 8.5 g/l NaCl in PBS, pH 7.4) before flow cytometry (FACS) analysis. Per sample, 10⁵ cells were counted using FACSCalibur and CellQuest Pro software (Becton Dickinson, Heidelberg, Germany). The fluorescent labeling of the nanoparticles via Lumogen® F Orange 240 (BASF, Ludwigshafen, Germany) allowed a detection at 524/539 nm.

6.1.4 Nanoparticle plasma protein binding assay

Human plasma samples were obtained and pooled from citrated blood of 15 healthy individuals according to institutional bioethics approval. PLA nanoparticles were incubated with equal amount of human plasma for different time points (5, 15, 30 and 60 minutes), loaded onto a sucrose cushion (0.7 M in PBS) and centrifuged through the cushion to separate nanoparticle-protein complexes from plasma (12,000 rpm for 20 min at 4 °C) (Figure S2). Pellets were washed three times with PBS and proteins were eluted from the recovered particles by adding an equal volume of SDS sample buffer (62.5 mM Tris-HCl pH 6.8; 2% w/v SDS, 10% glycerol, 50 mM DTT, 0.01% w/v bromophenol blue) to the pellet and incubated at 95 °C for 5 min. Proteins were separated on a 12% SDS-polyacrylamide gel. To visualize the kinetic evolution of the protein corona, the SDS-polyacrylamide gel was stained with Coomassie brilliant blue R-250 (Bio-Rad) and protein quantification was performed using the BioRad Protein Assay (Bio-Rad). To examine the presence of apolipoproteins in the nanoparticle-protein complex, proteins were transferred onto a polyvinylidene difluoride (PVDF) membrane. Membranes were blocked with 5% non-fat dry milk in TBS containing 0.01% Tween-20 and the following antibodies were used: α -apoA4 (Cell Signaling, Boston, MA, USA); α -apoE and rabbit- α -mouse IgG antibody conjugated with horseradish peroxidase (Santa Cruz, Dallas, TX, USA).

List of Acronyms

A β	Amyloid- β
AD	Alzheimer's disease
AICD	APP intracellular domain
AJ	Adherens junction
ALS	Amyotrophic lateral sclerosis
ANOVA	Analysis of variance
APP	Amyloid precursor protein
APPs	Soluble APP
ApoE	Apolipoprotein E
ApoA4	Apolipoprotein A4
BBB	Blood-brain barrier
Bcat	β -catenin
BSA	Bovine serum albumin
BSCB	Blood-spinal cord barrier
$^{\circ}$ C	Degrees celsius
C _{Cl}	Capacitance
cDNA	Complementary deoxyribonucleic acid
ChIP	Chromatin immunoprecipitation
Ci	Curie
CLSM	Confocal laser scanning microscopy
CNS	Central nervous system
COX	Cyclooxygenase
CSF	Cerebrospinal fluid
CTF	C-terminal fragment
DMSO	Dimethylsulfoxid
<i>E.coli</i>	<i>Escherichia coli</i>
FALS	Familial ALS
FoxO1	Forkhead box protein O1
G	Gram
GFP	Green fluorescent protein
GSM	γ -secretase modulators
H	hour
HEK	Human embryonic kidney
HPLC	high-performance liquid chromatography

Appendix

HRP	Horseradish peroxidase
IgG	Immunoglobulin G
kDa	Kilo Dalton
LB	Lysogeny broth
LRP	low density lipoprotein receptor-related protein
M	Milli
μ	Micro
M	Molar
Min	Minute
MAGUKs	Membrane-associated guanylate kinase-like proteins
NSAIDs	Nonsteroidal anti-inflammatory drugs
PAGE	Polyacrylamide gel electrophoresis
PBS	Phosphate-buffered saline
PCR	Polymerase chain reaction
PCS	Photon correlation spectroscopy
PI3K	Phosphatidylinositol-3-kinase
PD	Parkinson's disease
pMSCECs	Primary mouse spinal cord endothelial cells
PNS	Peripheral nervous system
ROS	Reactive oxygen species
rpm	Round per minute
RT	Room temperature
S	Second
SALS	Sporadic ALS
SEM	Standard error of the mean
SOD1	Cu/Zn-superoxide dismutase 1
TBS	Tris-buffered saline
TCF	T-cell factor
TER	Transendothelial resistance
TJ	Tight junctions
UV	Ultra violet
v/v	Volume per volume
VE	Vascular endothelial
WB	Western blot
w/v	Weight per volume
ZO	Zonula occludens

List of Scientific Contributions

Publications in Peer-Reviewed Journals

- **Meister S**, Storck SE, Hameister E, Behl C, Weggen S, Clement AB, Pietrzik CU (2015) Expression of the ALS-causing variant hSOD1G93A leads to an impaired integrity and altered regulation of claudin-5 expression in an in vitro BSCB model. *J Cereb Blood Flow Metab*, accepted 12th March 2015. doi:10.1038/jcbfm.2015.57
- **Meister S**, Zlatev I, Stab J, Docter D, Baches S, Stauber RH, Deutsch M, Schmidt R, Ropele S, Windisch M, Langer K, Wagner S, Briesen H, Weggen S, Pietrzik CU (2013) Nanoparticulate flurbiprofen reduces Abeta42 generation in an in vitro blood-brain barrier model. *Alzheimers Res Ther* 2013 5(6):51
- Maier W, Bednorz M, **Meister S**, Roebroek A, Weggen S, Schmitt U, Pietrzik CU (2013) LRP1 is critical for the surface distribution and internalization of the NR2B NMDA receptor subtype. *Mol Neurodegener* 8
- Wagner S, Zensi A, Wien SL, **Tschickardt SE**, Maier W, Vogel T, Worek F, Pietrzik CU, Kreuter J, von Briesen H (2012): Uptake mechanism of ApoE-modified nanoparticles on brain capillary endothelial cells as a blood-brain barrier model. *PLoS One* 7
- Pflanzner T, Petsch B, André-Dohmen B, Müller-Schiffmann A, **Tschickardt S**, Weggen S, Stitz L, Korth C, Pietrzik CU (2012) Cellular prion protein participates in amyloid- β transcytosis across the blood-brain barrier. *J Cereb Blood Flow Metab* 32(4)
- Jefferson T, Causevic M, Auf dem Keller U, Schilling O, Isbert S, Geyer R, Maier W, **Tschickardt S**, Jumpertz T, Weggen S, Bond JS, Overall CM, Pietrzik CU, Becker-Pauly C (2011) Metalloprotease Meprin β Generates Nontoxic N-terminal Amyloid Precursor Protein Fragments *in vivo*. *J Biol Chem* 286(31)

Conference Contributions

- **S. Meister**, I. Zlatev, J. Stab, D. Docter, S. Baches, R. H. Stauber, M. Deutsch, R. Schmidt, S. Ropele, M. Windisch, K. Langer, S. Wagner, H. v. Briesen, S. Weggen, C. U. Pietrzik, "Nanoparticulate flurbiprofen affects A β ₄₂ generation in an *in vitro* blood-brain barrier model", 13th Eibsee Meeting on Cellular Mechanisms of Neurodegeneration, Grainau, Germany, 23rd to 25th October 2013, poster presentation
- **S. Meister**, I. Zlatev, J. Stab, D. Docter, S. Baches, R. H. Stauber, M. Deutsch, R. Schmidt, S. Ropele, M. Windisch, K. Langer, S. Wagner, H. v. Briesen, S. Weggen, C. U. Pietrzik, "Nanoparticulate flurbiprofen affects A β ₄₂ generation in an *in vitro* blood-brain barrier model", 16th International Symposium "Signal Transduction in the Blood-Brain Barriers", Sümeg, Hungary, September 12th to 14th September 2013, oral presentation
- **S. Meister**, S. Storck, C. Behl, A. M. Clement, C. U. Pietrzik, "Impaired blood-brain barrier integrity of ALS spinal cord derived endothelial cells", 16th International Symposium "Signal Transduction in the Blood-Brain Barriers", Sümeg, Hungary, September 12th to 14th September 2013, poster presentation
- S. Storck, E. Hameister, **S. Meister**, D.A. Ridder, M. Schwaninger, C. Korth, S. Weggen, C. U. Pietrzik, "The role of LRP1 in A β clearance across the blood-brain barrier in Alzheimer's Disease", 16th International Symposium "Signal Transduction in the Blood-Brain Barriers", Sümeg, Hungary, September 12th to 14th September 2013, poster presentation
- **S. Meister**, J. Stab, I. Zlatev, D. Docter, S. Baches, R. H. Stauber, M. Deutsch, R. Schmidt, S. Ropele, M. Windisch, K. Langer, S. Wagner, H. v. Briesen, S. Weggen, C. U. Pietrzik, "Nanoparticulate flurbiprofen reduces A β ₄₂ generation in an *in vitro* blood-brain barrier model", 15th Workshop on barriers and transporters, Bad Herrenalb, Germany, 13th to 15th May 2013, oral presentation
- **S. Meister**, S. Storck, S. Isbert, C. Behl, A. M. Clement, C. U. Pietrzik, "Impaired blood-brain barrier integrity of ALS spinal cord derived endothelial cells", 15th Workshop on barriers and transporters, Bad Herrenalb, Germany, 13th to 15th May 2013, poster presentation
- S. Storck, **S. Meister**, D.A. Ridder, M. Schwaninger, C. U. Pietrzik, "A new mouse model to clarify the role LRP1 in A β clearance across the blood-brain barrier", 15th Workshop on barriers and transporters, Bad Herrenalb, Germany, 13th to 15th May 2013, poster presentation

-
- J. Stab, I. Zlatev, **S. Meister**, K. Langer, R. Wronski, M. Windisch, S. Ropele, R. Schmidt, M. Deutsch, C. Pietrzik, H. v. Briesen, S. Wagner, “Making transport possible: Flurbiprofen-loaded nanoparticles for the treatment of Alzheimer’s disease”, 15th Workshop on barriers and transporters, Bad Herrenalb, Germany, 13th to 15th May 2013, poster presentation
 - **S. Meister**, S. Baches, S. Weggen, C. U. Pietrzik, “Nanoparticulate flurbiprofen affects A β generation in an *in vitro* blood-brain barrier model“, 12th Eibsee Meeting on Cellular Mechanisms of Neurodegeneration, Grainau, Germany, 21st to 24th November 2012, poster presentation
 - **S. Meister**, M. Liebl, H. Witan, C. Behl, A. M. Clement, C. U. Pietrzik, “Characterization of the blood-spinal cord barrier (BSCB) in a mouse model for amyotrophic lateral sclerosis (ALS)“, 1st Biennial Meeting of the Rhine-Main Neuroscience network, Oberwesel, Germany, 20th to 22nd June 2012, poster presentation
 - **S. Meister**, M. Liebl, H. Witan, C. Behl, A. M. Clement, C. U. Pietrzik, “Characterization of the blood-spinal cord barrier (BSCB) in a mouse model for amyotrophic lateral sclerosis (ALS)“, 14th Workshop on barriers and transporters, Bad Herrenalb, Germany, 14th to 16th May 2012, poster presentation
 - **S. Meister**, H. Witan, C. Behl, A. M. Clement, C. U. Pietrzik, “Characterization of the blood-spinal cord barrier (BSCB) in a mouse model for amyotrophic lateral sclerosis (ALS)“, 4th Joint Labmeeting: The Pietrzik and Roebroek Groups, Mainz, Germany, 19th to 20th April 2012, oral presentation
 - **S. Tschickardt**, H. Witan, C. Behl, A. M. Clement, C. U. Pietrzik, “Characterization of the blood-spinal cord barrier (BSCB) in a mouse model for amyotrophic lateral sclerosis (ALS)“, 4th Tschagguns Meeting “Cellular and Molecular processes in neurodegenerative diseases“, Tschagguns, Austria, 30th January to 2nd February 2012, oral presentation
 - **S. Tschickardt**, C. U. Pietrzik, “Translational approach for blood-brain barrier penetration“, 11st Annual FTN/IAK Symposium “Molecular and Cellular Neuroscience“, Mainz, Germany, 9th December 2011, poster presentation
 - **S. Tschickardt**, C. U. Pietrzik, “Translational approach for blood-brain barrier penetration“, 11th Eibsee Meeting on Cellular Mechanisms of Neurodegeneration, Grainau, Germany, 21st to 24th November 2012, poster presentation

-
- **S. Tschickardt**, C. U. Pietrzik “Transportmechanismen der Blut-Hirn-Schranke”, 27th Symposium of the AGNP, Munich, Germany, 05th to 8th October 2011, oral presentation

RESEARCH

Open Access

Nanoparticulate flurbiprofen reduces amyloid- β_{42} generation in an *in vitro* blood–brain barrier model

Sabrina Meister¹, Iavor Zlatev², Julia Stab³, Dominic Docter⁴, Sandra Baches⁵, Roland H Stauber⁴, Mordechai Deutsch⁶, Reinhold Schmidt⁷, Stefan Ropele⁷, Manfred Windisch⁸, Klaus Langer², Sylvia Wagner³, Hagen von Briesen³, Sascha Weggen⁵ and Claus U Pietrzik^{1*}

Abstract

Introduction: The amyloid- β_{42} ($A\beta_{42}$) peptide plays a crucial role in the pathogenesis of Alzheimer's disease (AD), the most common neurodegenerative disorder affecting the elderly. Over the past years, several approaches and compounds developed for the treatment of AD have failed in clinical studies, likely in part due to their low penetration of the blood–brain barrier (BBB). Since nanotechnology-based strategies offer new possibilities for the delivery of drugs to the brain, this technique is studied intensively for the treatment of AD and other neurological disorders.

Methods: The $A\beta_{42}$ lowering drug flurbiprofen was embedded in polylactide (PLA) nanoparticles by emulsification-diffusion technique and their potential as drug carriers in an *in vitro* BBB model was examined. First, the cytotoxic potential of the PLA-flurbiprofen nanoparticles on endothelial cells and the cellular binding and uptake by endothelial cells was studied. Furthermore, the biological activity of the nanoparticulate flurbiprofen on γ -secretase modulation as well as its *in vitro* release was examined. Furthermore, the protein corona of the nanoparticles was studied as well as their ability to transport flurbiprofen across an *in vitro* BBB model.

Results: PLA-flurbiprofen nanoparticles were endocytosed by endothelial cells and neither affected the vitality nor barrier function of the endothelial cell monolayer. The exposure of the PLA-flurbiprofen nanoparticles to human plasma occurred in a rapid protein corona formation, resulting in their decoration with bioactive proteins, including apolipoprotein E. Furthermore, lumenally administered PLA-flurbiprofen nanoparticles in contrast to free flurbiprofen were able to modulate γ -secretase activity by selectively decreasing $A\beta_{42}$ levels in the abluminal compartment of the BBB model.

Conclusions: In this study, we were able to show that flurbiprofen can be transported by PLA nanoparticles across an *in vitro* BBB model and most importantly, the transported flurbiprofen modulated γ -secretase activity by selectively decreasing $A\beta_{42}$ levels. These results demonstrate that the modification of drugs via embedding in nanoparticles is a promising tool to facilitate drug delivery to the brain, which enables future development for the treatment of neurodegenerative disorders like AD.

Introduction

Alzheimer's disease (AD) is an age-related neurodegenerative disorder currently affecting more than 35 million people worldwide [1]. To date, the treatment of AD is only symptomatic and there is no cure for the disease [2]. AD is characterized by neuronal and synaptic loss, neurofibrillary tangle formation and extracellular deposits of amyloid- β ($A\beta$) peptides in susceptible brain regions, which result in learning and memory impairment [3]. $A\beta$

is generated through the sequential processing of the amyloid precursor protein (APP) by the β -secretase (BACE1) and the γ -secretase complex, and occurs in various isoforms between 36 and 46 amino acids in length, with $A\beta_{40}$ and $A\beta_{42}$ being the most prevalent variants [4-6]. Recently, we have demonstrated that APP is also processed by the metalloprotease meprin β , which might act as an additional enzyme, responsible for the release of N-terminal truncated $A\beta$ species and soluble N-terminal APP fragments, independent of BACE1 [7,8]. According to the amyloid hypothesis [9-11], abnormal accumulation or increased generation of $A\beta_{42}$ peptides in the brain is a primary event in the pathogenesis of AD [12-14].

* Correspondence: pietrzik@uni-mainz.de

¹Institute of Pathobiochemistry, University Medical Center of the Johannes Gutenberg University Mainz, Mainz, Germany

Full list of author information is available at the end of the article

Therefore, several strategies such as reducing A β generation, blocking its aggregation or enhancing A β clearance in the brain are thought to slow down the progression of the disease [15].

Besides APP, γ -secretase has more than 50 substrates with critical functions, such as cell signaling (for example, the Notch receptor), cell adhesion and apoptosis [16]. In earlier studies, we were able to demonstrate that the treatment of Chinese hamster ovary (CHO) cells with some nonsteroidal anti-inflammatory drugs (NSAIDs) such as indomethacin, ibuprofen and flurbiprofen specifically decreased the secretion of the A β_{42} peptides. This was accompanied by an increase of other A β isoforms (for example, A β_{37} and A β_{38}), indicating that NSAIDs subtly altered γ -secretase activity without significant impairment of other APP processing pathways or Notch signaling [17]. NSAIDs exert their principal therapeutic effects, reducing fever, pain and inflammation, by blocking the cyclooxygenase (COX)-mediated synthesis of inflammatory prostaglandins [18]. However, some NSAIDs were shown to selectively lower A β_{42} production *in vitro* and in mouse models of AD, independently of COX activity [17,19]. Later, small molecules with the ability to lower A β_{42} production without altering overall γ -secretase activity were termed γ -secretase modulators (GSM) [20]. Recently, the clinical development of the A β_{42} lowering agent tarenflurbil, the COX-inactive *R*-enantiomer of the NSAID flurbiprofen, has been stopped after failure in a Phase III clinical trial [21]. The results of this multicenter, randomized, double-blind, placebo-controlled trial did not show any slowing of cognitive decline after 18 months of treatment with tarenflurbil. While the reasons for the clinical failure of tarenflurbil are unknown, low penetration across the blood-brain barrier (BBB) and, consequently, insufficient target engagement in the brain may be likely explanations [21].

The BBB separates the circulating blood from the central nervous system (CNS) and is comprised of endothelial cells, astrocytes and pericytes. Tight junctions between the endothelial cells are an essential part of the BBB because they close the intracellular space and limit the paracellular flux of hydrophilic molecules across the BBB. The brain endothelial cells express a large number of specialized transporters and receptors, including carriers for glucose and amino acids. Therefore, the BBB plays a crucial role in the regulation of the constancy of the internal environment of the brain and is essential for the supply of the CNS with nutrients. Furthermore, it protects the brain from the peripheral circulation and toxic substances and restricts the transport of many therapeutically important drugs from the blood into the brain, including Alzheimer drugs, anticancer drugs, antibiotics and a wide variety of CNS-active drugs [22-24].

Over the past few years, a number of different strategies have been devised to overcome the BBB such as

osmotic opening of the tight junctions, the direct surgical administration of drugs into the brain or the development of drug carriers such as liposomes or nanoparticles [15,25-27]. However, the most notable and promising progression has been achieved by the use of nanotechnology. Liposomes as well as solid lipid nanoparticles or different polymeric nanoparticles have been successfully used for the transport of drugs across the BBB and into the brain [28]. Compared to free drug molecules or pro-drugs, the usage of nanoparticles possesses advantages such as a high drug-loading capacity of the nanoparticles. Furthermore, the drugs are protected against chemical or enzymatic degradation. In addition, nanoparticles can be actively targeted to a tissue via surface modifications of the nanoparticles [29].

In this study, we used polylactide (PLA) as the starting polymer for the nanoparticle preparation. By an emulsification-diffusion method, racemic flurbiprofen was embedded in the PLA nanoparticles. We decided to use flurbiprofen as a candidate substance since flurbiprofen has already been approved by the Food and Drug Administration (FDA) and is freely available as an over-the-counter medicine. We studied the transport of nanoparticulate flurbiprofen in an *in vitro* BBB model, and we could convincingly demonstrate that γ -secretase modulation *in vitro* was significantly enhanced after BBB penetration when flurbiprofen was delivered with nanoparticles compared to flurbiprofen alone.

Methods

Reagents and chemicals

Poly(L-lactide) (PLA, viscosity approximately 1.0 dL/g), flurbiprofen and polyvinyl alcohol (PVA) were obtained from Sigma (Steinheim, Germany). Lumogen[®] F orange 240 was provided by BASF (Ludwigshafen, Germany). All other reagents were of analytical grade and used as received.

Nanoparticle preparation

PLA nanoparticles were formed by an emulsification-diffusion technique. Briefly, 100 mg of PLA, 10 mg of flurbiprofen and 150 μ g of Lumogen[®] orange were dissolved in 2 ml dichloromethane (DCM). For the control PLA nanoparticles, 100 mg of PLA and 150 μ g of Lumogen[®] orange were dissolved in 2 ml DCM. For both formulations, the organic phase was added to 6 ml aqueous solution of PVA (2%, w/v). This mixture was homogenized in an ice bath for 30 minutes at 24,000 rpm (Ultra Turrax[®], IKA, Staufen, Germany) and diluted with 6 ml PVA solution (1%, w/v). DCM was removed by stirring the emulsion over night at room temperature. Finally, the particles were collected by centrifugation at 20,000 g for 10 minutes (Eppendorf, Hamburg, Germany) and washed twice with purified water before lyophilization.

Freeze-drying of the samples

For the lyophilization process a freeze-dryer Epsilon 1–4 (Martin Christ Gefriertrocknungsanlagen GmbH, Osterode am Harz, Germany) was used. Aliquots of the nanoparticles suspension (100 μ l) were dispensed into 2 ml Lyovials and diluted with 100 μ l trehalose solution (6%, w/v) as a cryoprotective agent. The freeze-drying cycle was performed according to an established protocol. First, the samples were frozen at -40°C for three hours. In the second step, primary drying was performed at a temperature of -34°C for 24 hours and a vacuum of 0.05 mbar, followed by a secondary drying phase for 11 hours at 20°C and a vacuum of 0.025 mbar. At the end of the drying process the vials were sealed and removed.

Nanoparticle characterization

Nanoparticles were analyzed with regard to particle diameter and polydispersity by photon correlation spectroscopy (PCS) and zeta potential was measured by microelectrophoresis using a Malvern Zetasizer Nano ZS (Malvern Instruments Ltd., Malvern, UK). Prior to measurement the samples were diluted with purified water.

Determination of flurbiprofen loading

The amount of flurbiprofen incorporated into the nanoparticles was determined by a HPLC method in which 1 mg nanoparticles was incubated in 1 ml acetonitrile for five minutes at room temperature. The sample was centrifuged (20,000 g for 10 minutes) and the chromatographic separation was carried out using aliquots of the supernatant. The aliquots (20 μ l) were injected into a Phenomenex Gemini NX 250 \times 4.6 mm, 5 μ m particle, C18 column (Phenomenex, Aschaffenburg, Germany). The flow rate was set to 1 ml/minute during the separation, with the mobile phase composed of acetonitrile and 0.1% (v/v) trifluoroacetic acid (57.5: 42.5, v/v). The eluate was analyzed at a wavelength of 245 nm.

In vitro release of flurbiprofen

For each point in time individual samples were prepared as follows: 1 mg nanoparticles were incubated in 1 ml phosphate buffer (0.1 mM, pH = 7.5) at 37°C under constant shaking. At defined points in time (0, 0.5, 1, 3, 5, 7, 24 hours) one sample was centrifuged (20,000 g for 10 minutes). The amount of the released drug was determined in the supernatant by HPLC as described above.

Nanoparticles reconstitution

The freeze-dried nanoparticles were always reconstituted prior to the cell culture experiments. Therefore, 40 mg nanoparticles were dissolved in 1 ml purified water and vortexed for two minutes.

Cell culture

The mouse brain endothelial cell line bEnd.3 (ATCC, Manassas, VA, USA) was cultured in DMEM (Gibco, Darmstadt, Germany) high glucose medium containing 10% fetal bovine serum and 100 U/ml penicillin/streptomycin (Gibco, Darmstadt, Germany). For the experiments, 5×10^4 cells per cm^2 were seeded and the experiments were performed after three days when the cells were post-confluent. APP751 overexpressing CHO cells (7WD10) were cultured in DMEM high glucose medium containing 10% fetal bovine serum, 1 mM sodium pyruvate (Gibco, Darmstadt, Germany), 100 U/ml penicillin/streptomycin and 400 μ g/ml geneticin (Calbiochem, Nottingham, UK). For the experiments, 3×10^4 cells per cm^2 were seeded, and after 24 hours cells were either treated or co-cultured with the bEnd.3 in the *in vitro* BBB model.

Measurement of cytotoxicity

The cytotoxicity of free flurbiprofen or PLA-flurbiprofen nanoparticles was assessed using the alamarBlue[®] reagent (Invitrogen, Karlsruhe, Germany). bEnd.3 cells were seeded on 96-well plates (Greiner, Frickenhausen, Germany) and after reaching post-confluency, cells were treated with increasing concentrations of free or nanoparticulate flurbiprofen, ranging from 25 μ M to 750 μ M (which corresponded to approximately 32 μ g/ cm^2 to 942 μ g/ cm^2 nanoparticles). The unit μ g per cm^2 refers to the amount of nanoparticles which are administered to the cells and this unit reflects possible local sedimentation on the surface of the cells, which locally might lead to different concentrations. After 72 hours, cells were incubated for another four hours with 1 \times alamarBlue[®] in medium. The absorbance was measured with an Anthos plate reader 2010 (Anthos Labtec, Salzburg, Austria) using a 570 nm measurement filter and a 600 nm reference filter. The cell viability was calculated as percentage of absorbance in relation to vehicle control treated cells.

Measurement of the transepithelial electrical resistance of endothelial cells

The transepithelial electrical resistance (TER) was used to analyze the toxicity of the nanoparticles for endothelial cells. bEnd.3 cells were seeded on 24-transwell cell culture inserts (ThinCerts[™], Greiner Bio-One, Frickenhausen, Germany) and placed into the cellZscope[®] device [30]. The TER of the cells was measured automatically every hour under physiological conditions by impedance spectroscopy. When cells were post-confluent, equal amounts of drug-loaded and unloaded nanoparticles (approximately 2.4 mg nanoparticles per cm^2) were added luminally and the TER was measured (this concentration corresponds to 750 μ M nanoparticulate flurbiprofen).

Cellular binding and uptake of nanoparticles

bEnd.3 cells were cultured in 24-well plates (Greiner, Frickenhausen, Germany) and treated with approximately 100 $\mu\text{g}/\text{cm}^2$ PLA-flurbiprofen nanoparticles for four hours at 37°C. After the incubation, cells were washed twice with PBS (Invitrogen, Karlsruhe, Germany) and subsequently trypsinized and harvested. Fixing was performed with FACS-Fix (10 g/L paraformaldehyde (PFA) and 8.5 g/L NaCl in PBS, pH 7.4) before flow cytometry analysis. Per sample, 10^4 cells were counted using FACSCalibur and CellQuest Pro software (Becton Dickinson, Heidelberg, Germany). The fluorescent labeling of the nanoparticles via Lumogen® F Orange 240 allowed a detection at 524/539 nm. To study the endocytotic uptake of the PLA nanoparticles, bEnd.3 cells were grown on glass coverslips (Marienfeld, Lauda-Königshofen, Germany) and treated with approximately 100 $\mu\text{g}/\text{cm}^2$ PLA-flurbiprofen nanoparticles at 4°C or 37°C for one hour or four hours. After the incubation, cells were put on ice and washed with PBS pH2 to remove the surface-bound nanoparticles, mimicking the acidic environment of endosomes where ligands dissociate from their receptor after internalization [31]. Cells were fixed with 4% PFA and 0.12 M sucrose in PBS for 10 minutes at room temperature and the cell nuclei were stained with 2 μM DRAQ5™ (Biostatus Limited, Leicestershire, UK) for 10 minutes at room temperature. Samples were embedded in Prolong® Gold antifade reagent (Invitrogen, Darmstadt, Germany) and the confocal laser scanning microscope (CLSM) study was performed with a CLSM equipped with ZEN 2008 software (LSM 710; Zeiss, Jena, Germany).

Treatment of 7WD10 with nanoparticles

To examine the biological activity of flurbiprofen-loaded nanoparticles, 7WD10 were treated with free or nanoparticulate flurbiprofen, ranging from 50 μM to 250 μM flurbiprofen. The administered concentration of the nanoparticles was adjusted to the free flurbiprofen, which corresponds to approximately 65 $\mu\text{g}/\text{cm}^2$ to 317 $\mu\text{g}/\text{cm}^2$ nanoparticles. After 48 hours, the supernatants were collected and centrifuged at 18,000 g for 20 minutes at 4°C. Levels of A β were measured by an A β specific ELISA.

Transport assay of nanoparticulate flurbiprofen in an *in vitro* BBB model

bEnd.3 cells were seeded on 24-transwell cell culture inserts. After reaching post-confluency, bEnd.3 cells were co-cultured with 7WD10 in the lower compartment and bEnd.3 cells were treated with 300 μM free flurbiprofen or nanoparticulate flurbiprofen, ranging from 300 μM to 750 μM flurbiprofen, which corresponds to approximately 380 $\mu\text{g}/\text{cm}^2$ to 942 $\mu\text{g}/\text{cm}^2$ nanoparticles. After 72 hours, the supernatants of the lower compartment

were collected and centrifuged at 18,000 g for 20 minutes at 4°C. Levels of A β were measured by an A β specific ELISA.

Measurement of A β species by ELISA

The levels of A β_{40} and A β_{42} peptides were determined using a cell-based sandwich ELISA assay as described [32]. Briefly, the monoclonal antibody IC16 (1:250 in PBS, pH 7.2) raised against amino acids 1 to 15 of the A β sequence was used as a capture antibody. To generate standard curves, synthetic A β_{40} and A β_{42} peptides (JPT Peptide Technologies, Berlin, Germany) were used. These A β peptides were solubilized in dimethyl sulfoxide (DMSO) at 10 $\mu\text{g}/\text{ml}$ and aliquots were stored at -80°C. The capture antibody was incubated overnight in 96-well high-binding microtiter plates at 4°C. After the capture antibody was removed, conditioned media samples (20 μl for detection of A β_{40} and 100 μl for A β_{42}) and freshly diluted A β peptide standards (125 to 6,000 pg/ml in PBS containing 0.05% Tween-20, 1% BSA) were added. Subsequently, C-terminal detection antibodies specific for A β_{40} and A β_{42} labeled with horseradish peroxidase (HRP) using the Pierce EZ-Link™ Plus Activated Peroxidase kit (Thermo Fisher Scientific, Rockford, IL, USA) were diluted in PBS containing 0.05% Tween-20, 1% BSA, added to each well, and incubated overnight at 4°C. Plates were washed three times with PBS containing 0.05% Tween-20 and once with PBS. Then, 50 μl of TMB (3,3',5,5'-Tetramethylbenzidine) ELISA Peroxidase Substrate (Interchim, Montluçon cedex, France) was added and incubated for 1 to 10 minutes at room temperature in the dark. The reaction was stopped by adding 50 μl of 2 M H₂SO₄ and the absorbance was measured using a Paradigm microplate reader (Beckman Coulter, Krefeld, Germany) at 450 nm. The levels of the A β_{40} and A β_{42} peptides were normalized to A β total (A β_{40} + A β_{42}) and the average of triplicate measurements for each concentration was normalized to the control condition (DMSO or unloaded PLA nanoparticles).

Nanoparticle plasma protein binding assay

To obtain human plasma, blood was taken at the ENT department at the Medical University Mainz from 15 different seemingly healthy donors in K₂EDTA coated tubes (Greiner, Frickenhausen, Germany) to prevent blood clotting. The blood samples were labeled anonymously and could not be traced back to a specific donor. Studies were approved by the local ethics committee of the University Medical Center of the Johannes Gutenberg-University of Mainz, and informed consent was obtained in accordance with the Declaration of Helsinki. The PLA nanoparticles were incubated with equal amounts of human plasma for different time points (5, 15, 30 and 60 minutes), loaded onto a sucrose cushion (0.7 M in PBS) and centrifuged through the cushion to separate nanoparticle-protein complexes from plasma (12,000 rpm for 20 minutes at 4°C).

Pellets were washed three times with PBS and proteins were eluted from the recovered particles by adding an equal volume of SDS sample buffer (62.5 mM Tris-HCl pH 6.8; 2% (w/v) SDS, 10% glycerol, 50 mM dithiothreitol (DTT), 0.01% (w/v) bromophenol blue) to the pellet and incubated at 95°C for five minutes. Proteins were separated on a 12% SDS-polyacrylamide gel. To visualize the kinetic evolution of the protein corona, the SDS-polyacrylamide gel was stained with Coomassie brilliant blue R-250 (Bio-Rad, München, Germany) and protein quantification was performed using the BioRad Protein Assay (Bio-Rad, München, Germany). To examine the presence of apolipoproteins in the nanoparticle-protein complex, proteins were transferred onto a polyvinylidene difluoride (PVDF) membrane. Membranes were blocked with 5% non-fat dry milk in Tris-buffered saline (TBS) containing 0.01% Tween-20 and the following antibodies were used: α -apoA4 (Cell Signaling, Boston, MA, USA); α -apoE and rabbit- α -mouse immunoglobulin G (IgG) antibody conjugated with HRP (Santa Cruz, Dallas, TX, USA).

Statistical analysis

All graphs and statistics were performed using the GraphPad Prism 4 software (GraphPad, La Jolla, CA, USA). Data were analyzed by two-way analysis of variance (ANOVA) coupled to Bonferroni post-tests for multiple comparisons. $P < 0.05$ was considered as statistically significance.

Results

Preparation and characterization of PLA nanoparticles

To investigate a novel approach to deliver potential drugs against AD into the brain, we established an *in vitro* BBB model to analyze the transport and functionality of the $A\beta_{42}$ lowering drug flurbiprofen embedded in PLA nanoparticles. The PLA-flurbiprofen nanoparticles were prepared by an emulsification-diffusion method. For the visualization of the nanoparticles, Lumogen® F Orange 240 (kindly provided by BASF) was added during the preparation. The particles had a size between 213.6 and 218.1 nm. The amount of incorporated flurbiprofen was determined by HPLC (Table 1).

Determination of cell toxicity

The cytotoxicity of the PLA-flurbiprofen nanoparticles was assessed using the alamarBlue® cell viability reagent. Therefore, post-confluent bEnd.3 cells were incubated with increasing concentrations of free flurbiprofen or

PLA-flurbiprofen nanoparticles. As reported earlier by us and others, free flurbiprofen has a cytotoxic potential at concentrations above 300 μ M (Figure 1A) [19,33]. In contrast, nanoparticulate flurbiprofen showed no cytotoxic potential (Figure 1B). The toxicity of the nanoparticles was further analyzed by the measurement of their influence on the integrity of endothelial cells (Figure 2). Therefore, the TER of the cells was measured by impedance spectroscopy using a cellZscope® device [30]. bEnd.3 were cultured on cell culture inserts and after reaching post-confluency, cells were treated with 750 μ M nanoparticulate flurbiprofen. The nanoparticles showed no interference with the TER development, even at this high concentration. Taken together, the cell viability as well as the integrity of the endothelial cells was not impaired by the nanoparticulate flurbiprofen and, therefore, any cytotoxic effect could be excluded.

Biological activity of nanoparticles

Although we could convincingly demonstrate the tolerance of endothelial cells to nanoparticulate flurbiprofen, we had to establish whether nanoparticulate flurbiprofen had any biological activity on modulating the γ -secretase function. Therefore, we first analyzed the *in vitro* release of flurbiprofen from the PLA nanoparticles at a physiological pH by incubating 1 mg nanoparticles in 1 ml phosphate buffer (pH = 7.5) at 37°C. By HPLC, we observed that flurbiprofen is constantly released from the nanoparticles over time with an initial rapid release followed by a slower exponential phase (Figure 3). Consequently, we analyzed the influence of nanoparticulate flurbiprofen on γ -secretase activity using APP overexpressing cells (7WD10). The 7WD10 cells were incubated with free flurbiprofen or PLA-flurbiprofen nanoparticles (both ranging from 50 μ M to 250 μ M). After 48 hours, tissue culture supernatants were collected and the amounts of $A\beta_{40}$ and $A\beta_{42}$ were measured by an $A\beta$ specific ELISA. As reported earlier by us and others, free flurbiprofen specifically modulates γ -secretase activity by decreasing the levels of $A\beta_{42}$ in a concentration dependent manner whereas the levels of $A\beta_{40}$ remained unaffected (Figure 4A) [17,19]. For the treatment with the PLA-flurbiprofen nanoparticles, the administered concentration of the nanoparticles was adjusted to the free flurbiprofen to compare the effects of the nanoparticulate and the free drug. The nanoparticulate flurbiprofen reduced the amount of the $A\beta_{42}$ peptides in a concentration dependent manner (Figure 4B). The levels of $A\beta_{40}$ remained unaffected. The

Table 1 Physicochemical characteristics of poly(lactide) (PLA) nanoparticles

Formulation	Mean particle diameter (nm)	Polydispersity index	Zeta potential (mV)	Flurbiprofen loading (μ g/mg)
PLA-flurbiprofen nanoparticles	218.1	0.053	-17.4	60.2
PLA nanoparticles	213.6	0.048	-27.6	-

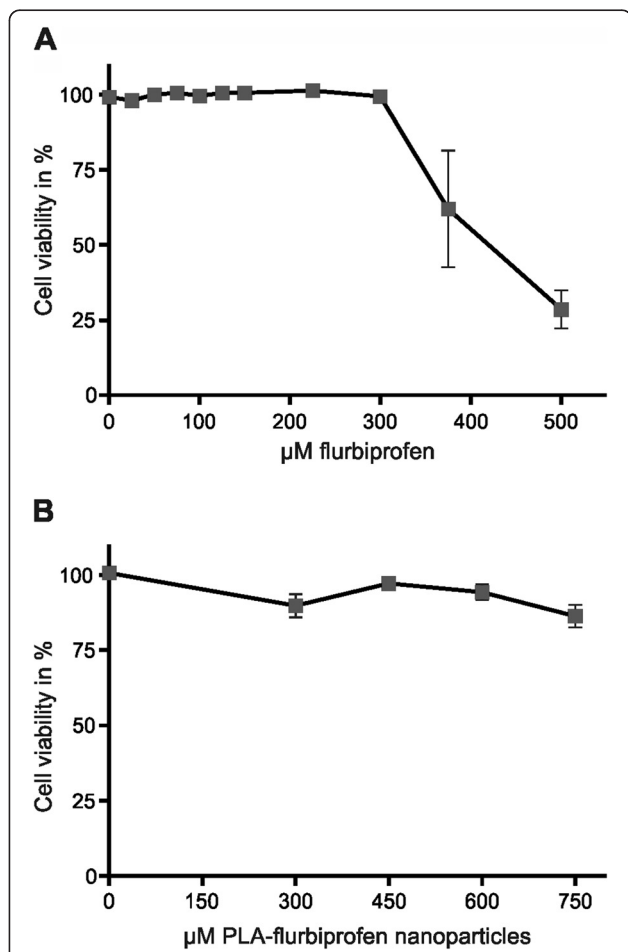


Figure 1 Cytotoxicity of free or nanoparticulate flurbiprofen. bEnd.3 cells were treated with the indicated concentrations of free flurbiprofen (A) or PLA-flurbiprofen nanoparticles (B) for 72 hours. The cytotoxicity was assessed after a four hour incubation with 1 × alamarBlue®. The absorbance was measured and the cell viability was calculated as a percentage of absorbance in relation to vehicle control treated cells. The data represent mean ± SEM of n ≥ 3. PLA, poly lactide; SEM, standard error of the mean.

decrease of the Aβ₄₂ levels by the PLA-flurbiprofen nanoparticles is achieved by the *in vitro* release of the drug from the nanoparticles, as shown in Figure 3. Thus, the nanoparticulate flurbiprofen exhibited a biological activity to modulate γ-secretase *in vitro* comparable to free flurbiprofen.

Cellular binding and uptake of nanoparticles

To analyze the potential of nanoparticulate flurbiprofen to cross a cellular monolayer, we first examined the cellular binding and uptake of the PLA-flurbiprofen nanoparticles by endothelial cells. Therefore, bEnd.3 cells were incubated with the nanoparticles for four hours at 37°C and subsequently analyzed by flow cytometry (Figure 5A). Compared to the untreated control, cellular binding of the PLA-flurbiprofen nanoparticles was

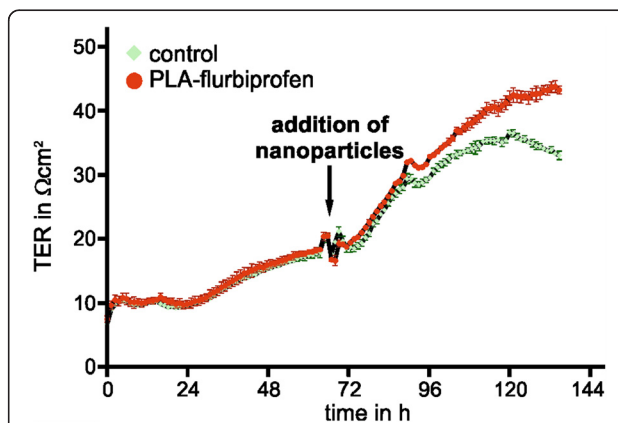


Figure 2 Influence of PLA-flurbiprofen nanoparticles on the integrity of the endothelial cell barrier. bEnd.3 cells were cultivated on cell culture inserts in a cellZscope® device. When cells were post-confluent, approximately 2.4 mg nanoparticles per cm² (corresponding to 750 µM nanoparticulate flurbiprofen) were added to the luminal side of the endothelial cells and the TER was measured every hour by impedance spectroscopy. PLA, poly lactide; TER, transepithelial electrical resistance.

detected. The cellular uptake of the nanoparticles was further studied by CLSM. Post-confluent bEnd.3 cells were incubated with nanoparticles for one to four hours at either 37°C or at 4°C as a control to inhibit endocytosis. At 4°C, the bEnd.3 cells exhibited no signal of the nanoparticles demonstrating that the nanoparticles were not endocytosed (Figure 5B). However, at 37°C, the nanoparticles were endocytosed by the bEnd.3 cells (Figure 5C) and this uptake increased with longer incubation time (Figure 5D).

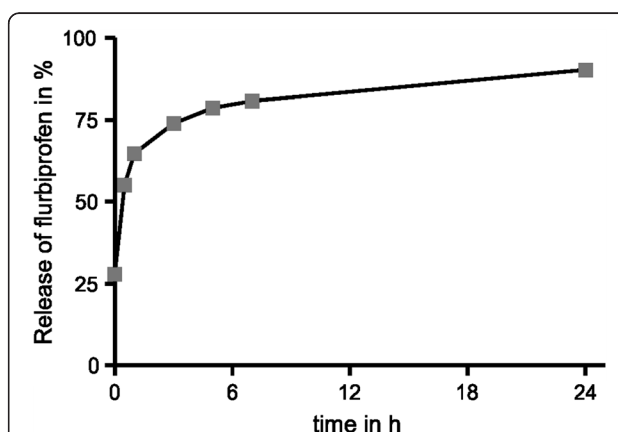
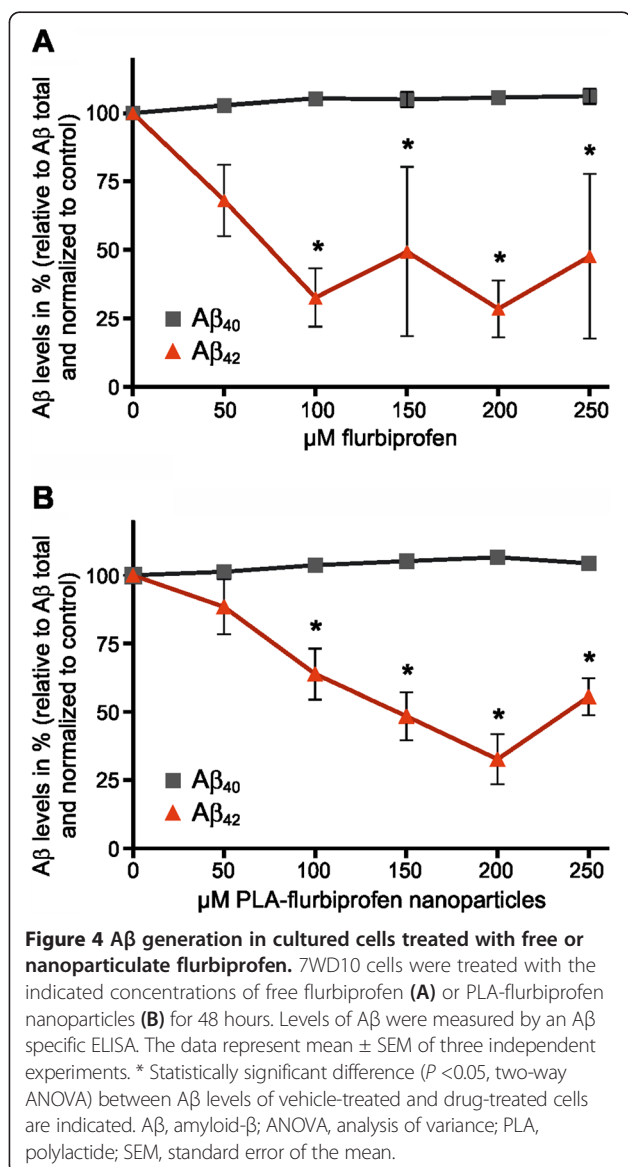


Figure 3 Flurbiprofen is released over time from the PLA nanoparticles. PLA-flurbiprofen nanoparticles were dissolved in an aqueous solution at pH 7.5 and the amount of flurbiprofen in the solution was measured by HPLC at different time points. The release is shown as the percentage of the total amount of incorporated flurbiprofen in the nanoparticles. PLA, poly lactide.



Transport of nanoparticles across endothelial cells

To study the ability of PLA nanoparticles to transport flurbiprofen across an *in vitro* BBB model, bEnd.3 cells were cultivated in the luminal compartment of cell culture inserts until a post-confluent monolayer had grown (Figure 6A). Then, 7WD10 were co-cultured abuminally together with the bEnd.3 cells. After confirmation of the tightness of the endothelial cell monolayer by TER measurement, nanoparticles were added to the bEnd.3 cells at the luminal side. As a readout for the transport of nanoparticulate NSAIDs, we collected the medium in the abuminal compartment after 72 hours and measured the γ -secretase activity by determining the levels of Aβ₄₀ and Aβ₄₂ using a specific ELISA. Furthermore, we measured the amount of flurbiprofen by HPLC. Luminally administered free flurbiprofen (300 μM) had

no effect on the levels of Aβ₄₀ and Aβ₄₂ in the abuminal compartment (Figure 6B). We only administered 300 μM free flurbiprofen in this experimental setup due to its cytotoxic potential at higher concentrations (Figure 2A). By HPLC, we measured the concentration of flurbiprofen in the abuminal compartment and we could detect that approximately 10% of the initial concentration was diffusing across the endothelial cell monolayer, which was not sufficient to reduce Aβ₄₂ (Table 2). When flurbiprofen-loaded nanoparticles were added luminally to the endothelial cells, Aβ₄₂ levels decreased in a concentration dependent manner whereas the levels of Aβ₄₀ remained unchanged (Figure 6C). Since the IC₅₀ for flurbiprofen induced γ -secretase modulation is about 150 to 200 μM, we hypothesize that the final concentration of flurbiprofen in the abuminal compartment, most likely still bound to nanoparticle components, is therefore sufficient to reduce the Aβ₄₂ levels. These results strongly indicate that the nanoparticles were transported in this *in vitro* BBB model and that the embedded flurbiprofen was able to reduce Aβ₄₂ levels by modulating the γ -secretase activity.

Human blood plasma corona of the nanoparticles

When nanoparticles enter a biological fluid, proteins rapidly compete for binding to the nanoparticle surface, leading to the formation of a protein corona that critically defines the biological identity of the particle. The properties of such a particle-protein complex differ significantly from those of the formulated particle. Hence, the further biological responses of the body as well as the biodistribution of the nanoparticles are expected to be influenced by the nanoparticle-protein complex [34]. Therefore, the PLA nanoparticles were incubated with human blood plasma for several time points and we examined the binding of plasma proteins to the nanoparticles. The protein binding profiles were visualized by SDS-PAGE, demonstrating that an exposure for five minutes was already sufficient for an efficient corona formation (Figure 7A). Also, the amount of corona proteins increased over time, albeit the corona seems to change only quantitatively rather than qualitatively. Furthermore, we examined the presence of apolipoproteins in the protein corona (Figure 7B). Apolipoproteins are part of the circulating lipoproteins and serve as receptor ligands for lipid and cholesterol uptake and metabolism, and it was suggested that apolipoprotein-modified nanoparticles are able to transport drugs across the BBB [35-38]. We observed that apolipoprotein E (ApoE) and apolipoprotein A4 (ApoA4) are already present in the nanoparticle-protein complex after five minutes of exposure, and that the amount of ApoA4 slightly decreased and the ApoE concentrations significantly increased over time. The formation of the apolipoprotein corona on the PLA nanoparticles indicates a potential

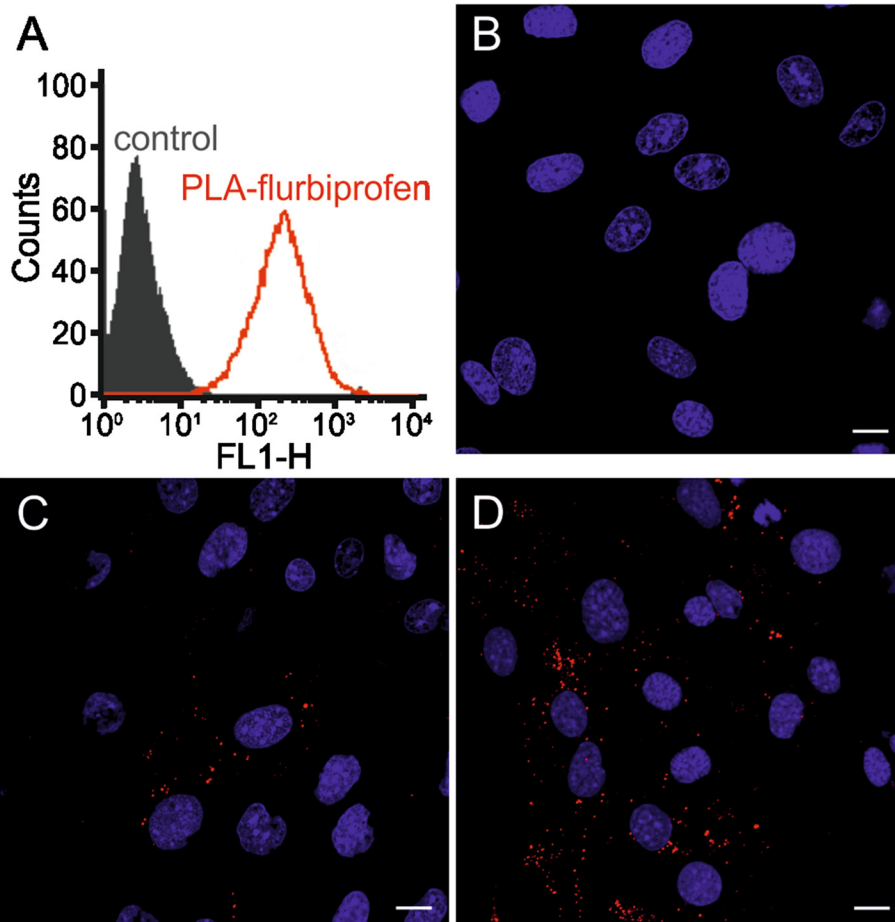


Figure 5 Cellular binding of the PLA-flurbiprofen nanoparticles. (A) bEnd.3 cells were treated with approximately 100 $\mu\text{g}/\text{cm}^2$ PLA-flurbiprofen nanoparticles for four hours at 37°C and the cellular binding was quantified by flow cytometry. The data are shown as histograms of the FL1-H channel (red: PLA-flurbiprofen nanoparticles, black: untreated control). (B-D) bEnd.3 cells were treated with approximately 100 $\mu\text{g}/\text{cm}^2$ nanoparticles. To inhibit endocytosis, the cells were treated at 4°C (B). For the cellular uptake, cells were treated for one hour (C) or four hours (D) at 37°C. After the incubation period, the cells were put on ice and washed with acidic PBS to remove the surface-bound nanoparticles. The cells were fixed with paraformaldehyde and cell nuclei were stained with DRAQ5TM. Scale bar, 10 μm . PLA, polylactide.

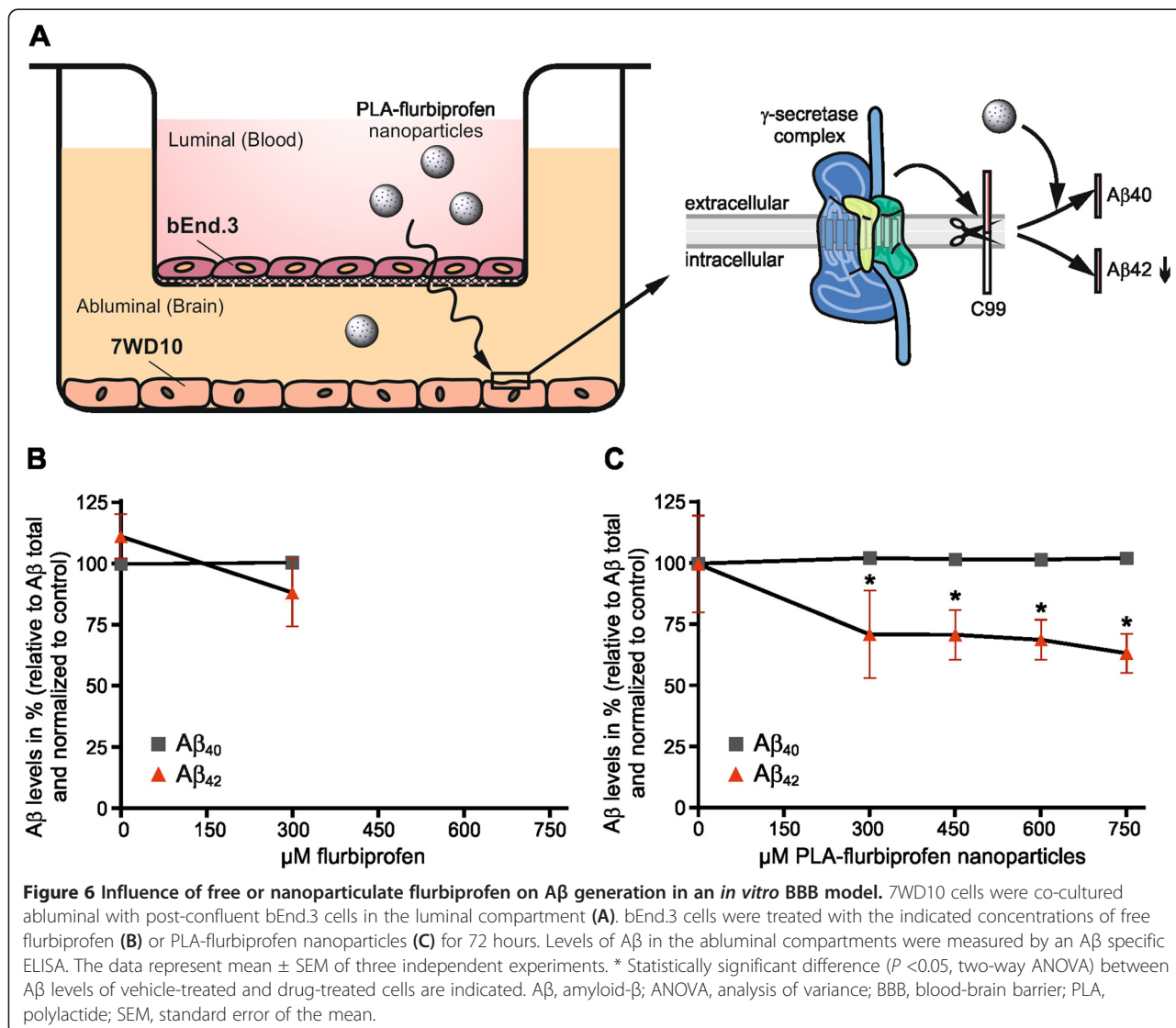
transport route of the nanoparticles through a lipoprotein receptor transcytosis pathway [37,39].

Discussion

AD is a severe neurodegenerative disease affecting more than 35 million people worldwide, and is characterized by memory impairment, neurofibrillary tangles formation and extracellular accumulation of $\text{A}\beta_{42}$ in insoluble plaques. The $\text{A}\beta_{42}$ peptide is generated through the proteolytic processing of APP, and its accumulation or increased generation is thought to be one of the primary events in the pathogenesis of AD [12-14,40]. According to this hypothesis, reduced generation or enhanced clearance of $\text{A}\beta_{42}$ peptides and plaques would be expected to modify the disease course in AD [41]. Recently, the $\text{A}\beta_{42}$ lowering agent tarenflurbil, the *R*-enantiomer of flurbiprofen, failed in a phase III clinical trial, presumably because it could

not cross the BBB in high enough concentrations [21]. Generally, brain penetration of CNS active drugs is mostly limited by the BBB, and several strategies have been devised to overcome this barrier to deliver therapeutic drugs to the brain [42]. To date, drug carriers, such as nanoparticles, have been studied intensively for neurological disorders, cancer and other diseases, and some of them are in different trial phases or even commercially available [43,44]. In this study, we examined the efficiency of nanoparticulate flurbiprofen to cross the BBB in order to decrease selectively the levels of $\text{A}\beta_{42}$ peptides in the brain.

We decided to study PLA-nanoparticle formulations because this starting material is FDA-approved, biodegradable and biocompatible [29,45]. In addition, we decided to use flurbiprofen as a GSM because it is also FDA-approved, commercially available and, most importantly, its GSM activity has been studied intensively

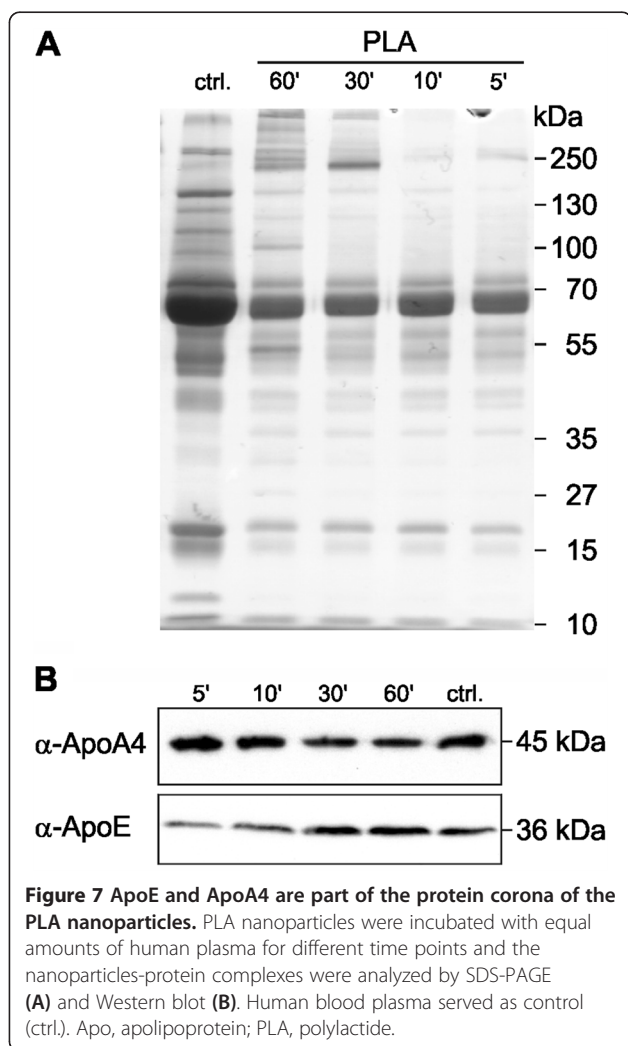


in vivo and *in vitro* [17,19]. First, the cytotoxic potential of the PLA-flurbiprofen nanoparticles in comparison to free flurbiprofen was investigated. Compared to free flurbiprofen, the PLA-flurbiprofen nanoparticles did not affect cell viability. Even if high amounts of nanoparticles were administered to the endothelial cells, and including that the nanoparticles may sediment in the culture medium on the surface of the cells which may lead to different local concentrations, these amounts did

not perturb the integrity of an endothelial barrier. Thus, the embedding of flurbiprofen in nanoparticles disguised its cytotoxic potential which enables the application of higher concentrations on endothelial cells without any cytotoxic potential. The cellular binding and uptake of the nanoparticles was observed by flow cytometry and CLSM. These data confirmed the cellular binding as well as a time-dependent uptake of the nanoparticles by endothelial cells. Next, the *in vitro* release of flurbiprofen from the

Table 2 Concentration of flurbiprofen in the abluminal compartment measured by HPLC

μM luminally administered	μM abluminally measured by HPLC	% of administered concentration
300 μM flurbiprofen	41.85	13.95
300 μM PLA-flurbiprofen nanoparticles	31.56	10.52
450 μM PLA-flurbiprofen nanoparticles	46.82	10.40
600 μM PLA-flurbiprofen nanoparticles	63.95	10.66
750 μM PLA-flurbiprofen nanoparticles	83.70	11.16



nanoparticles was investigated, which showed that the drug is constantly released over the time. Consequently, we examined the biological activity of the nanoparticulate flurbiprofen compared to free flurbiprofen in the APP overexpressing cell line 7WD10. Free flurbiprofen specifically decreased $A\beta_{42}$ levels with a maximal effect size of approximately 70%, in good agreement with previous studies [17,19]. For the PLA-flurbiprofen nanoparticles, a similar decrease in $A\beta_{42}$ levels was detected. Since flurbiprofen is released constantly over time from the PLA nanoparticles, its biological activity to modulate γ -secretase activity *in vitro* was comparable to free flurbiprofen. Based on these observations that the PLA-flurbiprofen nanoparticles were able to lower $A\beta_{42}$ levels and were endocytosed by endothelial cells, we studied their transport in an *in vitro* BBB model. In these experiments, the endothelial cells were cultured luminally on cell culture inserts (representing the blood side) with the 7WD10 cell line in the abluminal compartment (representing the brain side). In this experimental setup, free flurbiprofen did not reduce

$A\beta_{42}$ levels, because it was not sufficiently transported across the endothelial cell monolayer at high enough concentration. This is in agreement with phase I dosing studies of *R*-flurbiprofen in humans [46]. In these studies, healthy volunteers were treated for 21 days with up to 800 mg twice daily of *R*-flurbiprofen. Maximal plasma concentrations of *R*-flurbiprofen up to 185 μ M were measured, well in the range of the $A\beta_{42}$ -lowering activity of flurbiprofen in tissue culture experiments. However, flurbiprofen concentrations in the cerebrospinal fluid (CSF) of the volunteers were found to be more than 100-fold lower with an average CSF to plasma ratio of 0.5%. No significant changes in CSF $A\beta_{42}$ levels were observed in *R*-flurbiprofen treated individuals compared to placebo controls. In the failed Phase III clinical study of *R*-flurbiprofen, CSF drug concentration were not measured but the highest dose administered in the trial was identical to the phase I study, predicting similarly low brain concentrations [21]. Importantly, we could detect a significant decrease of $A\beta_{42}$ levels for the nanoparticulate flurbiprofen. In earlier studies, we were able to demonstrate that drug-loaded nanoparticles exhibited a higher biological activity than the free drug alone [47]. The nanoparticulate drug had a lower IC_{50} value than the free drug molecule resulting in a higher efficiency of the nanoparticulate formulation. Furthermore, the nanoparticles may gradually sediment in the culture medium on the surface of the cells, which can locally lead to higher concentrations of the nanoparticulate flurbiprofen compared to free flurbiprofen. For the HPLC measurements, the total capacity of the abluminal compartment was used and the total concentration of free or nanoparticulate flurbiprofen was measured. Thus, total concentration of the nanoparticulate flurbiprofen may not be higher compared to free flurbiprofen, but if the sedimentation of the nanoparticles is taken into account, the concentrations of the nanoparticulate flurbiprofen can be locally higher resulting in significantly decreased levels of $A\beta_{42}$. The embedding of flurbiprofen into nanoparticles not only disguises its cytotoxic potential, it further enables the administration of higher drug concentrations resulting in a sufficient transport of the drug across the endothelial cell monolayer. These data provide a proof of principle showing that even NSAIDs with low GSM activity can efficiently lower $A\beta_{42}$ levels if transported sufficiently across the BBB. As a potential transport mechanism we would like to highlight the presence of the lipoproteins ApoA4 and ApoE in the protein corona of the nanoparticles. In biological fluids, proteins and other biomolecules bind to the surface of the nanoparticles and build a corona which determines their biological properties. For instance, members of the apolipoprotein family enable the endocytotic uptake through lipoprotein receptors. In a recent study, we were able to show that ApoE-modified nanoparticles were actively endocytosed by endothelial cells and that the

low density lipoprotein receptor-related protein 1 (LRP1) is involved in this process [37]. Thus, the transport of the nanoparticulate flurbiprofen may be facilitated by the surface-bound proteins mimicking endogenous lipoproteins via endocytosis by transporters such as LRP1.

Conclusions

Over the past years, the application of nanotechnology-based strategies for the treatment or diagnosis of AD has been investigated by many groups [43,48]. Some approaches, like this study, focused on the encapsulation of molecules into nanoparticles for delivery to the brain; others dealt with a reduction of amyloid plaques toxicity or focused on the early detection of the disease [49]. In this study, we could show that after embedding in polymeric nanoparticles, flurbiprofen can be transported across the BBB and retains its biological activity. However, some improvements and optimizations of the nanoparticles are required for future applications. The use of other GSMs with higher potency, or surface modifications such as coupling the nanoparticles with peptides or ligands, which can achieve a higher bioavailability or a specific targeting to the brain, are just some examples for achievable improvements [15,20]. To date, an enormous amount of work has been invested in the sophisticated surface-functionalization of drug carriers to improve their targeting and/or bioactivity, but the potential impact of the protein corona on the success or failure of these strategies has been mostly neglected so far [34,50,51]. However, we show for the first time that the blood plasma protein corona on PLA nanoparticles is established rapidly, is complex and appears to change predominantly only quantitatively over time. The surface-functionalization of nanoparticles with apolipoproteins has been shown to facilitate translocation through the BBB [37,38,52], and we assume that the observed 'natural functionalization' of the PLA nanoparticles with ApoE and ApoA4 may facilitate the BBB transport of the nanoparticulate flurbiprofen via endocytosis using transporters such as LRP1 [37]. Whether further surface modifications may increase BBB transport remains to be investigated. The surface-functionalization of drug carriers is labor and cost-intensive and therefore often limited to (pre)clinical studies in nanobiomedicine. Since the protein corona is established in physiological environments, this 'natural biofunctionalization' should be exploited to improve the bioactivity of drug carriers to overcome these limitations.

Taken together, we were able to show that the modification of usually nonpermeable drugs via embedding in nanoparticles results in an efficient transport across an endothelial cell monolayer and that these nanotechnology-based strategies are very promising to generate novel therapeutic options for AD and other CNS diseases.

Abbreviations

AD: Alzheimer's disease; ApoA4: Apolipoprotein A4; ApoE: Apolipoprotein E; APP: Amyloid precursor protein; A β : Amyloid- β ; BBB: Blood-brain barrier; BSA: Bovine serum albumin; CHO: Chinese hamster ovary; CLSM: Confocal laser scanning microscopy; CNS: Central nervous system; COX: Cyclooxygenase; CSF: Cerebrospinal fluid; DCM: Dichloromethane; DMEM: Dulbecco's modified Eagle's medium; DMSO: Dimethyl sulfoxide; ELISA: Enzyme-linked immunosorbent assay; FDA: Food and Drug Administration; GSM: γ -secretase modulators; HPLC: High performance liquid chromatography; HRP: Horseradish peroxidase; NSAIDs: Nonsteroidal anti-inflammatory drugs; PBS: Phosphate-buffered saline; PFA: Paraformaldehyde; PLA: Polylactide; PVA: Polyvinyl alcohol; TER: Transepithelial electrical resistance.

Competing interests

The authors declare that they have no competing interests.

Authors' contributions

SM designed the studies and wrote the manuscript. IZ, JS, DD and SB performed experiments. SW and SyW contributed to the experimental design and the writing of the manuscript. RHS, MD, RS, SR, MW, KL and HB contributed to the writing of the manuscript. CUP supervised the experimental design and entire work of the manuscript. All authors read and approved the final manuscript.

Acknowledgements

We thank Roswitha Nehrbauß for excellent technical assistance and Michael Plenikowski for the illustrations. SM would like to thank the 'Hans and Ilse Breuer' Foundation for financial support. This work was additionally supported by the German Bundesministerium für Bildung und Forschung (BMBF) (01EW1009 to CUP and 01EW1010 to HB), the Deutsche Forschungsgemeinschaft (DFG-SPP1313), the ERA-NET NEURON 2nd call for translational research projects 2009, the Austrian Science Fund (FWF) project I453, the Carl-Zeiss Stiftung (ChemBioMed) and the Stiftung Rheinland-Pfalz für Innovation (InnoRP1076).

Author details

¹Institute of Pathobiochemistry, University Medical Center of the Johannes Gutenberg University Mainz, Mainz, Germany. ²Institute of Pharmaceutical Technology and Biopharmacy, University of Muenster, Muenster, Germany. ³Department of Cell Biology and Applied Virology, Fraunhofer Institute for Biomedical Engineering, St. Ingbert, Germany. ⁴Molecular and Cellular Oncology/Mainz Screening Center (MSC), ENT-Department, University Medical Center of the Johannes Gutenberg University Mainz, Mainz, Germany. ⁵Department of Neuropathology, Heinrich Heine University, Duesseldorf, Germany. ⁶The Biophysical Interdisciplinary Schottenstein Center for the Research and Technology of the Cellome, Bar Ilan University, Ramat gan, Israel. ⁷Department of Neurology, Medical University of Graz, Graz, Austria. ⁸NeuroScios GmbH, St. Radegund/Graz, Austria.

Received: 14 August 2013 Accepted: 16 October 2013

Published: 27 Nov 2013

References

1. Querfurth HW, LaFerla FM: **Alzheimer's disease.** *N Engl J Med* 2010, **362**:329-344.
2. Alzheimer's Association: **Alzheimer's disease facts and figures.** *Alzheimers Dement* 2012, **2012**:131-168.
3. LaFerla FM, Oddo S: **Alzheimer's disease: Abeta, tau and synaptic dysfunction.** *Trends Mol Med* 2005, **11**:170-176.
4. Haass C, Selkoe DJ: **Cellular processing of beta-amyloid precursor protein and the genesis of amyloid beta-peptide.** *Cell* 1993, **75**:1039-1042.
5. Burdick D, Soreghan B, Kwon M, Kosmoski J, Knauer M, Henschen A, Yates J, Cotman C, Glabe C: **Assembly and aggregation properties of synthetic Alzheimer's A4/beta amyloid peptide analogs.** *J Biol Chem* 1992, **267**:546-554.
6. Kuo YM, Emmerling MR, Vigo-Pelfrey C, Kasunic TC, Kirkpatrick JB, Murdoch GH, Ball MJ, Roher AE: **Water-soluble Abeta (N-40, N-42) oligomers in normal and Alzheimer disease brains.** *J Biol Chem* 1996, **271**:4077-4081.
7. Jefferson T, Causevic M, auf dem Keller U, Schilling O, Isbert S, Geyer R, Maier W, Tschickardt S, Jumpertz T, Weggen S, Bond JS, Overall CM, Pietrzik CU, Becker-Pauly C: **Metalloprotease meprin beta generates NCT**

- N-terminal amyloid precursor protein fragments in vivo. *J Biol Chem* 2011, **286**:27741–27750.
8. Bien J, Jefferson T, Causevic M, Jumpertz T, Munter L, Multhaupt G, Weggen S, Becker-Pauly C, Pietrzik CU: **The metalloprotease meprin beta generates amino terminal-truncated amyloid beta peptide species.** *J Biol Chem* 2012, **287**:33304–33313.
 9. Selkoe DJ: **The molecular pathology of Alzheimer's disease.** *Neuron* 1991, **6**:487–498.
 10. Hardy J, Allsop D: **Amyloid deposition as the central event in the aetiology of Alzheimer's disease.** *Trends Pharmacol Sci* 1991, **12**:383–388.
 11. Hardy JA, Higgins GA: **Alzheimer's disease: the amyloid cascade hypothesis.** *Science* 1992, **256**:184–185.
 12. Golde TE: **Alzheimer disease therapy: can the amyloid cascade be halted?** *J Clin Invest* 2003, **111**:11–18.
 13. Wyss-Coray T: **Inflammation in Alzheimer disease: driving force, bystander or beneficial response?** *Nat Med* 2006, **12**:1005–1015.
 14. McGowan E, Pickford F, Kim J, Onstead L, Eriksen J, Yu C, Skipper L, Murphy MP, Beard J, Das P, Jansen K, Delucia M, Lin WL, Dolios G, Wang R, Eckman CB, Dickson DW, Hutton M, Hardy J, Golde T: **Abeta42 is essential for parenchymal and vascular amyloid deposition in mice.** *Neuron* 2005, **47**:191–199.
 15. Sahni JK, Doggui S, Ali J, Baboota S, Dao L, Ramassamy C: **Neurotherapeutic applications of nanoparticles in Alzheimer's disease.** *J Control Release* 2011, **152**:208–231.
 16. Haapasalo A, Kovacs DM: **The many substrates of presenilin/gamma-secretase.** *J Alzheimers Dis* 2011, **25**:3–28.
 17. Weggen S, Eriksen JL, Das P, Sagi SA, Wang R, Pietrzik CU, Findlay KA, Smith TE, Murphy MP, Bulter T, Kang DE, Marquez-Sterling N, Golde TE, Koo EH: **A subset of NSAIDs lower amyloidogenic Abeta42 independently of cyclooxygenase activity.** *Nature* 2001, **414**:212–216.
 18. Warner TD, Mitchell JA: **Cyclooxygenases: new forms, new inhibitors, and lessons from the clinic.** *FASEB J* 2004, **18**:790–804.
 19. Eriksen JL, Sagi SA, Smith TE, Weggen S, Das P, McLendon DC, Ozols VV, Jessing KW, Zavitz KH, Koo EH, Golde TE: **NSAIDs and enantiomers of flurbiprofen target gamma-secretase and lower Abeta 42 in vivo.** *J Clin Invest* 2003, **112**:440–449.
 20. Bulic B, Ness J, Hahn S, Rennhack A, Jumpertz T, Weggen S: **Chemical biology, molecular mechanism and clinical perspective of gamma-secretase modulators in Alzheimer's disease.** *Curr Neuropharmacol* 2011, **9**:598–622.
 21. Green RC, Schneider LS, Amato DA, Beelen AP, Wilcock G, Swabb EA, Zavitz KH, Tarenfluril Phase 3 Study Group: **Effect of tarenfluril on cognitive decline and activities of daily living in patients with mild Alzheimer disease: a randomized controlled trial.** *JAMA* 2009, **302**:2557–2564.
 22. Abbott NJ, Chugani DC, Zaharchuk G, Rosen BR, Lo EH: **Delivery of imaging agents into brain.** *Adv Drug Deliv Rev* 1999, **37**:253–277.
 23. Abbott NJ, Ronnback L, Hansson E: **Astrocyte-endothelial interactions at the blood-brain barrier.** *Nat Rev Neurosci* 2006, **7**:41–53.
 24. Madara JL: **Tight junction dynamics: is paracellular transport regulated?** *Cell* 1988, **53**:497–498.
 25. Craparo EF, Bondi ML, Pitarresi G, Cavallaro G: **Nanoparticulate systems for drug delivery and targeting to the central nervous system.** *CNS Neurosci Ther* 2011, **17**:670–677.
 26. Brightman MW, Hori M, Rapoport SI, Reese TS, Westergaard E: **Osmotic opening of tight junctions in cerebral endothelium.** *J Comp Neurol* 1973, **152**:317–325.
 27. Rapoport SI, Robinson PJ: **Tight-junctional modification as the basis of osmotic opening of the blood-brain barrier.** *Ann N Y Acad Sci* 1986, **481**:250–267.
 28. Silva GA: **Nanotechnology applications and approaches for neuroregeneration and drug delivery to the central nervous system.** *Ann N Y Acad Sci* 2010, **1199**:221–230.
 29. Tosi G, Costantino L, Ruozi B, Forni F, Vandelli MA: **Polymeric nanoparticles for the drug delivery to the central nervous system.** *Expert Opin Drug Deliv* 2008, **5**:155–174.
 30. Wegener J, Abrams D, Willenbrink W, Galla HJ, Janshoff A: **Automated multi-well device to measure transepithelial electrical resistances under physiological conditions.** *Biotechniques* 2004, **37**:590–594, 596–597.
 31. Koo EH, Squazzo SL: **Evidence that production and release of amyloid beta-protein involves the endocytic pathway.** *J Biol Chem* 1994, **269**:17386–17389.
 32. Hahn S, Bruning T, Ness J, Czirr E, Baches S, Gijzen H, Korth C, Pietrzik CU, Bulic B, Weggen S: **Presenilin-1 but not amyloid precursor protein mutations present in mouse models of Alzheimer's disease attenuate the response of cultured cells to gamma-secretase modulators regardless of their potency and structure.** *J Neurochem* 2011, **116**:385–395.
 33. Grosch S, Tegeer I, Schilling K, Maier TJ, Niederberger E, Geisslinger G: **Activation of c-Jun-N-terminal-kinase is crucial for the induction of a cell cycle arrest in human colon carcinoma cells caused by flurbiprofen enantiomers.** *FASEB J* 2003, **17**:1316–1318.
 34. Monopoli MP, Aberg C, Salvati A, Dawson KA: **Biomolecular coronas provide the biological identity of nanosized materials.** *Nat Nanotechnol* 2012, **7**:779–786.
 35. Kreuter J, Shamenkov D, Petrov V, Ramge P, Cychutek K, Koch-Brandt C, Alyautdin R: **Apolipoprotein-mediated transport of nanoparticle-bound drugs across the blood-brain barrier.** *J Drug Target* 2002, **10**:317–325.
 36. Wagner S, Kufleitner J, Zensi A, Dadparvar M, Wien S, Bungert J, Vogel T, Worek F, Kreuter J, von Briesen H: **Nanoparticulate transport of oximes over an in vitro blood-brain barrier model.** *PLoS One* 2010, **5**:e14213.
 37. Wagner S, Zensi A, Wien SL, Tschickardt SE, Maier W, Vogel T, Worek F, Pietrzik CU, Kreuter J, von Briesen H: **Uptake mechanism of ApoE-modified nanoparticles on brain capillary endothelial cells as a blood-brain barrier model.** *PLoS One* 2012, **7**:e32568.
 38. Zensi A, Begley D, Pontikis C, Legros C, Mihoreanu L, Wagner S, Buchel C, von Briesen H, Kreuter J: **Albumin nanoparticles targeted with Apo E enter the CNS by transcytosis and are delivered to neurones.** *J Control Release* 2009, **137**:78–86.
 39. Pflanzner T, Janko MC, Andre-Dohmen B, Reuss S, Weggen S, Roebroek AJ, Kuhlmann CR, Pietrzik CU: **LRP1 mediates bidirectional transcytosis of amyloid-beta across the blood-brain barrier.** *Neurobiol Aging* 2011, **32**:2323. e1-11.
 40. Selkoe DJ: **Alzheimer's disease: genes, proteins, and therapy.** *Physiol Rev* 2001, **81**:741–766.
 41. Hardy J: **The amyloid hypothesis for Alzheimer's disease: a critical reappraisal.** *J Neurochem* 2009, **110**:1129–1134.
 42. Partridge WM: **Blood-brain barrier delivery.** *Drug Discov Today* 2007, **12**:54–61.
 43. Re F, Gregori M, Masserini M: **Nanotechnology for neurodegenerative disorders.** *Nanomedicine* 2012, **8**:S51–S58.
 44. Kumari A, Yadav SK, Yadav SC: **Biodegradable polymeric nanoparticles based drug delivery systems.** *Colloids Surf B: Biointerfaces* 2010, **75**:1–18.
 45. Li S: **Hydrolytic degradation characteristics of aliphatic polyesters derived from lactic and glycolic acids.** *J Biomed Mater Res* 1999, **48**:342–353.
 46. Galasko DR, Graff-Radford N, May S, Hendrix S, Cottrell BA, Sagi SA, Mather G, Laughlin M, Zavitz KH, Swabb E, Golde TE, Murphy MP, Koo EH: **Safety, tolerability, pharmacokinetics, and Abeta levels after short-term administration of R-flurbiprofen in healthy elderly individuals.** *Alzheimer Dis Assoc Disord* 2007, **21**:292–299.
 47. Wagner S, Rothweiler F, Anhorn MG, Sauer D, Riemann I, Weiss EC, Katsen-Globa A, Michaelis M, Cinatl J Jr, Schwartz D, Kreuter J, von Briesen H, Langer K: **Enhanced drug targeting by attachment of an anti alphav integrin antibody to doxorubicin loaded human serum albumin nanoparticles.** *Biomaterials* 2010, **31**:2388–2398.
 48. Roney C, Kulkarni P, Arora V, Antich P, Bonte F, Wu A, Mallikarjuna NN, Manohar S, Liang HF, Kulkarni AR, Sung HW, Sairam M, Aminabhavi TM: **Targeted nanoparticles for drug delivery through the blood-brain barrier for Alzheimer's disease.** *J Control Release* 2005, **108**:193–214.
 49. Brambilla D, Le Droumaguet B, Nicolas J, Hashemi SH, Wu LP, Moghimi SM, Couvreur P, Andrieux K: **Nanotechnologies for Alzheimer's disease: diagnosis, therapy, and safety issues.** *Nanomedicine* 2011, **7**:521–540.
 50. Wilson B: **Therapeutic compliance of nanomedicine in Alzheimer's disease.** *Nanomedicine (Lond)* 2011, **6**:1137–1139.
 51. Rizzo LY, Theek B, Storm G, Kiessling F, Lammers T: **Recent progress in nanomedicine: therapeutic, diagnostic and theranostic applications.** *Curr Opin Biotechnol* 2013. doi: 10.1016/j.copbio.2013.02.020.
 52. Michaelis K, Hoffmann MM, Dreis S, Herbert E, Alyautdin RN, Michaelis M, Kreuter J, Langer K: **Covalent linkage of apolipoprotein e to albumin nanoparticles strongly enhances drug transport into the brain.** *J Pharmacol Exp Ther* 2006, **317**:1246–1253.

10.1186/alzrt225

Cite this article as: Meister et al.: Nanoparticulate flurbiprofen reduces amyloid- β_{42} generation in an *in vitro* blood-brain barrier model. *Alzheimer's Research & Therapy* 2013, **5**:51

Curriculum vitae

